Dedicated to innovation in aerospace

PUBLIC

NLR-CR-2023-140 | September 2023

SUSTAINair - Rivet detection

KET8: Robotic dismantling of EoL aircraft structures for maximised recyclate value

CUSTOMER: European Commission

Royal NLR - Netherlands Aerospace Centre

Dedicated to innovation in aerospace

SUSTAINair - Rivet detection

KET8: Robotic dismantling of EoL aircraft structures for maximised recyclate value

Problem area

The current recycling rate per aircraft is claimed to be 85% by weight, this is synonym for serious downgrading to mixed fraction waste, ending up in aluminium food trays or drink cans. Different materials cannot be separated in an economically viable way, as these are joined by rivets, more than 40.000 for a fuselage only. Latest shredder developments typically used in the EoL processing today, are able to classify shredded fractions, but cannot solve the inherent fact that mechanically joined multi-materials cannot be separated, leading to serious downgrading of the aluminium.

Description of work

Determine which Non-Destructive Testing method is most suitable to detect the rivets and which technique is best suited for the extraction of rivet coordinates which can be provided to the water-jet cutting robot. The following NDT methods were evaluated: Eddy Current Array, Ultrasonic Phased Array and Optical Lock-In Thermography, supported by 3D structural light scanning.
Investigation was performed on actual Airbus A330 and A340 fuselage panels.

REPORT NUMBER
NLR-CR-2023-140

AUTHOR(S)
A.F. Bosch
H.P. Jansen

REPORT CLASSIFICATION
UNCLASSIFIED

DATE
September 2023

KNOWLEDGE AREA(S)
Aerospace Materials

DESCRIPTOR(S)
NDI (Non-Destructive Inspection)
Thermography
EoL (End of Life)
Recycling

Results and conclusions

1. The PAUT inspection is for this application the least practical and sensitive. First reason is the need for a couplant. Although it is not much it still need some light spray of water. Another reason is the relative thin skin of aluminium, which results in multiple echoes, which makes it much harder to detect the right signal and therefore the right component.
2. ECA has a good detectability with respect to all geometrical features. But in practical performance, contact type method and small FOV it makes the ECA method less practical for this application.
3. OLT has a good detectability with respect to all geometrical features. The main advantages of OLT over ECA is the speed of inspection, the larger field of view and it is a non-contact technique.
4. Thermographic images can be mapped on top of a 3D model, which is acquired by 3D structural light scanning. This enables the extraction of a rivet coordinate in X, Y, Z position instead of X,Y position within the image.

Applicability

This study has shown that the Lock-In Thermography method is well suited to detect geometrical features such as: rivets, stringers, joints etc.
This result provides the aircraft recycling industry direction to further develop disassembling concepts in a cost effective way. Besides the possibilities of automating disassembly activities there is an substantially contribution to prevention of downgrading of high-performance aerospace materials.

Royal NLR
Anthony Fokkerweg 2
1059 CM Amsterdam, The Netherlands
p) +31 88 511 3113
e) info@nlr.nl i) www.nlr.nl

Dedicated to innovation in aerospace

PUBLIC

NLR-CR-2023-140 | September 2023

SUSTAINair - Rivet detection

KET8: Robotic dismantling of EoL aircraft structures for maximised recyclate value

CUSTOMER: European Commission

AUTHOR(S):

A.F. Bosch NLR
H.P. Jansen NLR

Royal NLR - Netherlands Aerospace Centre

CUSTOMER	**European Commission**
CONTRACT NUMBER	**101006952**
OWNER	**NLR**
DIVISION NLR	**Aerospace Vehicles**
DISTRIBUTION	**Unlimited**
CLASSIFICATION OF TITLE	**UNCLASSIFIED**

APPROVED BY:		**Date**
AUTHORS	A. Bosch P. Jansen	10-03-2023 10-03-2023
REVIEWER	J. Platenkamp	10-03-2023
MANAGING DEPARTMENT	P. Arendsen	10-05-2023

Contents

Abbreviations

ACRONYM	DESCRIPTION
A/C	Aircraft
AELS	Aircraft End-of-Life Solutions
AIT	Austrian Institute of Technology GmbH
ArUco	Augmented Reality University of Cordoba
DLR	German Aerospace Center
DNW	German-Dutch Wind Tunnels
EC	Eddy Current
ECA	Eddy Current Array
EoL	End of Life
ET	Eddy Current Testing
Hz	Hertz
IR	Infrared
IRT	Infrared Thermography
KET	Key Enabling Technology
LT	Lock-In Thermography
LKR	Leichtmetallkompetenzzentrum Ranshofen GmbH
LWIR	Long Wave Infrared
MHz	Mega Hertz
MWIR	Medium Wave Infrared
NDI	Non Destructive Inspection
NDT	Non Destructive Testing
NLR	Royal NLR - Netherlands Aerospace Centre
OLT	Optical Lock-in Thermography
PAUT	Phased Array Ultrasonic Testing
SWIR	Short Wave Infrared
UT	Ultrasonic Testing
WP	Work Package

1 Introduction

SUSTAINair is addressing the major challenge of 'Greening of Aircraft' in a way, that environmental benefits are meeting economic viability and European competitiveness at once. In contrast to the automotive sector, where End of Life (EoL) regulations are in place for years already, the EoL of aircraft does not have any legal regulation at all. When a commercial aircraft is retired today, on average after a 17-20 year service life, spare components of any value are taken off and re-sold on the spare market. The remaining of the airframe remains either corroding on the parking space in the hope it will be re-brought to service again, or in case of scrapping is shredded in pieces and sold per ton at very low values.

Although the current recycling rate per aircraft is claimed to be 85% by weight, this is synonym for serious down grading to mixed fraction waste, ending up in Aluminium food trays or drink cans. Different materials cannot be separated in an economically viable way, as these are joined by rivets, >40.000 for a fuselage only. Latest shredder developments typically used in the EoL processing today, are able to classify shredded fractions, but cannot solve the inherent fact that mechanically joined multi-materials cannot be separated, leading to serious downgrading. Purpose of this investigation is to supply a set of (X,Y,(Z)) coordinates for a waterjet cutting robot, this robot uses waterjet to remove the rivet lines from a certain part of a fuselage skin. Therefore substantially contributing to prevention of down grading of high-performance aerospace materials.

This investigation is part of WP2 Task 2.1 which forms the basis for the 8th Key Enabling Technology (KET8) of the SUSTAINair programme and this report describes the investigation to detect the rivets and rivets lines of an aircraft fuselage. A short summary of this report has been used as input for deliverable 2.2 of the SUSTAINair project [1].
The NLR is working with the following partners in this work package.

- **DLR – German Aerospace Center in Hamburg, Germany**
  DLR is developing a method to convert our coordinates into a machine (robot) useable instructions.
- **AIT-LKR - Leichtmetallkompetenzzentrum Ranshofen GmbH**
  AIT-LKR is responsible for the dismantling/recycling partnering with ConSus.
- **ConSus - ANT Stationary Cutting Solutions GmbH in Lübeck, Germany**
  ConSus facilitates the waterjet cutting robot.
- **AELS - Aircraft End-of-Life Solutions BV**
  AELS is an aircraft disassembly and dismantling company in Enschede, The Netherlands

The original plan was to receive the fuselage sections of a Belgium company AEROCIRCULAIR, but after their bankruptcy they were replaced by AELS as a partner in this programme. For this investigation 14 fuselage sections of different Airbus A/C were provided by AELS. The fuselage sections were used to perform inspections with different NDT methods:

- Eddy Current Array (ECA)
- Ultrasonic Phased Array (PAUT) with roller probe
- Optical Lock-in Thermography
- 3D optical light scanning

Goal: Determine which technique is most suitable to detect the rivets and which technique is best suited for the extraction of rivet coordinates which can be provided to the water-jet cutting robot.

2 Techniques

In this chapter the different NDT methods are described, which were used to detect the rivets, rivet lines and other components of the back-up structure in the fuselage sections.

2.1 Eddy Current (ET)

Although not used in this investigation, a quick explanation of the technique to understand the principle of Eddy Current Testing, as the Eddy Current Array (ECA) is derived from this. Eddy current (EC) inspection (or testing, ET) is a primary method for the in-service inspection of metallic aircraft components. The method is based on the response of induced currents that are caused in a conductive material when that material is subjected to an alternating electromagnetic field. Special probes, basically containing one (or more) coil(s), are used (Figure 2). A variable frequency oscillator feeds the coil by means of an alternating electrical current. The coil generates an alternating electromagnetic field (primary field H_p) in the test material. In accordance with the law of induction, circular electrical currents called eddy currents are induced into the material, their paths being parallel to the surface and perpendicular to the direction of the applied field. The eddy currents give rise to a secondary electromagnetic field H_s which by induction is directed opposite to, and therefore lessens, the primary field H_p. The eddy current response can be detected by measuring the phase and magnitude of the coil impedance. Material defects (e.g. cracks), now, will interrupt the induced eddy current flow and can hence be detected by a change in the coil impedance response, see Figure 1. A key advantage of the EC method is that no coupling medium is required between the probe and test material.

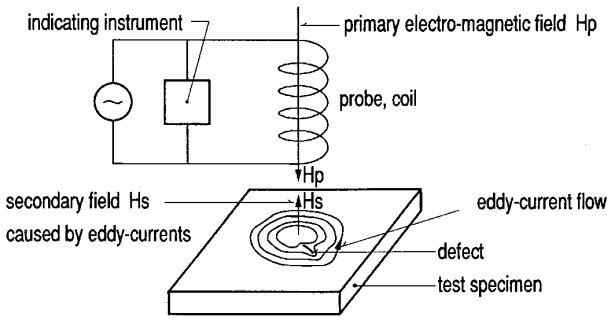

Figure 1: Eddy Current inspection technique

2.2 Eddy current array (ECA)

Eddy current array (ECA) inspection is a development in EC testing involving special multiple-coil probes and multi-channel EC equipment. The coils (generally of same design) are placed side-by-side in the probe (array) and data acquisition is done by using a multiplexer that avoids mutual inductance between the individual coils. Each EC coil in the probe produces a signal relative to the phase and amplitude of the structure below it. This data is referenced to an encoded position and time and represented graphically as a 2-dimensional C-scan image.

As a result, a wide-surface coverage of EC inspection can be done in a one-pass scan, see Figure 2. A key advantage of ECA inspection is an increase in scanning speed with respect to (single coil) EC while maintaining high resolution.

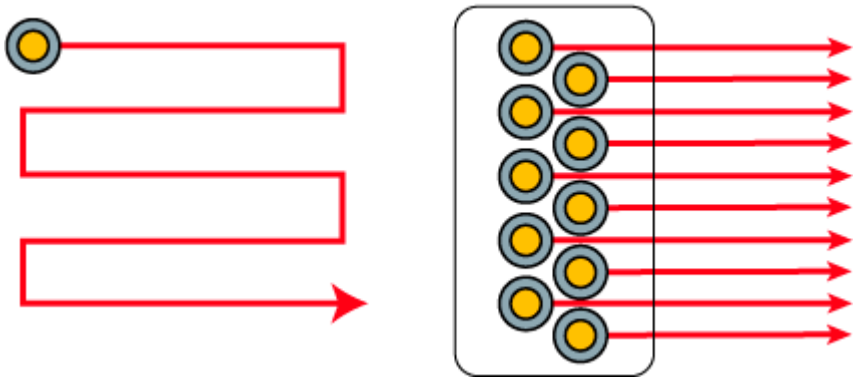

Figure 2: Benefit of ECA inspection with an array probe: one-pass scanning (ECA) versus conventional raster scanning with a single probe. [2]

Figure 3: ECA probes [2]

A typical aerospace application for ECA probes is the inspection of fastener rows for (sub)surface cracks. Formerly, this was done with so-called sliding probes that were centred on the fastener centre-line and subsequently scanned along the fastener row. The often complicated EC responses had to be analysed for any defect indications i.e. deviations from the 'standard' EC response of defect-free fasteners. The same complicated EC responses applies to ECA, but using monitoring gates the signals of interest are displayed on a C-scan image which immediately identifies any deviated areas, see Figure 5.

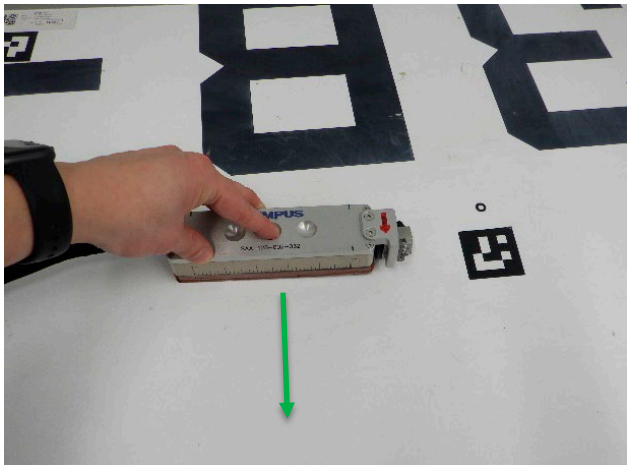

Figure 4: ECA scanning over the surface of the panel

Figure 5: Example of a typical C-scan image of stringers under the skin of the panel (not to scale)

2.3 Ultrasonic (UT)

Same case as with the Eddy Current part, Conventional UT was not used in this investigation but a quick description of the technique to understand the principle of Ultrasonic Testing, as the Phased Array (PAUT) is derived from this. Ultrasonic inspection (conventional) is a primary technique for the inspection of composite and metal components. The technique makes use of high-frequency sound waves, in fact propagating mechanical vibrations with a frequency in the range of about 0.5 - 50 MHz that are introduced into the material of interest. Because air is not an adequate transmitting medium for ultrasonic waves, a coupling medium such as water or gel has to be used between the transducer and the material. At interfaces of different materials, a part of the sound beam is reflected and the other part is transmitted into the material, see Figure 6. The reflection and transmission signals can be displayed and analysed on a scope. Depending on the material condition, attenuation of the sound beam due to the microstructure or local defects can occur. The time difference between reflected signals gives information about the “defect” depth in the material.

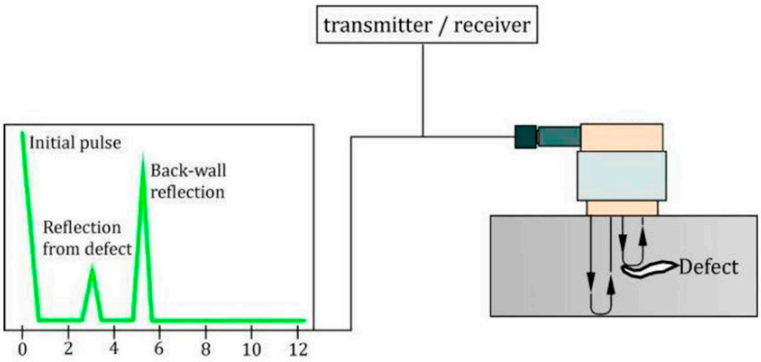

Figure 6: Principle of ultrasound inspection [3]

2.4 Ultrasonic Phased Array (PAUT)

Manual UT inspection with a single UT transducer is possible but not very practical. But a more attractive UT inspection technique has emerged, the so-called ultrasonic phased array technique (PAUT). This is a special UT technique that makes use of transducers consisting of multiple ultrasonic elements (currently up to 256 elements) that can each be driven independently. The PA transducers can have a different geometry (e.g. linear, matrix and annular) (See Figure 7) and the PA beams can be steered, scanned, swept and focused electronically by applying different electronic time delays to the elements. (See Figure 8).

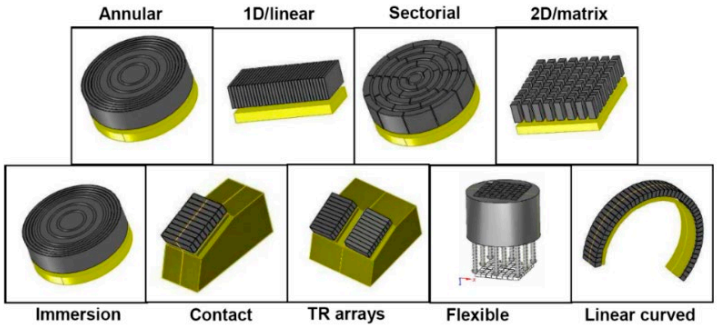

Figure 7: Examples of phased array transducer configurations [4]

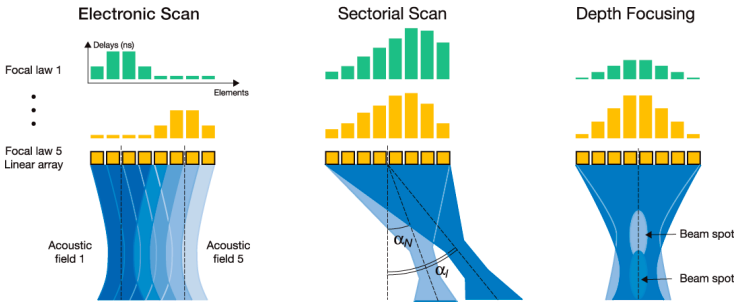

Figure 8: Time shifting wave fronts enables linear scanning, angulating/sweeping and focussing of the sound beam [5]

In this case we use the linear scan, this is a scan in which the acoustic beam moves along the major axis of the array without any mechanical movement. A single focal law is multiplexed across groups of active elements, creating either a straight beam or a beam at a single angle that advances the length of the probe.

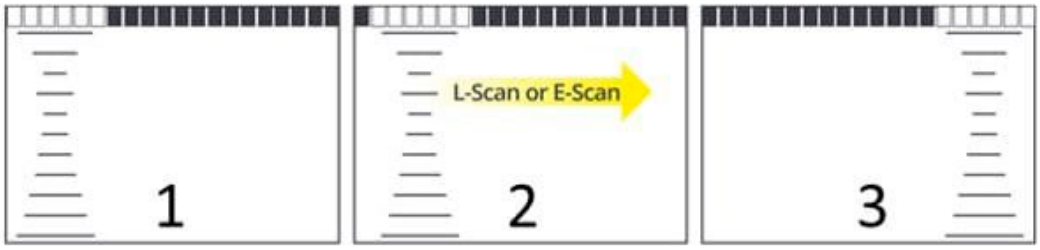

Figure 9: Principle of Linear (electronic) scanning [6]

There is also a special PAUT application that uses only little couplant. An example is the Wheel probe a.k.a. RapidScan™ of Sonatest Ltd. that employs a UT phased array probe housed within a rubber coupled and water-filled wheel probe. See Figure 10.

A wheel probe is an ultrasonic transducer assembly that allows rolling contact of a transducer over an inspection surface. The transducer assembly scans over the (curved) surface generally in more or less straight scan line, but steering of the wheel probe is also possible. An outer part of the assembly rotates, allowing the wheel to roll over the surface, while an inner part of the assembly holds the ultrasonic transducer at fixed angles relative to the surface. The conformable, rubber tyre is acoustically matched to water, providing low loss coupling into the test part. The probe can be used generally with a fine water spray on the test part which is used for optimum coupling.

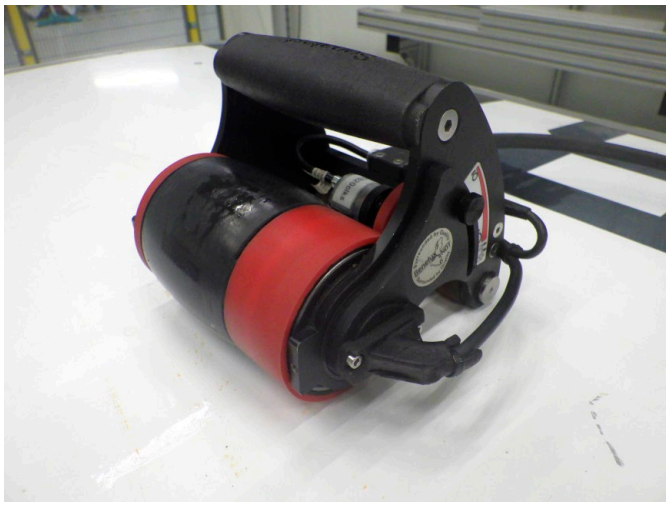

Figure 10: Sonatest Wheel probe with 5L64 PAUT transducer

2.5 Thermography (IRT)

Infrared Thermography (IRT) is a non-contact NDT method that monitors the heat radiation pattern on the surface of a test part. The method employs light just above the visible part of the electromagnetic spectrum, in the range of about 2 ~ 14 µm, see Figure 11. The 1 to 3µm is usually referred as short wave, 3 to 6µm medium wave and the 8 to 15µm as long wave. The split between the MW and LW bands is caused by the atmosphere attenuation of the 6 to 8 µm wavelengths due to absorption of the thermal infrared radiation by carbon dioxide (CO_2), water (H_2O) and ozone (O_3).

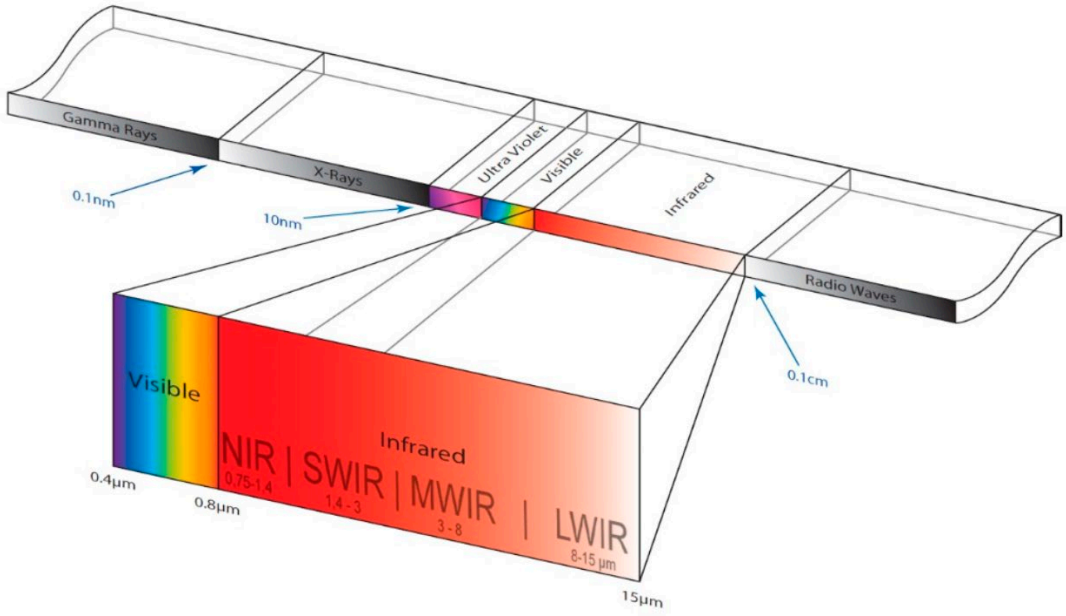

Figure 11: Electromagnetic spectrum with the infrared region highlighted (SWIR – short wave, MWIR- medium wave and LWIR – long wave) [7]

Passive and active IR techniques can be distinguished, however for NDT purposes the active technique is mostly used. Active IR involves temperature measurement of object surfaces that is subjected to a thermal excitation. When an object has a constant surface temperature (thermal equilibrium) it is not possible to detect deviations. When an object is excitated either by an external heat source or by mechanical vibrations, the differences in surface temperature are caused by internal features (discontinuities/geometry). For the NDT application, it is not necessary to measure absolute surface temperatures but only the temperature differences. Knowledge of the internal geometry of the object inspected is detrimental to differentiate between discontinuities and geometrical indications.

The principle of optical lock-in thermography is based on the application of a periodic input energy wave (in this case halogen lamps) to the surface of the object being examined and analysing the resulting local temperatures on the surface of the object. When the input energy wave penetrates the object's surface, is it absorbed and phase shifted. When the input wave reaches for example a defect the input wave is partially reflected. The reflected portion of the wave interferes with the incoming input wave at the surface of the object, causing a phase shift in the local surface temperature. This change is detected by the infrared camera. The internal structure of the object being examined can then be derived by evaluating the phase shift of the local surface temperatures in relation to the input energy wave. A schematic picture of the process is shown in Figure 12.

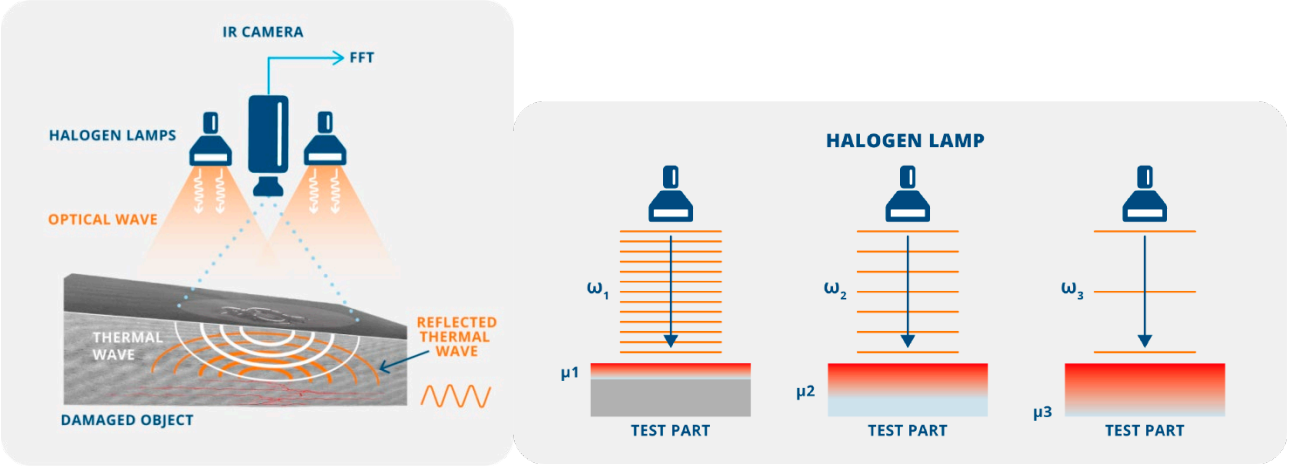

Figure 12: Principle of lock-in thermography and the relation of frequency and penetration depth

The applied frequencies determine the inspection depth. The higher frequencies are surface sensitive and lower frequencies are more suitable to detect deeper defects. Thermography is a sub-surface technique for relative thin structures and does not allow for inspection of very thick components. Lock-in thermography (LT) uses a (low-frequency) sinusoidal modulated heating which is imposed on the test part using halogen lamps. The test part is monitored with an IR camera several times per modulation cycle in order to obtain an image of the temperature modulation of the surface. Absorption of modulated radiation generates a thermal wave on the surface. This wave propagates into the interior where it is reflected at boundaries and defects, and finally returns back to the surface where it is superposed with the next wave [5], resulting in a phase shift between the modulation wave and the temperature on the surface. Figure 12 shows a schematic overview of the process and the data from a defect and non-defect region. Figure 12 also shows three types of situations, high frequency, medium frequency and low frequency. For a high frequency, the thermal diffusion length μ is small, resulting in low penetration depth of the sample. Only information about the subsurface can be obtained. With a decrease in frequency the penetration depth becomes higher and information deeper in the sample is obtained. At low frequencies the entire sample can be penetrated as shown in the third figure.

2.6 3D Scanning

The ATOS 5 MV1000 system is a blue light optical scanner which scans three-dimensional objects and converts the images to high density point clouds. This allows accurate measurement and capture of the shape and size of the visible surface of 3D objects. The scanning is based on optical triangulation and stereo-viewing. A projector is used to project striped fringe patterns onto the object's surface. These images are captured simultaneously by the two measurement cameras from different angles. Reference markers are used on the object (or around the object) to be able to stitch the individual scans together. With the help of digital image processing, 3D-coordinates are computed fast and with high accuracy. The captured scan data is then automatically integrated in the reference marker framework. The additional data captured with two cameras of the ATOS system are used to verify the calibration of the system, detect movements and high ambient light changes during the measurement and verify the matching accuracy of the individual scans into the global coordinate system. Figure 13 Shows the system and schematic representation.

Figure 13: ATOS 5 MV1000 system (left), and the schematic representation of the working of this system [8]

3 Reference specimens

In total 14 fuselage panels were provided by AELS for this investigation. These panels are cut fuselage sections from two Airbus aircraft types. 8 Airbus A330 panels and 6 panels of an Airbus A340. The 14 fuselage panels can roughly be divided into 2 sizes, six smaller sized panels (approx. 1 x 0.7 metres) from an A340 and eight larger (approx. 1.5 x 1 metres) sized panels from an A330. For easier identification and tracking the panels were all marked with an NLR product number and separately photographed from front side (outside fuselage) and back side (inside fuselage).

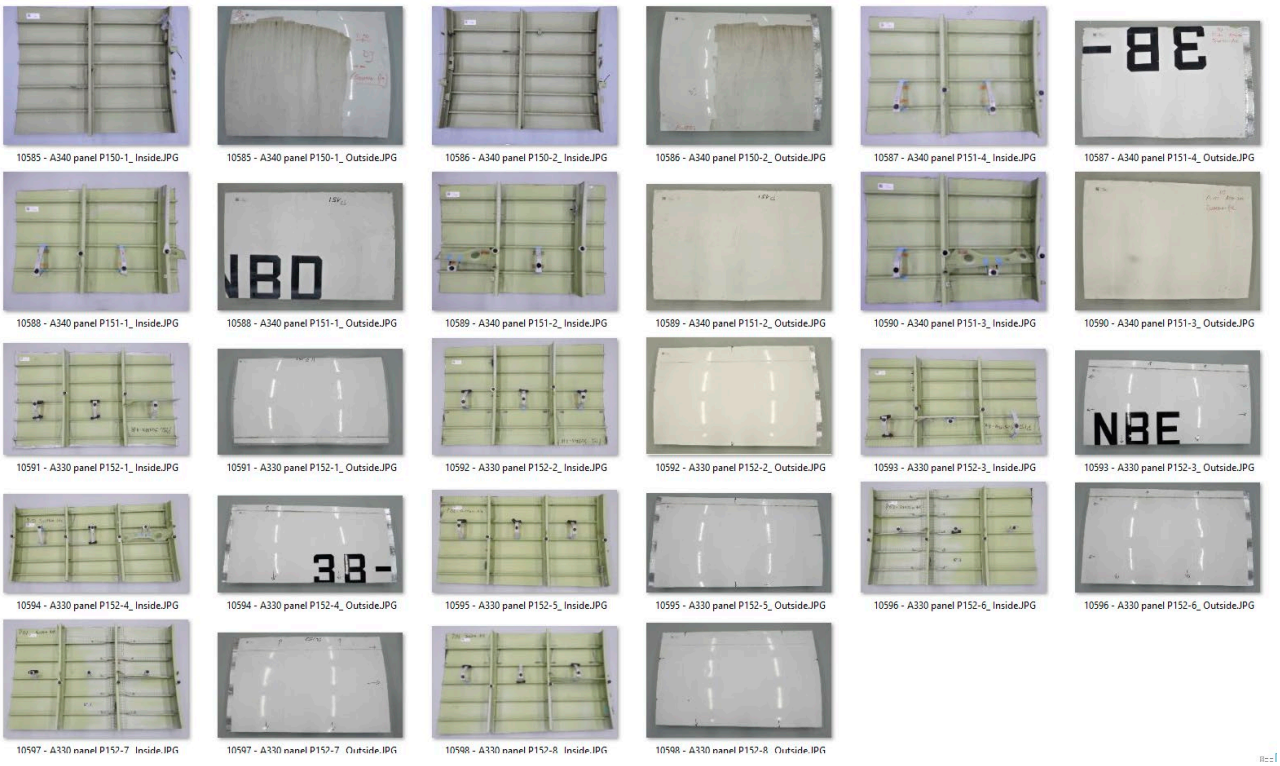

Figure 14: Front side and Back side photographs of the 14 panels that have been supplied by AELS

The used identification numbers are an NLR internally reference and tracking system (PDS) this system stores all information regarding a component or specimen during fabrication. In this case this numbered system is also useful for identification of these 14 panels.

Table 3-1 shows the cross reference between the NLR numbers and the identification found on the panels. Additional information is listed in the remarks section.

Table 3-1: NLR ID numbers

NLR ID number	Panel name	Remarks
10585	A340 panel P150-1	Thick rough paint on front side of panel
10586	A340 panel P150-2	Thick rough paint on front side of panel
10587	A340 panel P151-4	Black adhesive numbers on skin and dull white surface paint
10588	A340 panel P151-1	Black adhesive numbers on skin and dull white surface paint
10589	A340 panel P151-2	Dull white surface paint
10590	A340 panel P151-3	Dull white surface paint
10591	A330 panel P152-1	Longitudinal joint (lap-joint)
10592	A330 panel P152-2	Longitudinal joint (lap-joint)
10593	A330 panel P152-3	Longitudinal joint (lap-joint) and black adhesive numbers on skin
10594	A330 panel P152-4	Longitudinal joint (lap-joint) and black adhesive numbers on skin
10595	A330 panel P152-5	Longitudinal joint (lap-joint)
10596	A330 panel P152-6	Circumferential (butt-joint) and longitudinal joints (lap-joint)
10597	A330 panel P152-7	Circumferential (butt-joint) and longitudinal joints (lap-joint)
10598	A330 panel P152-8	Longitudinal joint (lap-joint)

Reference panel used for investigations by NLR and finally send to DLR

The 6 A340 panels consist of 2 bays with, depending of the cut area, 2 or 3 frames. The 8 A330 panels consist of 3 bays with 3 or 4 frames. The skins are made of 2024 Aluminium, painted with a glossy white paint on the outside and green primer on the inside. Paint thickness on the panels is 250-300µm. On some panels there are black identification letters and numbers adhered and other have a thick rough paint on them. Probably to cover up some identification numbers.

A fuselage panel consist of an aluminium sheet (skin) with multiple parts attached to it, this is also known as back-up structure. Back-up structures can be stringers, frames, clips, brackets and so on. On Figure 15 and Figure 16 the different parts of the back-up structure of these panels can be identified.
There are different types and size rivets used in the panels. The 2 types are punched rivets and ‘threaded rivets’ called HI-LOK fasteners. HI-LOK is a simple two-part fastener system. Consistent torque on each fastener is achieved by a breakoff groove in the self-locking HI-LOK collar. When the correct torque level is reached the hexagon part of the collar snaps off. Depending on the back-up structure configuration these fasteners or rivets have different sizes and lengths.

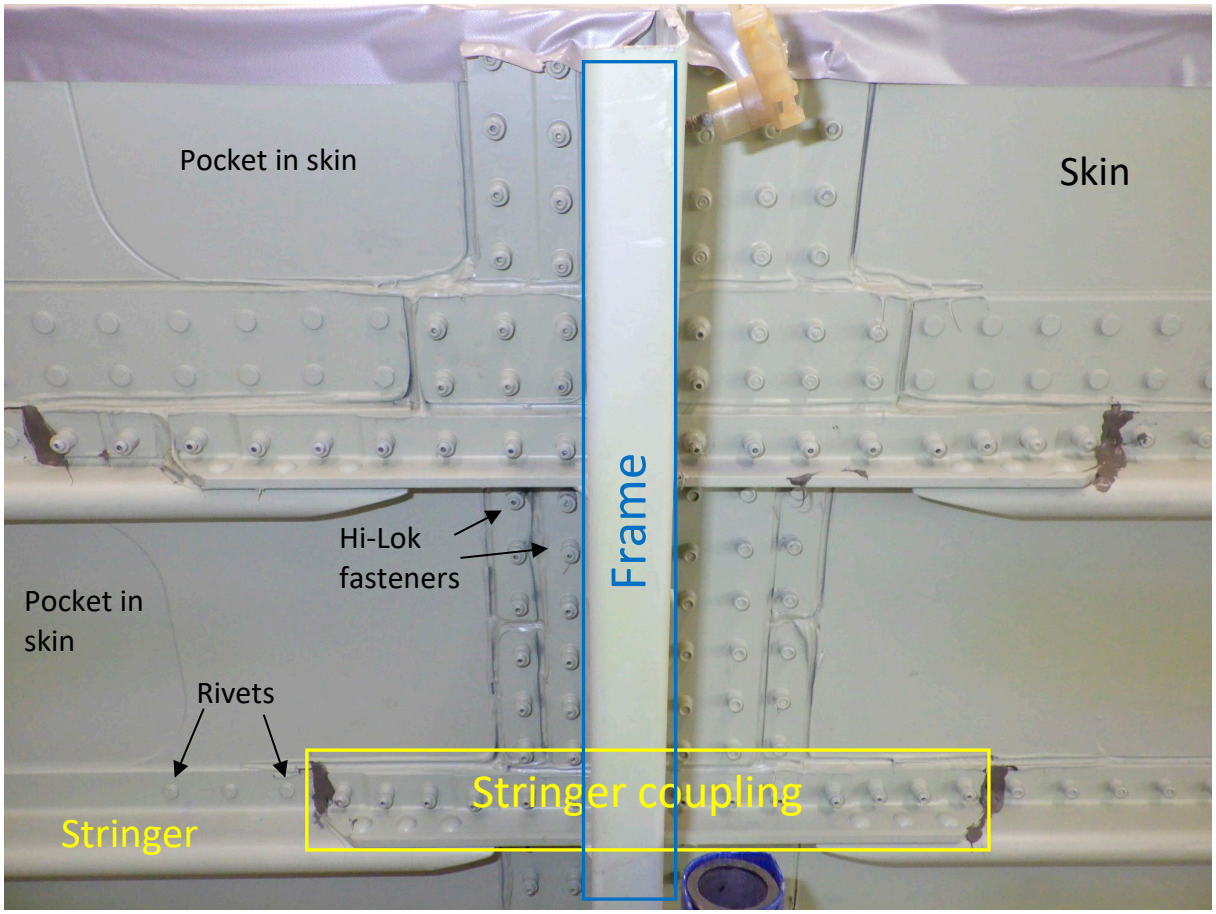

Figure 15: Back-up structure identification on A330 panel

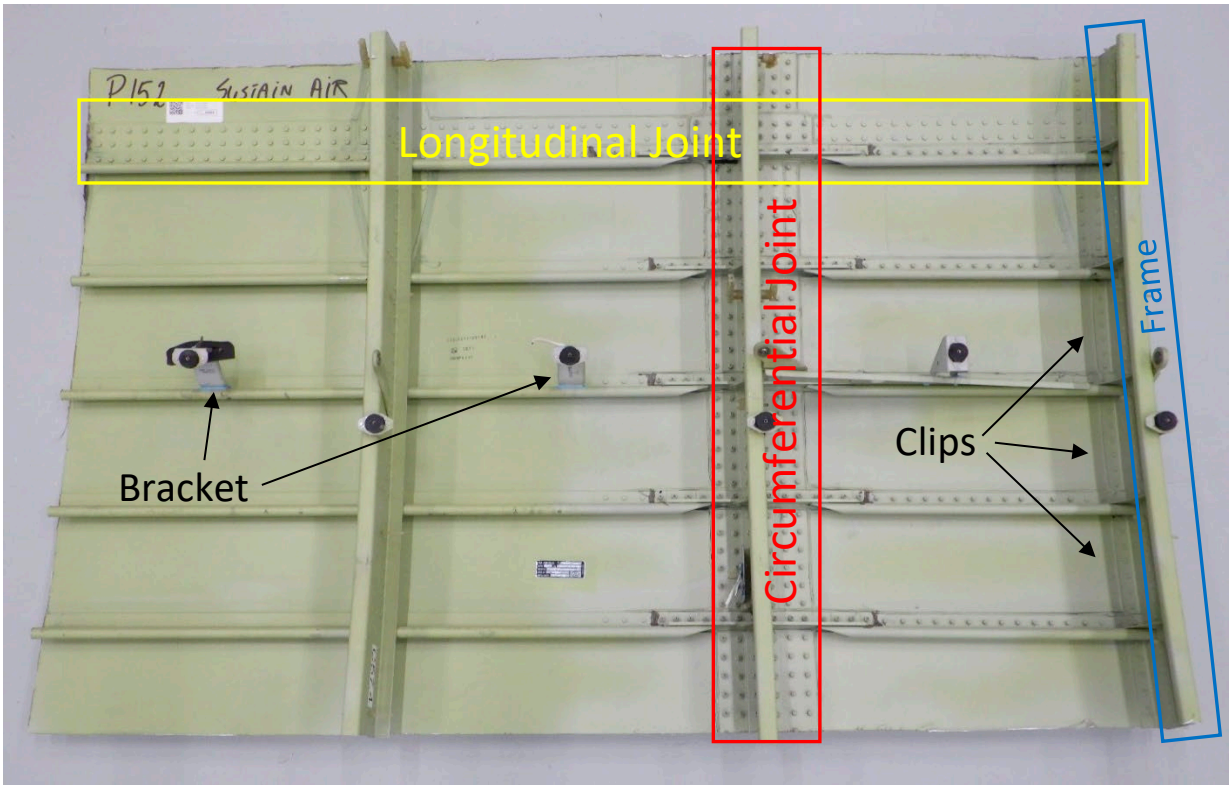

Figure 16: Back-up structure identification on A330 panel

The stringers are mostly bonded to the skin and on some areas, e.g. close to stringer couplings, also riveted to the skin. Clips are used to make a connection between frames and skin. The larger A330 panels all have a longitudinal joint and two panels (10596 and 10597) also a circumferential joint connection.

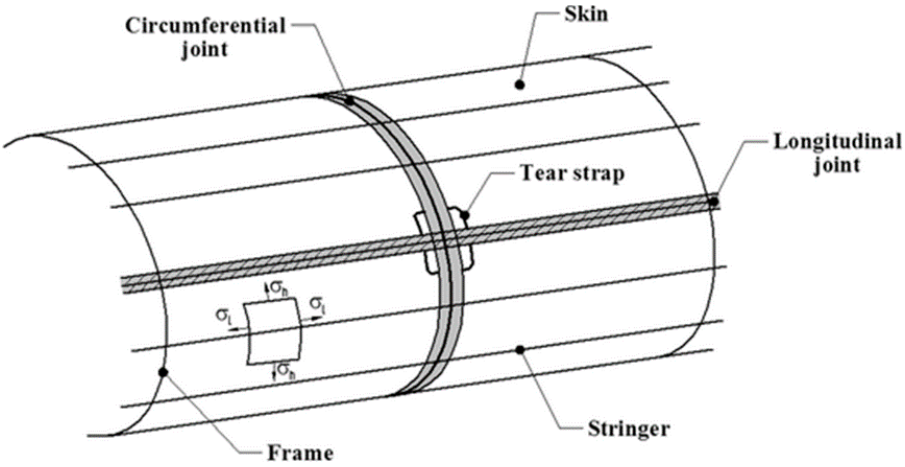

Figure 17: Different joints on aircraft [9]

Circumferential joints are used to couple two sections of fuselage together. These sections are coupled by a butt-joint connection. With typically two rows of 3 fasteners and a butt-strap connecting the two fuselage halves. Longitudinal joints are commonly lap-joint connections, which couple two sheets of skins together with a row of three fasteners.

On Figure 18 the difference of the two used joint connection types are shown.

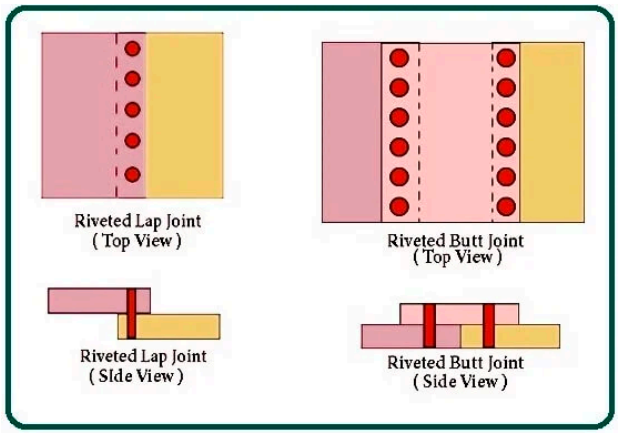

Figure 18: Lap-joint and butt-joint. Ref:mechanicaljungle.com [10]

For a clear comparison between the NDT methods without too many variables of different panels, 2 panels out of the 14 were selected on which all the experimental tests described in chapter 2 were performed.

The 10587 is one of the smaller series panels (A340) and was selected because a part of a sticker (black letter and number) is adhered to the skin, probably a registration number or similar. The contrasting black sticker on the white surface can have a large influence on the test results, especially for optical NDT methods.

Figure 19: Panel 10587 (inside view picture mirrored)

The 10597 is a larger panel (A330), here the surface finish is only white paint but this panel has both a longitudinal and a circumferential joint. Therefore consist of many rivets and joint configuration differences which made this panel interesting to perform the experimental NDT tests on.

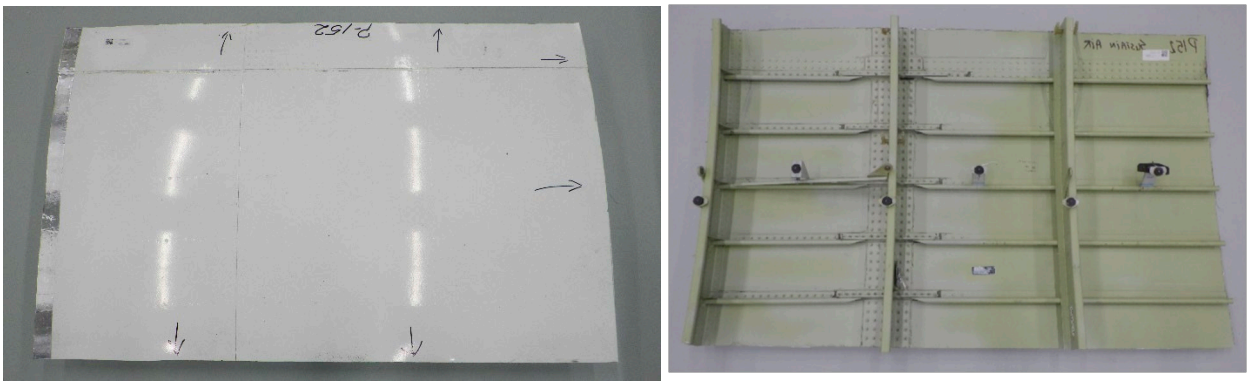

Figure 20: Panel 10597 (inside view picture mirrored)

4 Initial experiments

The techniques as described in chapter 2 were used to inspect the 2 panels and trying to detect the rivets and back-up structure as clear as possible of the panels.

4.1 3D scan

A 3D scan has been performed on the selected panels 10587 and 10597. The 3D scan can capture the entire outside geometry of the component. It is not possible to detect rivets that are hidden beneath a thick layer of paint, so this technique is not suited for rivet detection. However, the technique will be used to get more details of the component under investigation and to provide 3D coordinates for the cutting robot. For the panels that were received both the front side and the back side are visible. By scanning both the front side and the back side the thickness of the aluminium skin can be measured, as well as pockets and rivets can be located from the back side of the panel. This cannot be done in a production scenario, where only the outside of the fuselage is visible. Figure 21 shows photographs of 3D scanning process. The panel is scanned by manually moving the scanner around the panel.

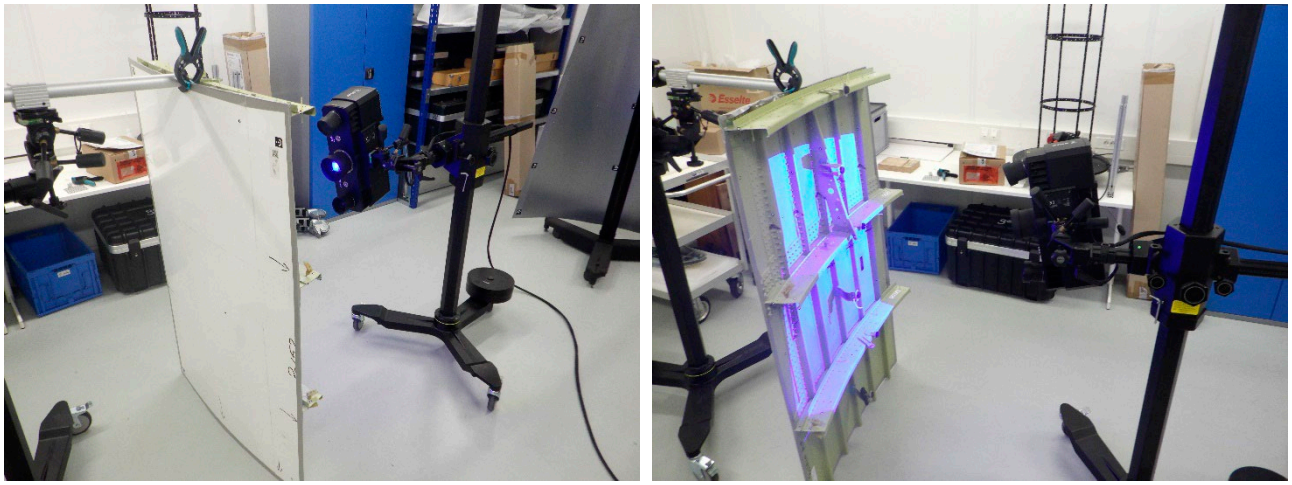

Figure 21: Photographs of the 3D scanning of panel 10597

The surface mesh of the front side of panel 10587 and 10597 obtained by the 3D scan are shown in Figure 22. For panel 10587 not a single rivet can be detected since they are covered with paint. For panel 10597 some rivets are visible from the surface mesh, but not with clear contrast with the rest of the surrounding.

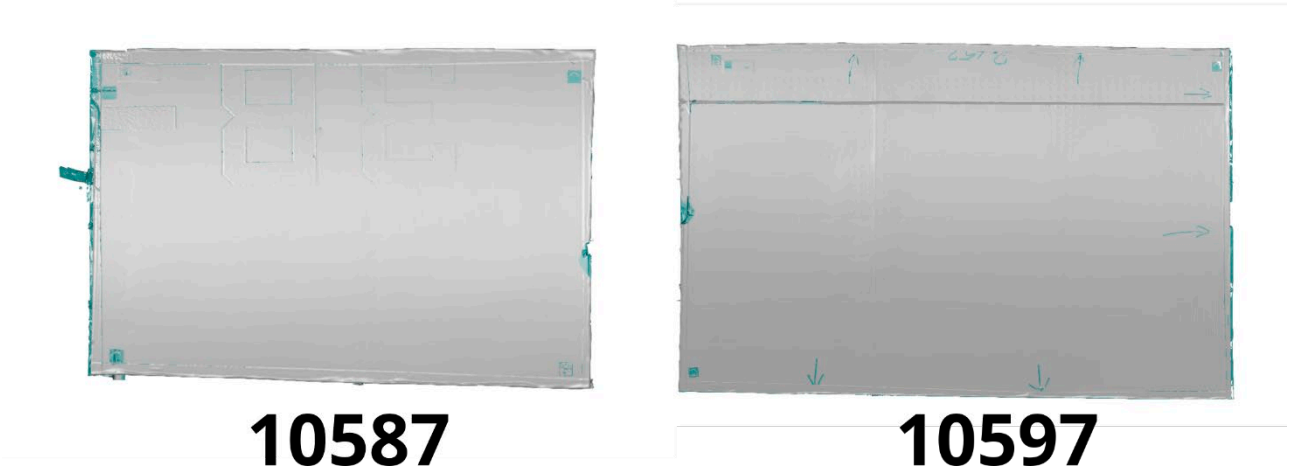

Figure 22: Surface mesh of the front side of both panels obtained by 3D scanning

The back side of these panels were also scanned, as shown in Figure 23. From the back side the structural details of the panels can be seen. In this case, the stringers, frames, clips, rivets and HI-LOK fasteners are visible. Unfortunately, scanning of the back side of the sample is not feasible in a production setting, rendering this results unsuitable for the real business case.

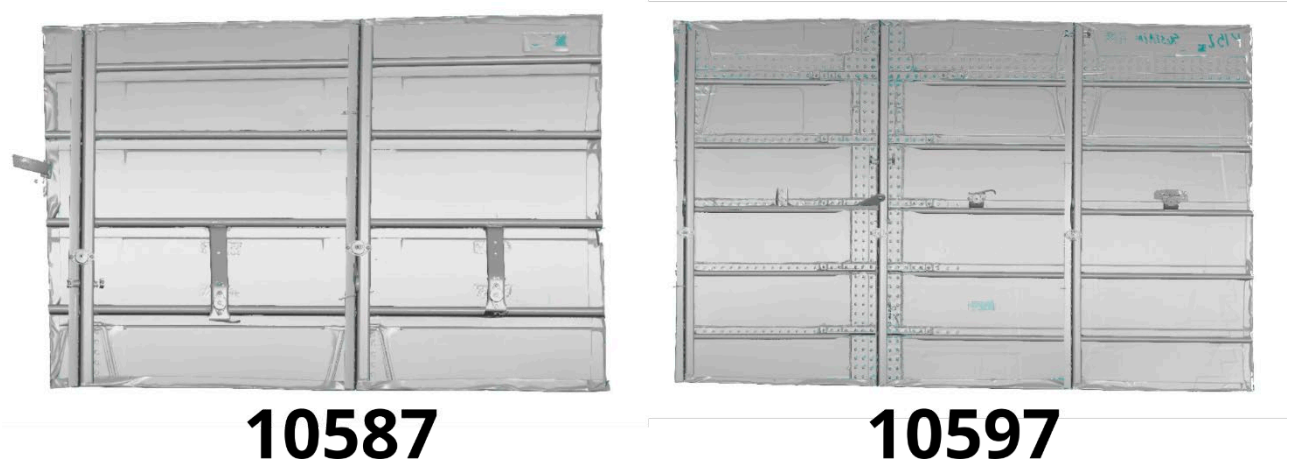

Figure 23: Surface mesh of the back side of both panels obtained by 3D scanning (mirrored such that it corresponds to the optical photographs)

Since both the front and the back side of the panels are scanned the thickness of the panel can be expressed by a colour plot from the front side, as shown in Figure 24. The overall skin thickness of the A340 fuselage amounts to 1.84 mm and the stringers and frames are clearly visible in the image due to the increase in thickness. Additionally, the rivets can also be clearly seen from these images. The results of the A330 fuselage part (10597) show a distinct skin thickness. At the left side of the circumferential joint (panel 10597) the skin thickness amounts to 1.89 mm while on the right side of the joint the skin is thicker, approximately up to 2.2 mm . From these images the stringers and frames can be clearly seen as well as the skin pockets. For this part the rivets and Hi-LOK fasteners can also clearly be detected.

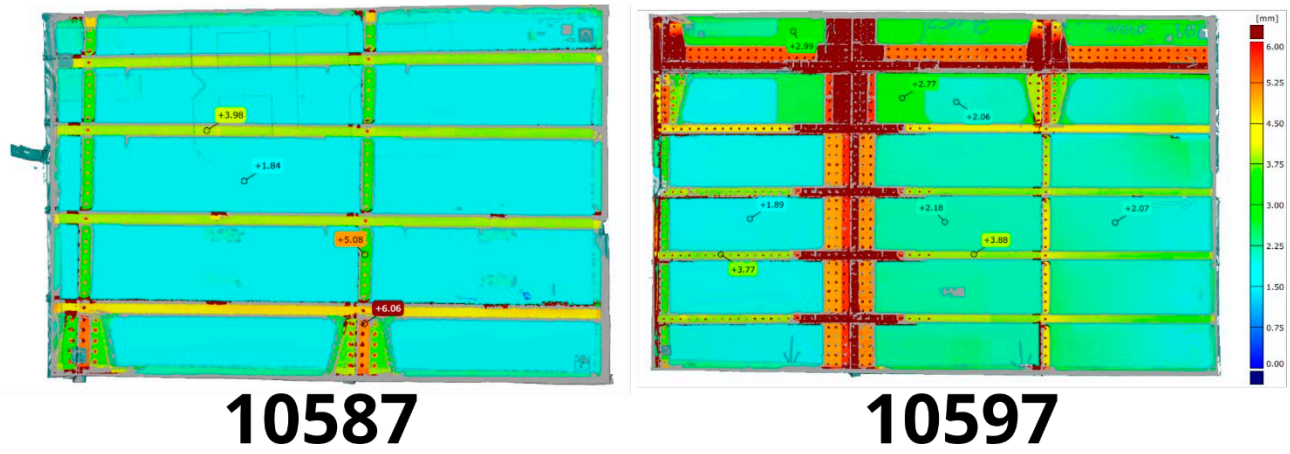

Figure 24: Material thickness map obtained by scanning both the front and the back side of the panels

Results from 3D scanning will be used two fold. First, it serves a check to see if all rivets have been detected by the NDT methods under consideration. Second, the 3D will be used in order to get the coordinates of the rivet locations in 3 dimensions, which will be described in Chapter 6.

4.2 Experimental inspection ECA

For Eddy Current Array (ECA) inspection an Olympus Omniscan MX with ECA module was used. The Omniscan MX of Olympus (now Evident) is a modular platform which can be used with Eddy Current as well as with Ultrasound.
A module on the rear of the instrument can be changed depending on the desired technique. The Eddy Current Array probe was the Olympus SAA-128-002-032. This ECA sliding probe has 32 coils, a centre frequency of 2kHz and a scanning width of 128 mm. The coils are mounted in a flexible 'sponge-like' material. This material makes that the surface of the probe can adapt to a curvature or light irregular surfaces. On the probe an encoder wheel is mounted which is used for the positioning and dimensioning of components (rivets, stringers etc) in the scan axis, synchronizing data acquisition with probe movement.

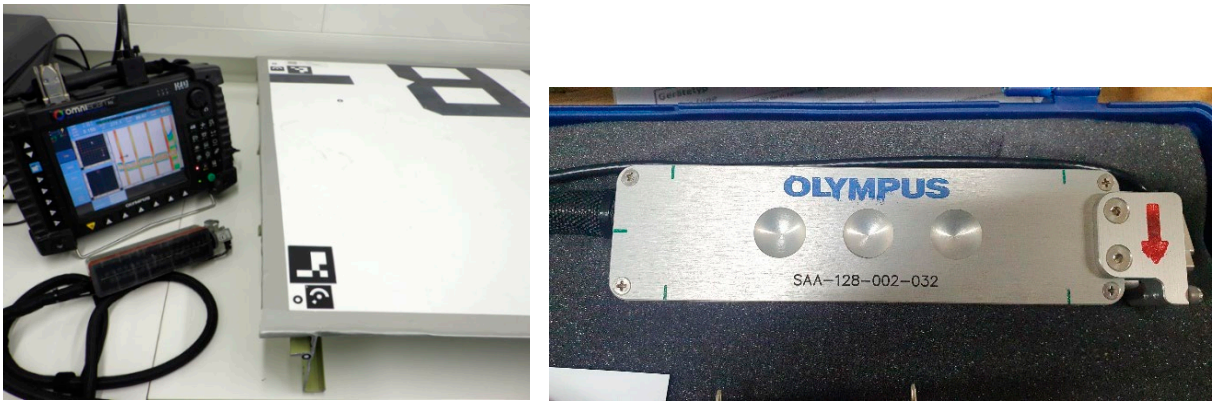

Figure 25: Omniscan MX with ECA module and SAA-128-002-032 sliding probe

Prior inspection the equipment is set-up for this specific configuration. This set-up was done on a clean part of the panel (i.e. only skin without stringer or rivets underneath it)

The set-up consist of different settings such as the phase angle of the eddy current signal, the horizontal and vertical gains, calibrating the encoder and determine the desired scan length. The scans were performed from the top of the panel to the bottom of the panel following the cord line of the surface. The most difficult part here is to inspect in a straight line. Without any guidance from a ruler it is almost impossible. If not scanned in a straight line you get very distorted pictures. (E.g. a curved stringer or rivet line)After the scan the file needs to be saved and the next scan can be carried out along the previous scan with an offset of approx. 128 mm etc. For panel 10587 nine scans were recorded, these can be stitched together afterwards in a graphical editing software program to have 1 image of a certain inspection area.

Another option is to use a clicker for the index steps. This is a manual switch which adds an extra axis to inspection setup. This clicker can be pressed after a scan line, the encoder skips a predefined distance and then the next scanline can be recorded in the same file. Disadvantage is that the file size becomes large which slows down the processing power of the equipment (limitation of the Omniscan MX).

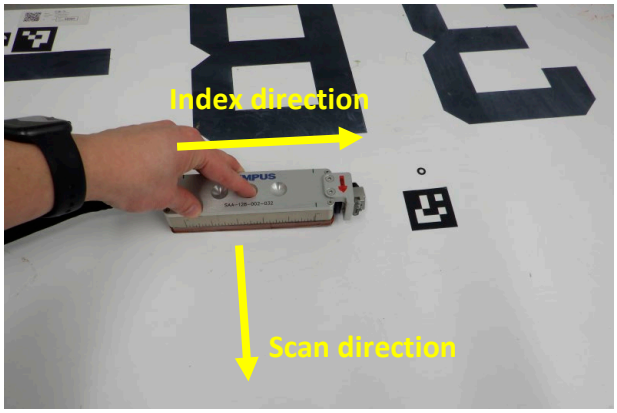

Figure 26: ECA Inspection on panel 10587

Eddy Current is a very suitable technique to detect any changes, anomalies or deviating materials in a metallic structure. And in this case the detection of the rivets and stringers in the panel is for this technique not any problem. In Figure 27 the results can be observed of 1 scan line on the panel from top to bottom (shown on the picture from left to right). The scan was following a rivet line and clearly the different stringers are visible, and in the end a 3 row rivet area is shown. The image is not to scale and therefore compressed in the scan axis. But the test results are good and the rivets and stringers can be detected clearly. After some post-processing of the data the C-scan image can be scaled to have the scan axis in the same ratio as the index axis, this can be seen in Figure 28. Here the detected rivets are displayed round and the stringers are in the right proportions to each other.

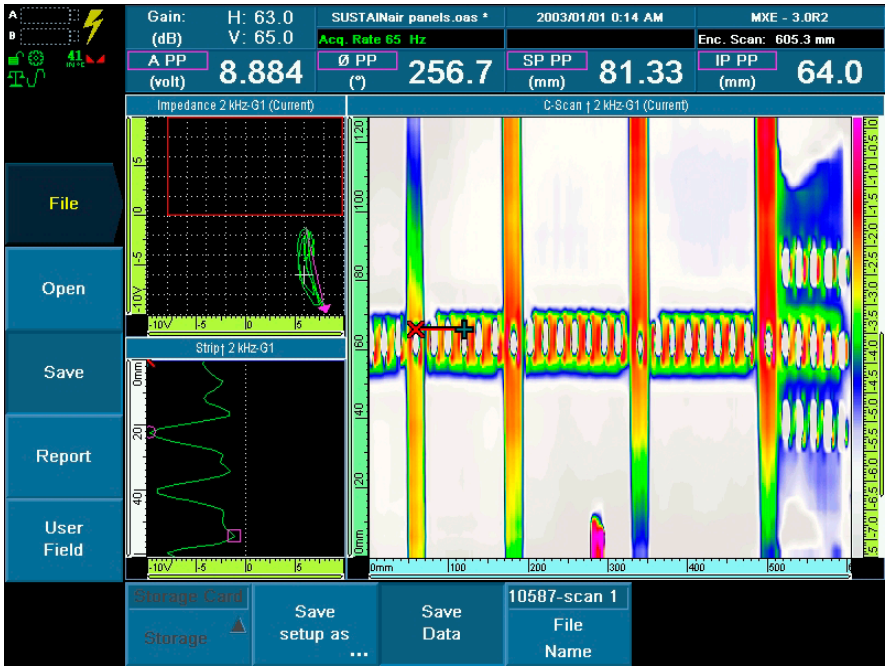

Figure 27: ECA result of stringers and rivet row of panel 10587 (not scaled in the scan axis)

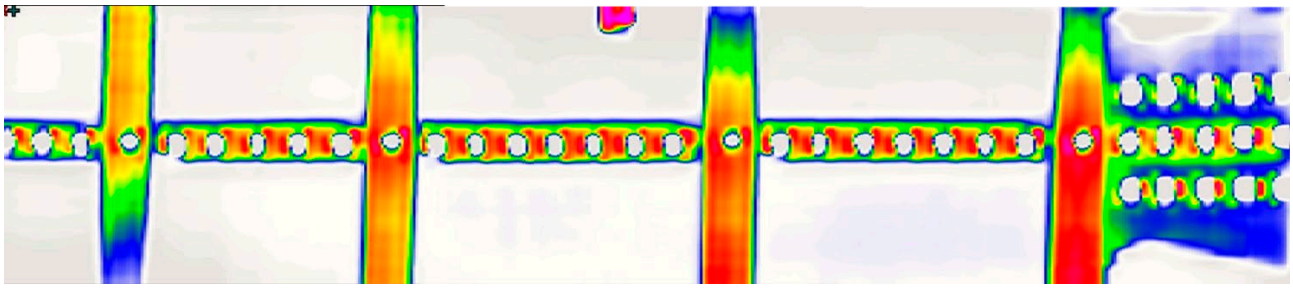

Figure 28: Scaled ECA C-scan image of the rivet line and 4 stringers on panel 10587

4.3 Experimental inspection PAUT

For Ultrasonic phased array (PAUT) inspection also the Olympus Omniscan MX was used, however the ECA module was swapped for an ultrasound phased array module: OMNI-M-PA 16:128. The used probe was the Sonatest wheel probe CWP-05-64-08-05-OMNI. Inside the wheel probe a 5 MHz, 64 element PAUT transducer is mounted with an effectively scan width of 44 mm.

The set-up for the inspection was done on the same area as it was for the ECA inspection: A single sheet of aluminium skin. For the ultrasonic method a light spray of water is necessary to obtain a good coupling between the probe and the surface. The scans were performed in the same way as the ECA inspection from the top of the panel to the bottom of the panel following the cord line of the surface. Here very similar issue as with the ECA inspection, is to keep the scan lines straight to prevent distorted images.

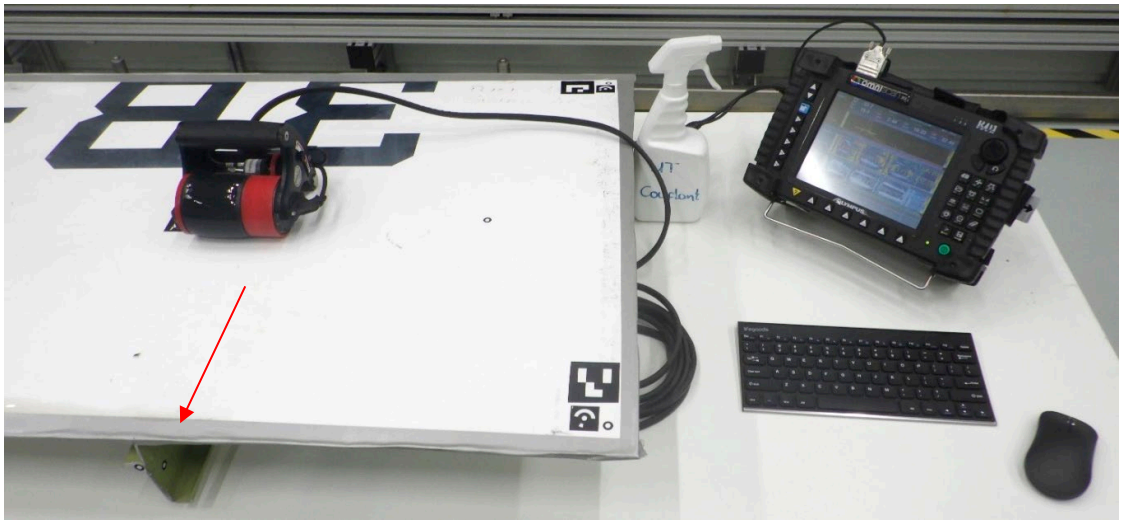

Figure 29: PAUT inspection on panel 10587 with the red arrow indicating the scan direction

As can be seen in Figure 30 the rivets and stringers can be detected but it is more difficult to interpret the signals from the aluminium structure. Multiple echoes due to the relative thin skin and layered structures (e.g. bonded stringer to skin) of the panel, makes it difficult to get a good inspection set-up. When there is disturbance cause by sealant or any other anomaly the returned ultrasound signal is reduced and this has an influence on the test results. This can be seen where the clips are mounted to the skin, around the edges of the clips there is a significant loss of ultrasound signal, resulting in blue coloured areas (more dampening) in those areas.

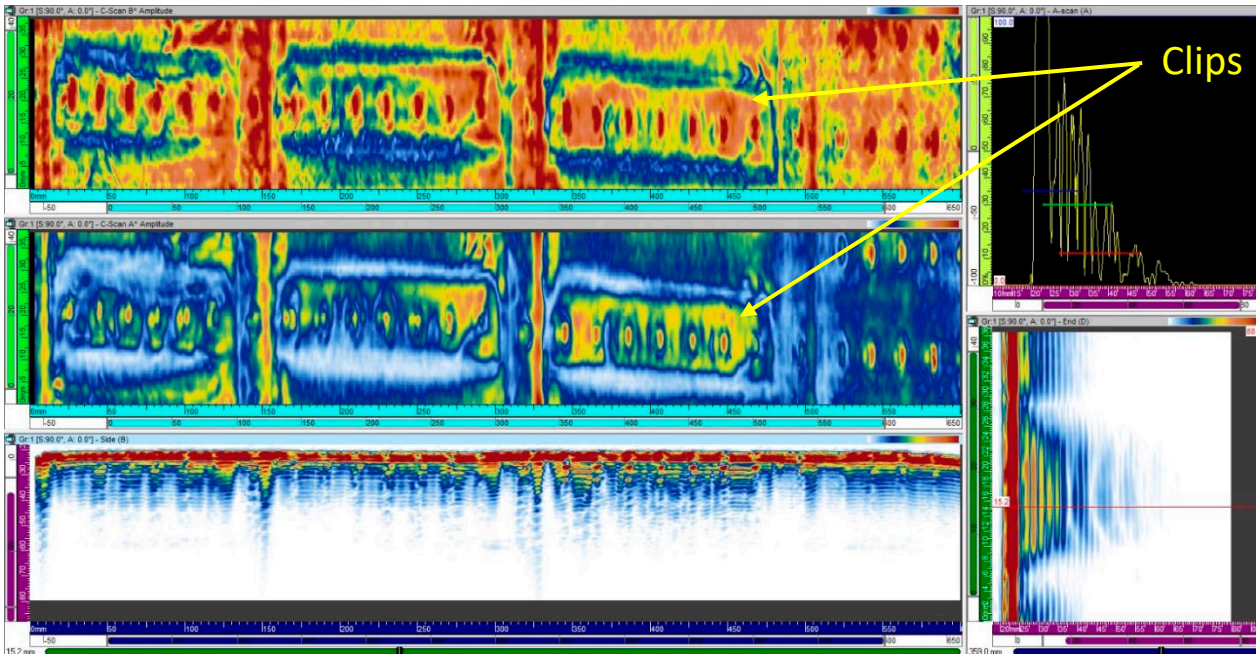

Figure 30: PAUT result of same rivet row and stringers as performed with the ECA inspection

In Figure 30 the PAUT results can be observed of 1 scan line on the panel from top to bottom (shown in the picture from left to right). The scan was following the same rivet line as with the ECA inspection and clearly the difference is visible between the two techniques. At the PAUT dataset the rivet line is more difficult to separate from the backwall (in this case the aluminium skin). Also the reduced inspection width of 44 mm is clearly visible compared to the 128 mm of the ECA probe.

4.4 Experimental inspection IRT

The Thermography set-up consists of an IRCAM Taurus 1310k SM infrared camera, two 2 kW halogen lamps, a signal generator and a computer for data logging. A picture of the setup is shown in Figure 31. The IRCAM Taurus 1310k camera has a resolution of 1280x1024 pixels and can record with a full frame rate of 179 Hz. The camera detects IR radiation in the band of 3.4 to 4.9 µm. The signal generator is controlled by the computer with the DisplayIMG 7 software from edevis GmbH.

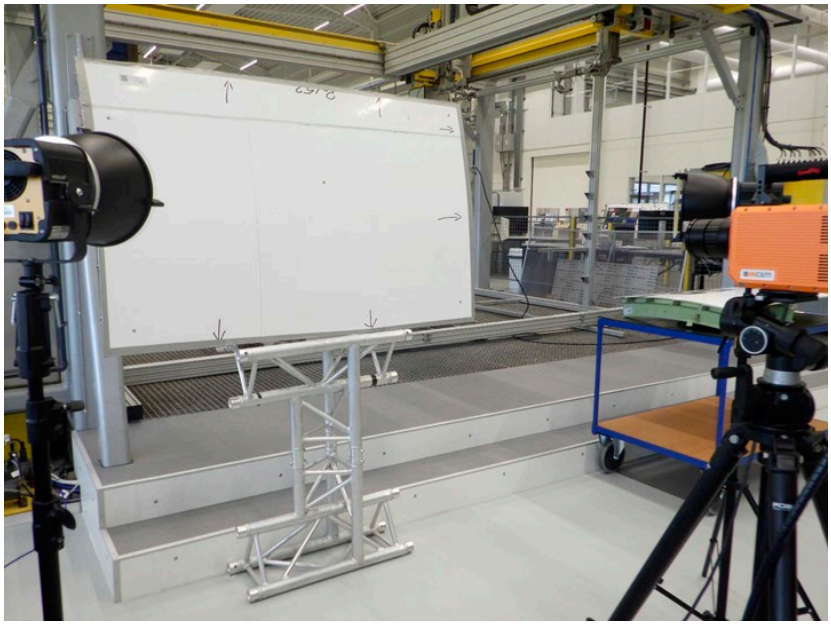

Figure 31: IRT inspection setup

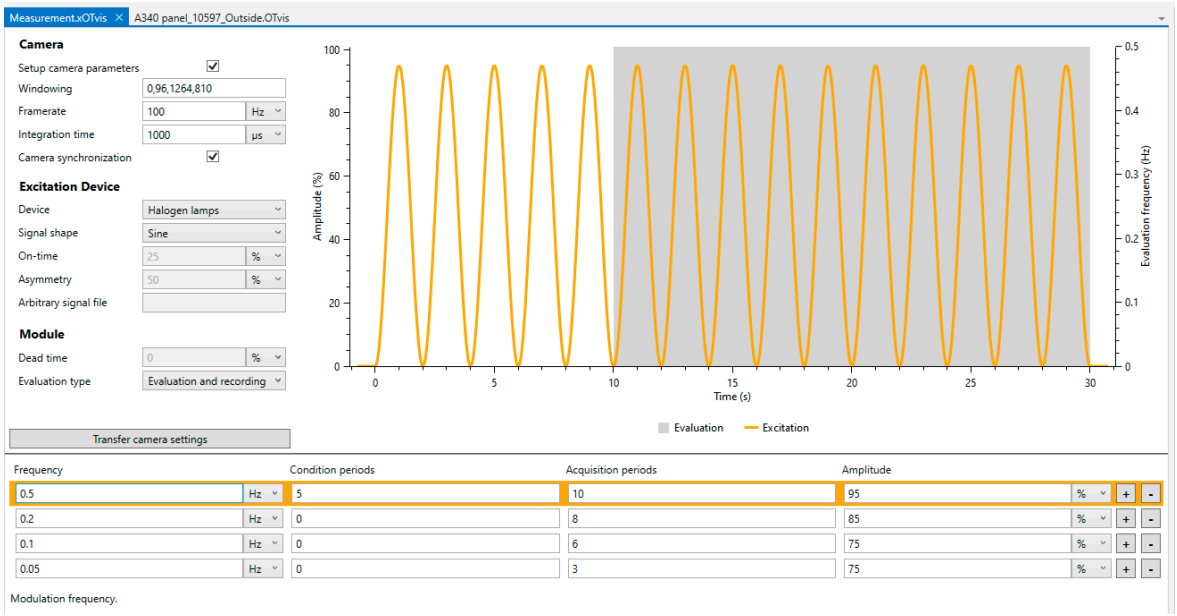

Figure 32: Initial inspection settings

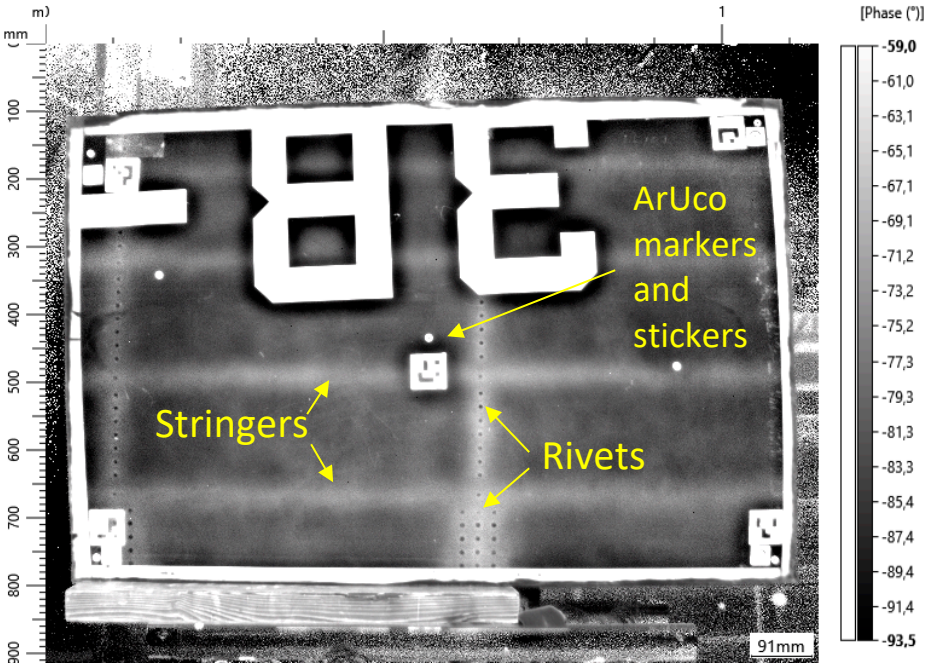

Figure 33: Visibility of components after Optical Lock-In IRT at 0.1Hz on panel 10587

In Figure 33 the test result at 0.1Hz is shown. With this frequency the stringers can be easily detected from the darker background. The individual rivets are also good detectable. The rivets and rivet line under the black adhesive stickers are not visible.

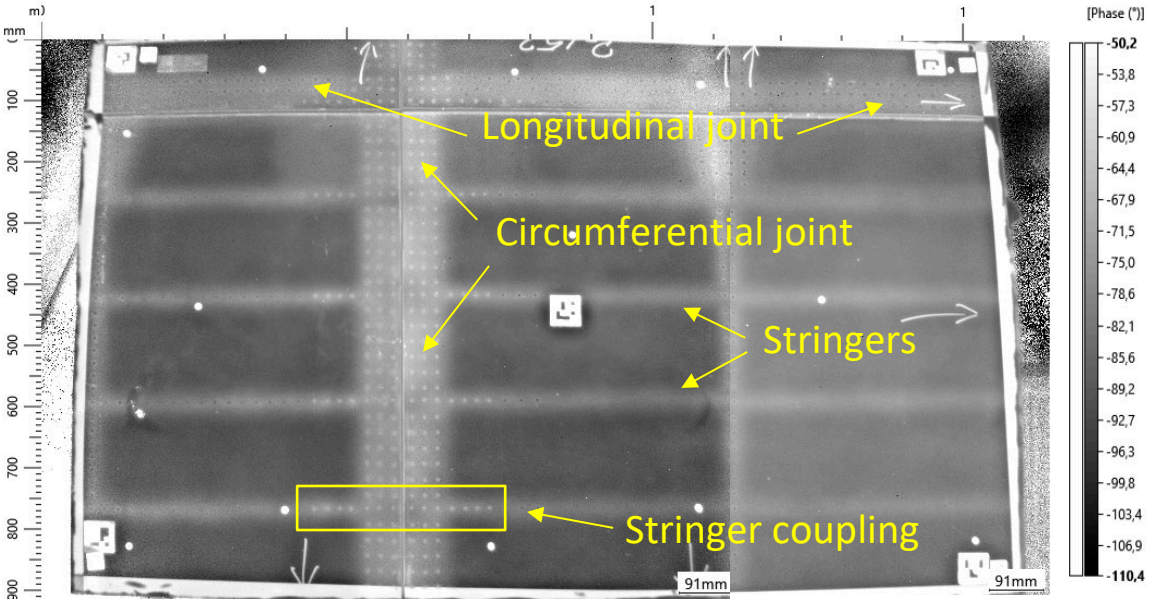

Figure 34: Visibility of components after Optical Lock-In IRT at 0.1Hz on panel 10597

In Figure 34 the test results at 0.1Hz are shown. With this frequency the stringers can be easily detected from the darker background. The circumferential butt-joint is clearly visible as well as the longitudinal lap-joint. The individual rivets are good detectable and the contours of the pockets in the skin are visible.

4.5 Experimental tests conclusion

Table 4-1 shows the pros and cons from each NDT method. The ECA technique is good in detection of rivets and stringers but the inspection is for large surfaces slow and the alignment of the probe with respect to the joints and rivet lines is difficult. The PAUT inspection is for this application the least practical and sensitive. Due to the need for couplant, although it is not much it still need some light spray of water. Another is the relative thin skin of aluminium which results in multiple echoes, which makes it much harder to detect the right signal and therefore the right component. IRT is the most useful technique of these, the main benefit is the large field of view and that it is non-contact. No issues with couplant or rough surfaces.

Based on the experiments performed on the fuselage reference panels, thermography is found to be a fast, global and non-contact technique that requires no coupling or complex scanning equipment. Panels with a surface area up to 1 m² can be inspected with a single exposure technique and still gives a good performance in detecting rivets, back-up structures and even differences in skin thicknesses. This method was selected to be the most suitable NDT method for detecting rivets in a fuselage panel.

Table 4-1 Pros and cons of the evaluated NDT methods

Inspection	ECA	PAUT	IRT
Detection rivets	++	+	++
Detection stringers	++	+	++
Detection joints	+	+	+
Detection skin pockets	o	o	+
Field of view	128 mm	44 mm	~ 1m²
Portability	+	+	o
Contactless	no	no	yes
Couplant required	no	yes	no
Inspection speed	o	o	++

A 3D scan has been performed on the selected panels 10587 and 10597. The 3D scan can capture the entire outside geometry of the component. It is not possible to detect rivets that are hidden beneath a thick layer of paint, so this technique is not suited for rivet detection. However, the technique will be used to get more details of the component under investigation and to provide 3D coordinates for the cutting robot which will be described in Chapter 6.

5 Optimization of IRT

From the initial test results, thermography (IRT) is considered to be the best choice for the fast detection of rivets and rivet lines. The initial thermography experiments were done in order to estimate the feasibility of thermography to detect rivets. Settings used for this initial study were not optimized with respect to the best rivet detectability and speed of inspection. This chapter will contain are more detailed approach in order to obtain the best settings. Three topics were investigated:

- Lock-in frequency for best contrast.
- Needed spatial resolution to detect a rivet.
- Effect of the amount of heating on the detectability of the rivets.

The optimized contrast is considered for:

- Stringer and skin
- Rivet and skin
- Rivet and rivet area
- HI-LOK fastener and fastener area
- Pocket area in skin

5.1 Lock-in frequency for best contrast

A multitude of frequencies were investigated. Started at a relative high frequency (4Hz) and stepped down in 8 steps to the lowest frequency used (0.05Hz).Table 5-1 shows an overview of the thermography settings which were used to inspected the panels with IRT.

Table 5-1: Settings IRT inspection

Frequency [Hz]	Conditioning periods	Acquisition periods	Amplitude [%]
4	20	40	95
2	10	30	95
1	0	30	95
0.8	0	20	95
0.5	0	20	95
0.3	0	6	95
0.1	0	3	95
0.05	0	2	95

The following terminology is used in Table 5-1**:**

Excitation frequency: The frequency at which the excitation source is modulated.

Conditioning periods: Defines the number of full signal periods during which the excitation signal is output while no data acquisition takes place yet. This time period is used for conditioning and for producing a steady state of the thermal wave.

Acquisition periods: During this stage, the image signal is acquired and analysed (in full periods).

Amplitude: Amplitude level of the excitation source as a percentage of maximum power.

In the following pictures (see Figure 35 and Figure 36) the relation of the applied frequency vs the detection of the different components can be seen. For all different frequencies applied on these two panels see page 39 Appendix A.

In Figure 35 can be seen that the higher frequencies have more noise in the images and the lower frequencies have the tendency to become more fuzzier. For panel 10587 at 4 Hz some of the stringers can be seen as well as some rivets, but not all. At a lower frequency of 2 Hz the rivets become more clear, but the stringers are not detected anymore. At 0.5 Hz, the rivets due not have a clear contrast, while at 0.1 Hz the contrast between the sound material and the rivets is the higher. The rivets that are located under the black paint are not visible anymore with these frequencies.

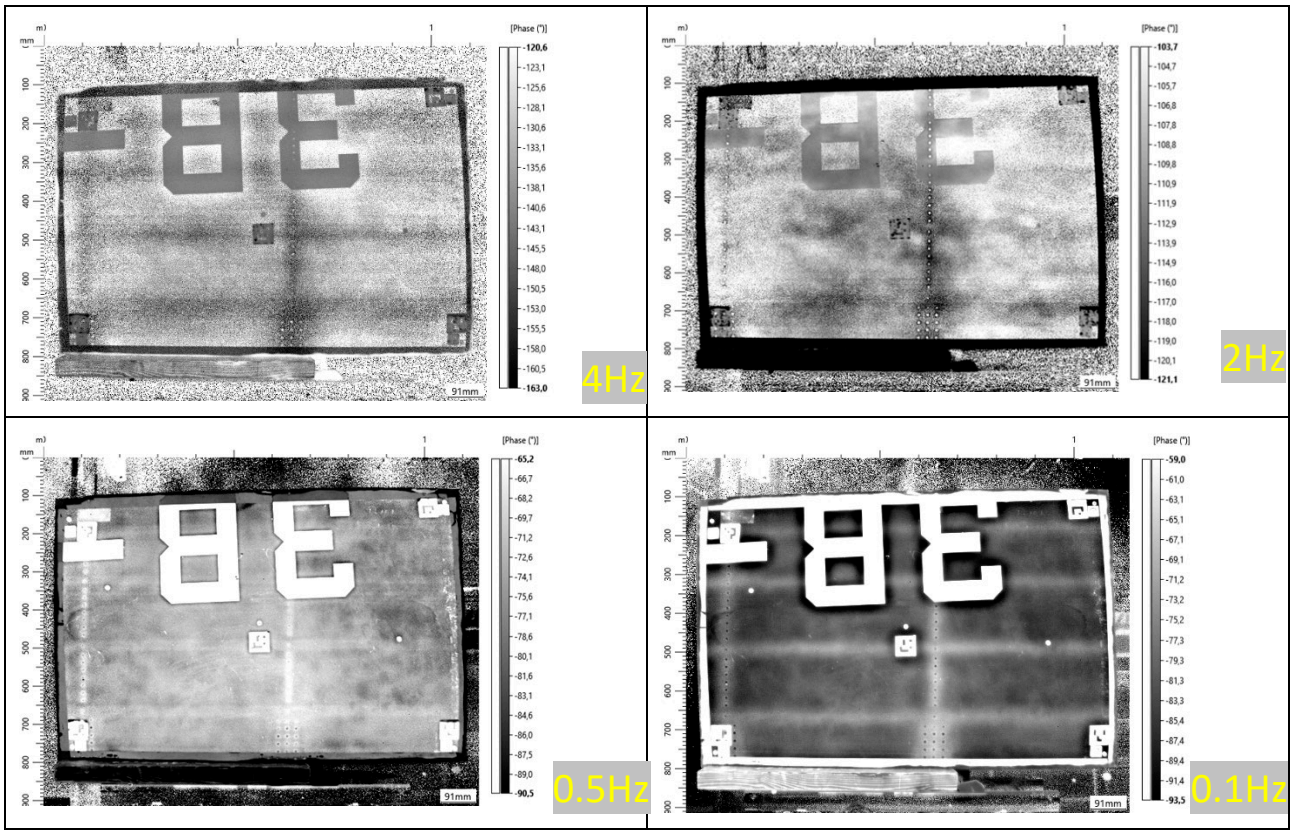

Figure 35: Overview of panel 10587 inspected with IRT at different frequencies

In Figure 36 can be seen that the again the higher frequencies have more noise in the images and the lower frequencies are more fuzzier. For panel 10597 at 4 Hz the contour of the stringers and the larger circumferential joint show up darker against the light grey skin. At the frequency of 2 Hz a little bit more detail appear and some individual rivets can be seen. At 0.5 Hz most of the backup structure can be seen: rivets, joints, stringers and the pockets in the skin. At 0.1 Hz the detail of the shallower rivets disappears a bit and are less clearly visible. The longer rivets in the circumferential and longitudinal joints are still visible.

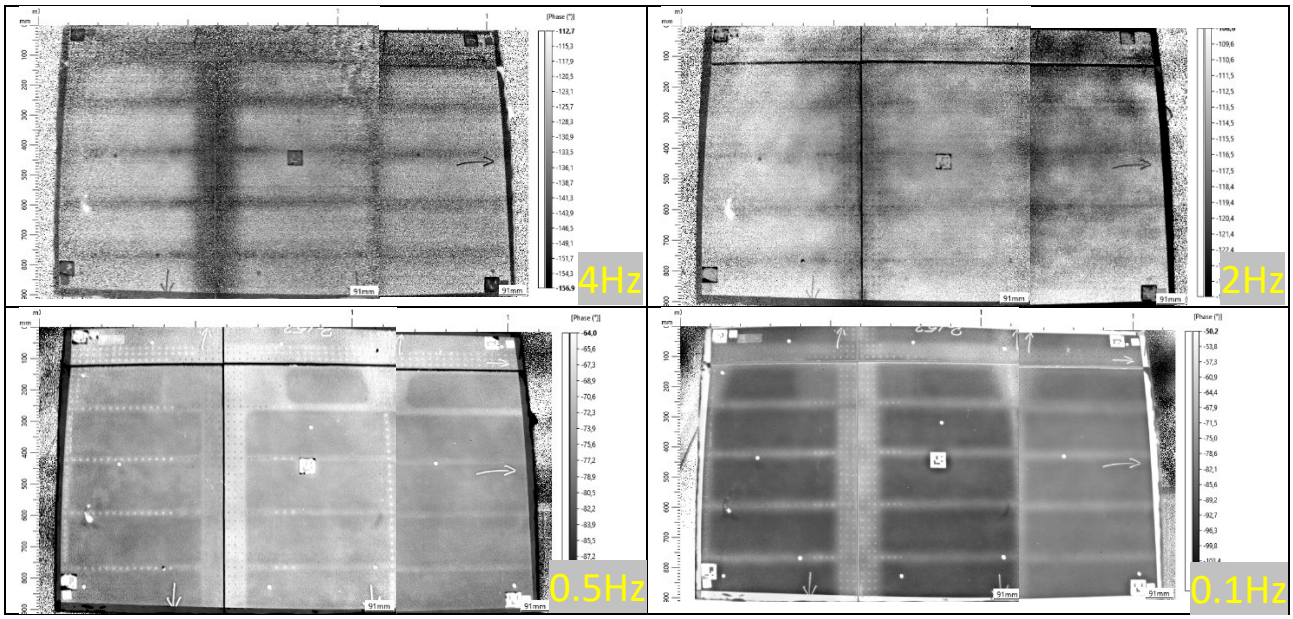

Figure 36: Overview of panel 10597 inspected with IRT at different frequencies

To summarise the detection of all different components the following Table 5-2 and Table 5-3 shows an overview per panel which components are good, partly or not detectable. This is presented with 3 colours.
Colour representation:

	Good detection of component
	Partly or poor detection of component
	No detection of component

Table 5-2: Detectability of different components of panel 10587

	10587							
Frequency [Hz]	**4**	**2**	**1**	**0.8**	**0.5**	**0.3**	**0.1**	**0.05**
Detection of:								
Rivets								
Rivet line								
Stringers								
Rivets under black sticker								
Image quality								

On the 2 Hz image the rivets and rivet line is clearly visible on the white paint as well on the black surface (adhesive sticker). The stringers and rivet lines for this configuration are best visible at 0.1Hz. In order to detect the rivets as fast as possible, which would be the case during an industrial environment the best frequency would be 2 Hz is this case. For this FOV of approximately 1 square metre the inspection time is for 2 Hz 20 seconds and for the 0.05 Hz 40 seconds. (with the used a conditioning and acquisition cycles) So an inspection at lower frequency would require twice the amount of time needed for an inspection at high frequency. Any inspection time optimization is possible but is not further investigated in this report.

Table 5-3: Detectability of different components of panel 10597

	10597							
Frequency [Hz]	**4**	**2**	**1**	**0.8**	**0.5**	**0.3**	**0.1**	**0.05**
Detection of:								
Rivets								
Fasteners								
Rivet line								
Stringers								
Circ. joints								
Long. joints								
Skin pockets								
Image quality								

In the 4Hz image the contours of the circumferential joint is visible, but it is a noisy image and no further details can be observed. The lower the frequency the more details become visible and the cleaner the image is. From the table above the highest frequency which can detect all components is 0.5Hz. On 0.5Hz most of the back-up structure is visible as well as the detection of the single rivets in the circumferential joint. The inspection time for this frequency is 10 seconds. Note that the results in this investigation are part of the complete sequence so included the heat applied by the previous frequencies. Only applying the 0.5Hz will have different results. The best frequency for inspection with respect to both speed and detectability strongly depends on the component thickness and material used and should be optimized per aircraft type.

5.2 Needed spatial resolution

In order to be able to identify individual rivets the spatial resolution of the thermographic inspections should be sufficient. Spatial resolution will be specified in the number of mm per pixel. If the resolution is taken to small, no individual rivets can be detected. Subsequently, if the resolution is taken too large a lot of scans would be needed to cover an entire fuselage. Figure 37 shows thermographic inspections of the same area on panel 10587, but at different resolutions. In order to change the resolution the camera was moved closer or farther from the panel surface. Starting at a high resolution of 0.8 mm/px all individual rivets can be clearly seen. Decreasing the resolution to 1.0 or 2.1 mm/px still allows for the detection of individual rivets. At a lower resolution of 3.6 mm/px not all individual pixels can be detected anymore.

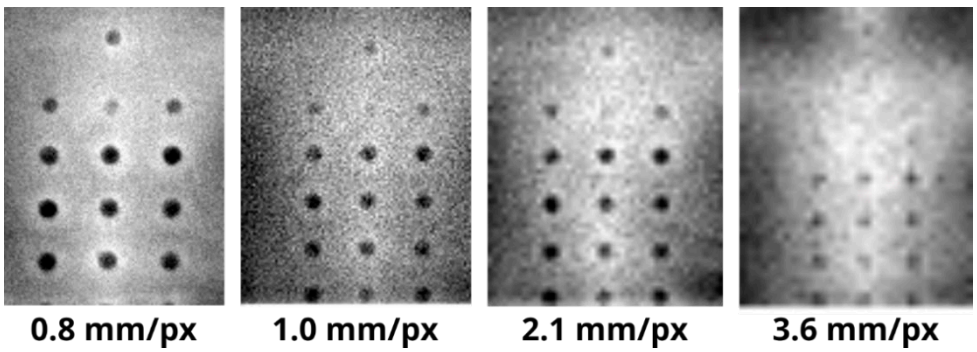

Figure 37: Thermographic images at different resolution on panel 10587. Each image has been enlarged such shat it covers the same area. FOV of the area amounts to 80x108 mm

The needed resolution depends on the size of the rivets that need to be detected. In this case the rivets are 6.2 and 7.7 mm. As a rule of thumb at least 3 pixels are needed to be able to identify a feature in an image. In this case, using this rule rivets with 10.8 mm can be detected at the lowest resolution. The rivets are smaller, which leads to the bad detectability as shown in Figure 37 (3.6 mm/px). All panels have been measured at 1.8 mm/px, which allows for scanning of the smaller panels in a single FOV. This resolution is slightly better than the 2.1 mm/px enabling the detection of all rivets. For the larger panels two FOV's are needed to scan the entire panel. The FOV amounts to 1152 mm by 931 mm.

5.3 Effect of the amount of heating

The contrast that is obtained in the phase images is mainly determined by frequency. However, the amount of noise that is present in these images is determined by the amount of heating power that can be supplied to the surface. The thermographic inspections are done on metals, which have a high heat conductivity, resulting in a lot of needed power to heat up the component. During the experiments, it became clear that the position of the lamps w.r.t. the panels are essential in order to detect rivets on the surface. The total output power of the lamps was fixed at 4kW, but the distance the lamps have with respect to surface determines the area over which this power will be divided. If lamps are close to the surface the power per unit area is higher as compared to the situation where the lamps are farther away from the surface. As an example, Figure 38 shows the thermographic images at three different frequencies, but at two different lamps positions. In the left column the lamps were put closer to the surface resulting in a higher power per unit area. For the column on the right the lamps were places farther away from the surface, resulting in a lower power per unit area. The most prominent differences can be seen at a high frequency of 2.00 Hz. In the case of higher power, the rivets can be detected better than in the case of low power, due to amount of noise that is present. At a lower frequency of 0.500 Hz this effect decreases and at 0.100 Hz there is now real difference between the two images. At low frequencies, due to the lower on-time of the lamps enough temperature difference can be achieved while this is not the case at low power and high frequency modulation.

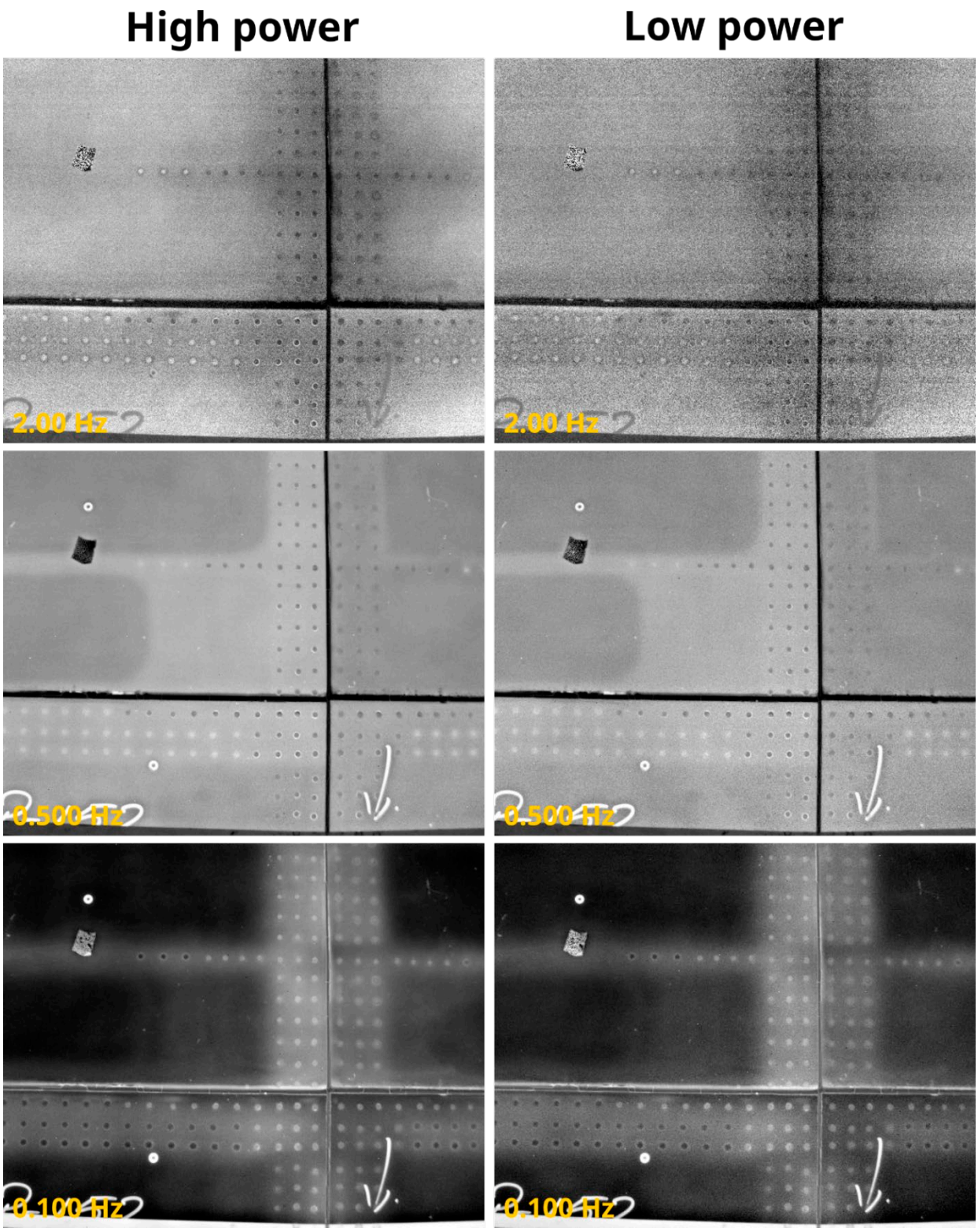

Figure 38: Thermographic inspection on panel 10597, showing the influence of lamp power

In the case of the experiments that have been performed the total amount of power available was the bottleneck for increasing the FOV more, and not the spatial resolution. This is especially true for the high frequencies used during investigation.

6 Coordinate system

The results from the inspections can be mapped on top of the surface mesh that has been obtained with 3D scanning. This allows for the extraction of the rivets position in the X,Y,Z format. This chapter describes the method that has been used to add the images to the 3D surface and to extract the coordinates from this procedure. First, the location of the rivets need to be extracted from the 2D thermographic phase image. The resulting outcome of this extraction will be X, and Y coordinates of the centre of a rivet in pixel units. This automatic subtraction of the rivets is currently be done by the DLR, so here will we only focus on transforming the 2D information to 3D.

6.1 Mapping of thermographic data

From the 3D scan information is obtained in the form of a point cloud with X,Y,Z values. From the thermography inspection only 2D information is available. For cutting procedures it is mandatory to also know the z information of the structure under investigation. The images of the thermographic inspection can be mapped on top of the 3D data by making use of the reference markers that are used for 3D Scanning. Figure 39 shows the markers that have been used as common reference points (marked by the red circle). Inside of the GOM software the common markers need to be selected both on the 3D surface mesh and within the IRT image. Once this is done, the image can be mapped on top of the point cloud, resulting in RGB values at the X,Y,Z values of the point cloud. An user can now manually select the rivets and extract the X,Y,Z coordinates of the rivet location. Unfortunately, the mapping progress is done inside of the GOM software which uses propitiatory software for the transformation of the image to the surface mesh. This does not allow to gain access to the transformation matrix, making it difficult to transform the location of the rivets inside of the thermographic image to 3D point coordinates.

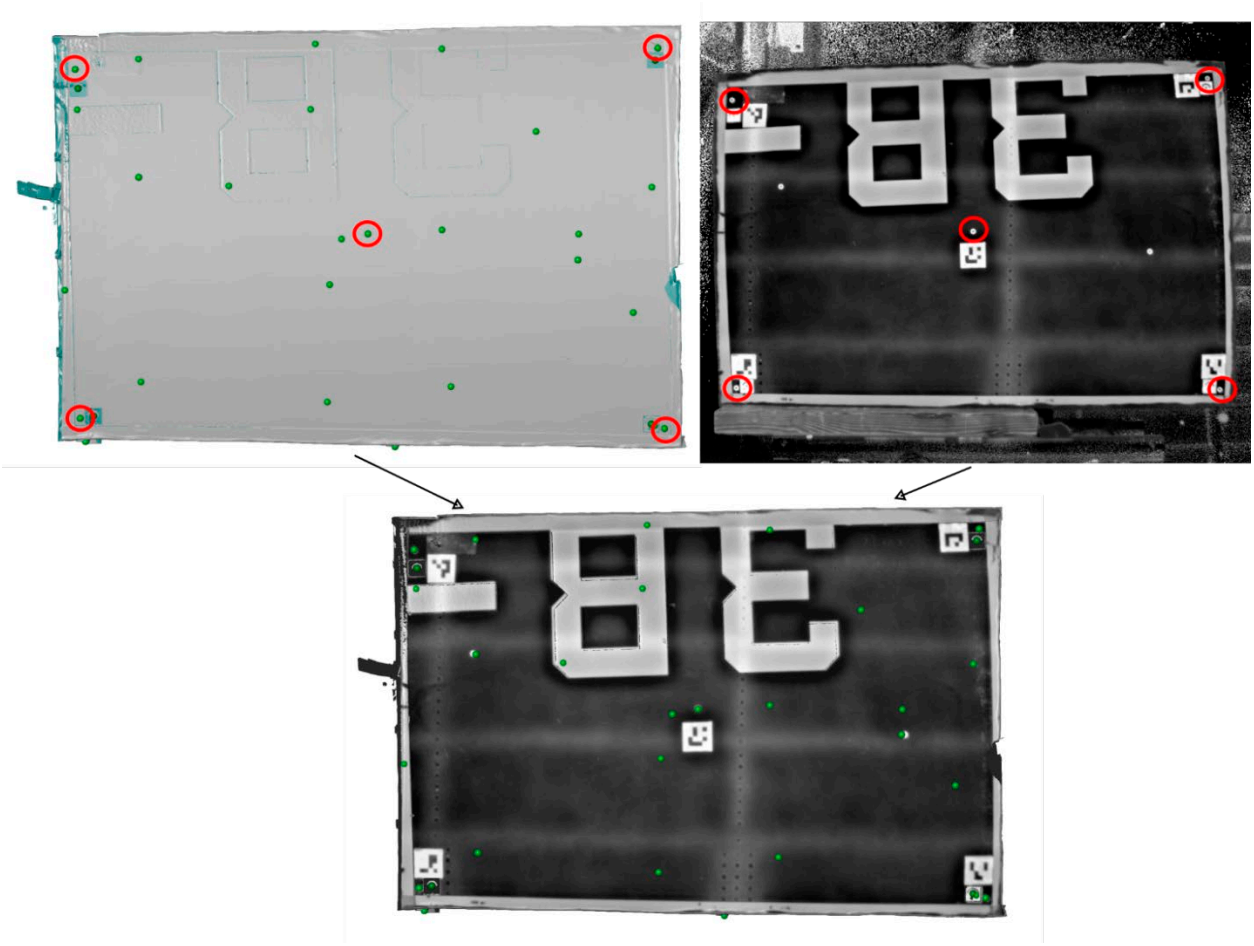

Figure 39: Mapping procedure using common ref points in the 3D scan and IRT picture

A possible work around can be found by using ArUco markers that the DLR uses for their vision system.

6.2 ArUco markers

DLR uses ArUco markers for their vision system that is integrated at their robots. ArUco markers are square markers containing a pattern in which codec information can be stored, see Figure 40. ArUco stands for Augmented Reality University of Cordoba, that is where it was developed in Spain. These markers can be detected in 3D space and have been added to panels 10587 and 10597. These markers are also present within the IRT phase images and can also be extracted from these images. Figure 41 shows a coloured mesh that has been produced by mapping an optical photograph of the component. From this coloured mesh the location of the markers in 3D coordinates can be extracted, as shown in the image for the top left corner and the centre of the marker.

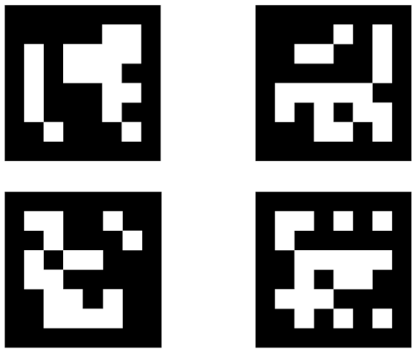

Figure 40: Example of 4 ArUco markers [11]

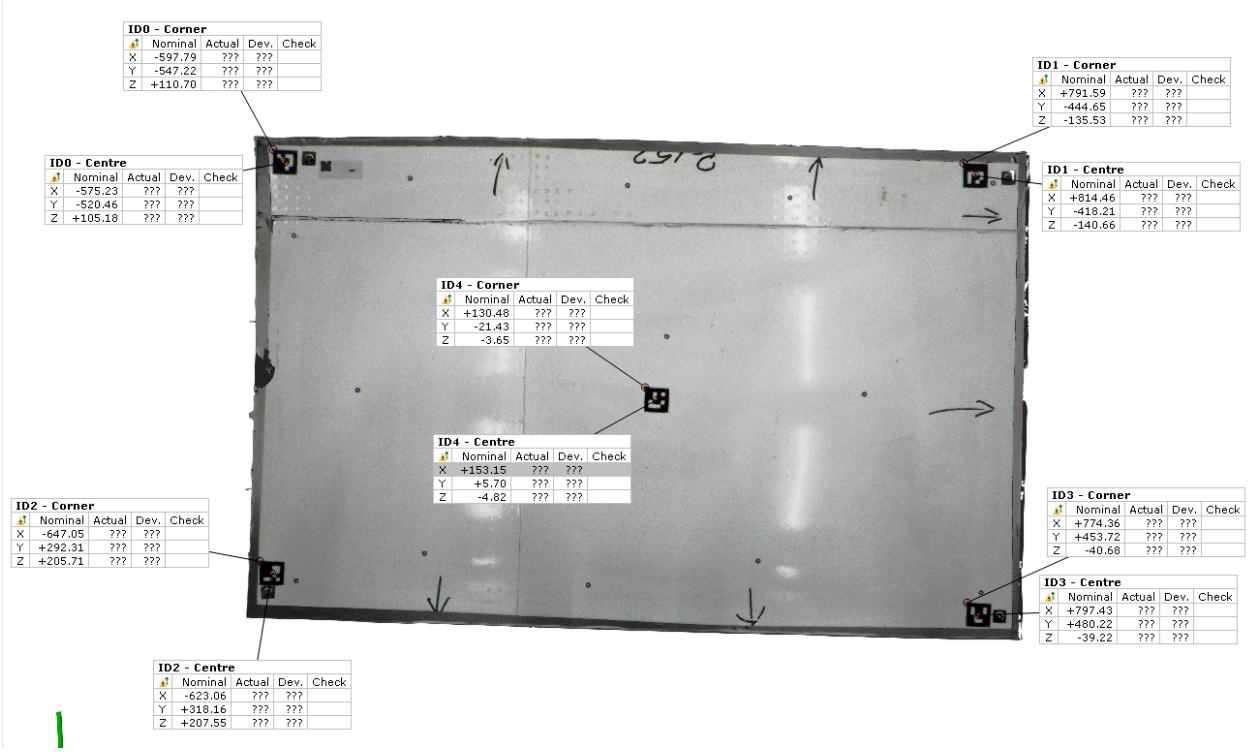

Figure 41: Mapped photograph of the ArUco markers, displaying the coordinates of the top left corner and the centre of the marker, respectively

Using a similar approach DLR should also be able to extracted the coordinates using their approach.

7 Conclusions

In this report we investigated the methods to detect the rivets and back-up structures in an aircraft fuselage. The NDT methods were Eddy Current Array, Ultrasonic Phased Array and Optical Lock- In Thermography.

1. The PAUT inspection is for this application the least practical and sensitive. A first reason for this is the need for a couplant. Although it is not much it still need some light spray of water. Another reason is the relative thin skin of aluminium, which results in multiple echoes, which makes it much harder to detect the right signal and therefore the right component.
2. ECA has a good detectability with respect to all geometrical features. But in practical performance, contact type method and small FOV makes the ECA method less practical for this application.
3. OLT has a good detectability with respect to all geometrical features. The main advantages of OLT over ECA is the speed of inspection, the larger field of view and it is a non-contact technique.

Optical Lock-In Thermography is based on the application of a periodic input (frequency) of heat energy to the surface of the object. This frequency determines in great manor the detectability of the rivets and other components of the back-up structure as can be seen from the results in chapter 5. Therefore an optimization effort was performed to be able to specify the frequencies resulting in the best detectability of the rivets. The configuration differences between the panels has influence on the detectability of the rivet lines at a certain frequency. For example the results on the smaller A340 panel are different from the larger A330 panel at the same frequency. It is therefore necessary to adjust the inspection frequency per aircraft type.

The minimal resolution required to be able to detect a rivet has also been investigated. In order to cover large area's with thermography, the FOV must be taken as large as possible. However, at some point the decrease in resolution will make it impossible to detect rivets anymore. In this case the sweet spot for resolutions is between 1.0 and 2.1 mm/px, but this depends on the rivet size. Generally speaking 3 pixels are needed to be able to detect a single rivet, and therefore the resolution depends on the size of the rivet. Additionally, the amount of heating power has also been investigated. In case of insufficient heating power the detectability of the rivets decreases. So in a final design this should be taken into account.

Thermographic images can be mapped on top of a 3D model, which is acquired by 3D structural light scanning. This enables the extraction of a rivet coordinate in X, Y, Z position instead of X,Y position within the image. This is still a manual step within the software that is used by the NLR. In order to get automatic extraction of rivet locations DLR will first perform automatic rivet detection on the thermographic images, which can later on be transformed into 3D space by making use of the ArUco markers.

This project has received funding from the European Union's Horizon 2020 research and innovation programme under grant agreement No 101006952.

8 References

[1] SUSTAINair, “D2.2 Rivet removal demonstrator using robotics and water jet cutting,” [Online]. Available: https://www.sustainair.eu/media-resources/deliverables/.

[2] Olympus Industrial Solutions, “Eddy current array tutorial,” Olympus, [Online]. Available: https://www.olympus-ims.com/en/ndt-tutorials/eca-tutorial/.

[3] Zoran Bergant, Joseph Janez and Janez Grum, “ULTRASONIC C-SCAN TESTING OF EPOXY/GLASS FIBER COMPOSITE,” in *The 14th International Conference of the Slovenian Society for Non-Destructive Testing*, Bernardin, Slovenia, 2017.

[4] S. Mahaut, “http://www.researchgate.net/,” EXTENDE, [Online]. Available: https://www.researchgate.net/figure/Different-designs-and-operation-modes-of-phased-array-probes. [Accessed 02 08 2023].

[5] Noël Dubé, Advances in Phased Array, Waltham, MA 02453, USA: Olympus, 2017.

[6] M.-P. Despaux, “https://sonatest.com/blog2/archive/2020/07/test,” Sonatest , 07 2020. [Online].

[7] M. Hayk, “https://www.ametek-land.com/,” 29 06 2021. [Online]. Available: https://www.ametek-land.com/pressreleases/blog/2021/june/thermalinfraredrangeblog.

[8] C. Funke, “GOM 3D Metrology Systems,” in *SCR-Forum*, Weissenburg, 2016.

[9] Skorupa, Andrzej & Skorupa, Małgorzata, “Riveted Lap Joints in a Pressurized Aircraft Fuselage,” 2012.

[10] Mechanical Jungle, “Mechanical Jungle,” [Online]. Available: https://mechanicaljungle.com/rivets-and-types-of-riveted-joints/. [Accessed 27 07 2023].

[11] “www.element14.com,” 20 06 2021. [Online]. Available: https://community.element14.com/challenges-projects/project14/photography/b/blog/posts/window-opening-monitor-with-aruco---installing-opencv-on-the-raspberry-pi-4b.

Appendix A Optimization of IRT frequencies

Panel 10587:

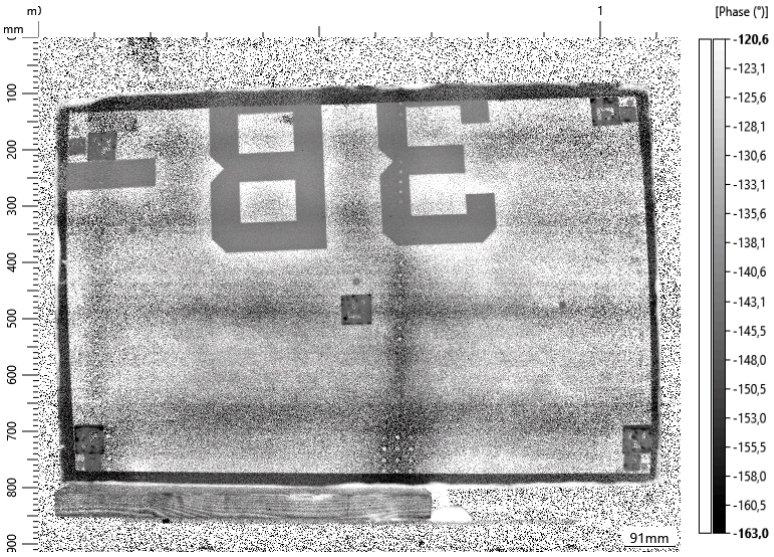

Figure 42: Panel 10587@ 4Hz

4Hz

- The overall image is quite noisy due to the lack of heat (result of the high frequency)
- Contour of stringers are visible
- Rivets partly visible at the rivet line under the black adhesive sticker.
- Rivets partly visible at the rivet line under the white paint and at the bottom of the panel (3 rivet row area)

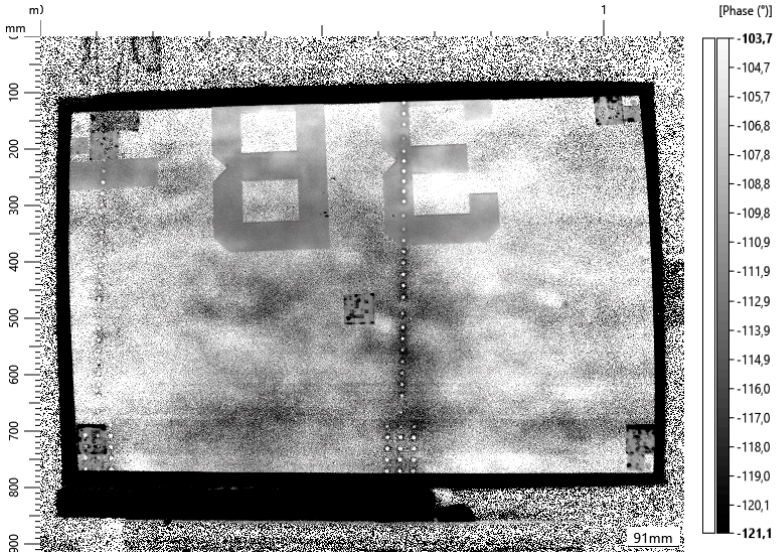

Figure 43: Panel 10587 @ 2Hz

2Hz

- Overall image less noisy than the 4Hz image but still significantly
- The whole rivet line is clearly visible
- Stringers are not visible

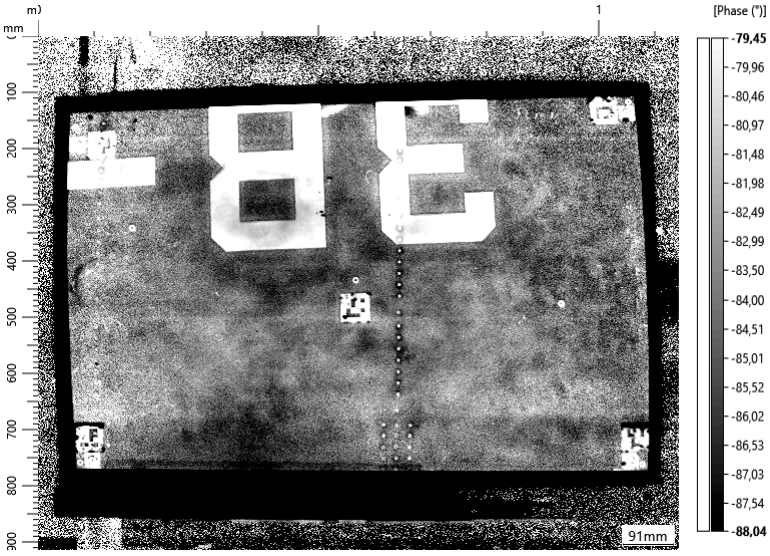

Figure 44: Panel 10587 @ 1Hz

1Hz

- Overall image: some darker areas on the surface
- Rivet line is under the white painted surface is clearly visible
- Rivet line under black sticker <u>not</u> or very limited visible
- Stringers are not visible

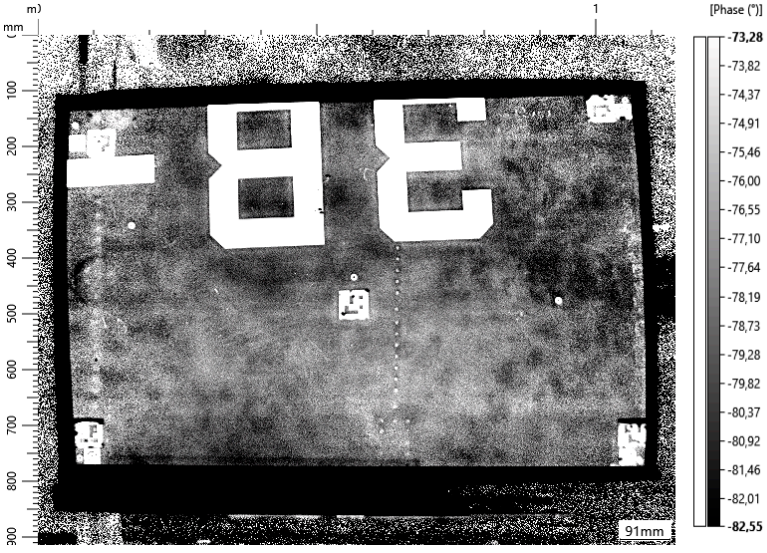

Figure 45: Panel 10587 @ 0.8Hz

0.8Hz

- Overall image: some darker areas on the surface
- Rivet line is under the white painted surface is visible
- Rivet line under black sticker <u>not</u> visible
- Stringers are not visible

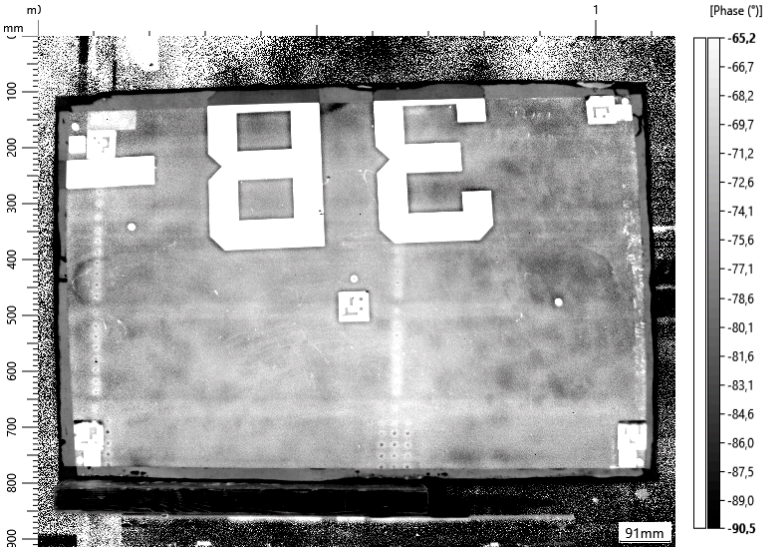

Figure 46: Panel 10587 @ 0.5Hz

0.5Hz

- Overall image is cleaner, less noisy
- Rivet line is under the white painted surface is visible but detectability of the individual rivets is less
- Rivet line under black sticker not visible
- Stringers are vaguely visible

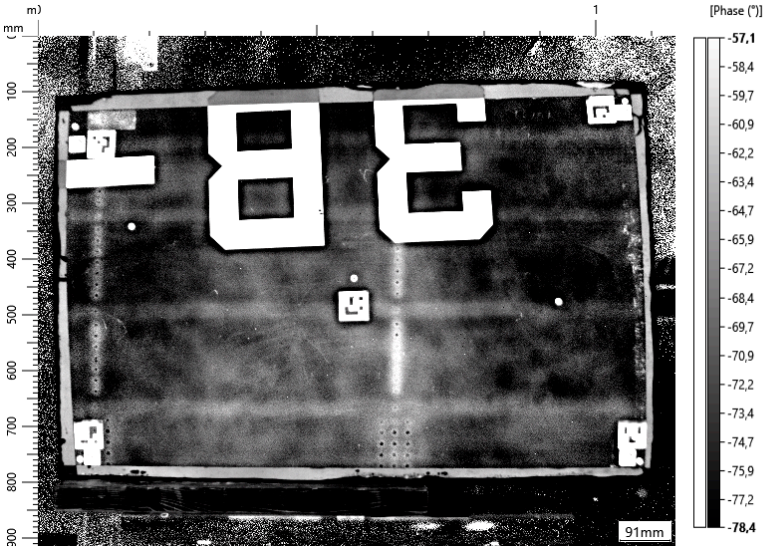

Figure 47: Panel 10587 @ 0.3Hz

0.3Hz

- Overall image is cleaner, less noisy
- Rivet line is under the white painted surface is partly visible
- Rivet line under black sticker not visible
- Stringers are visible

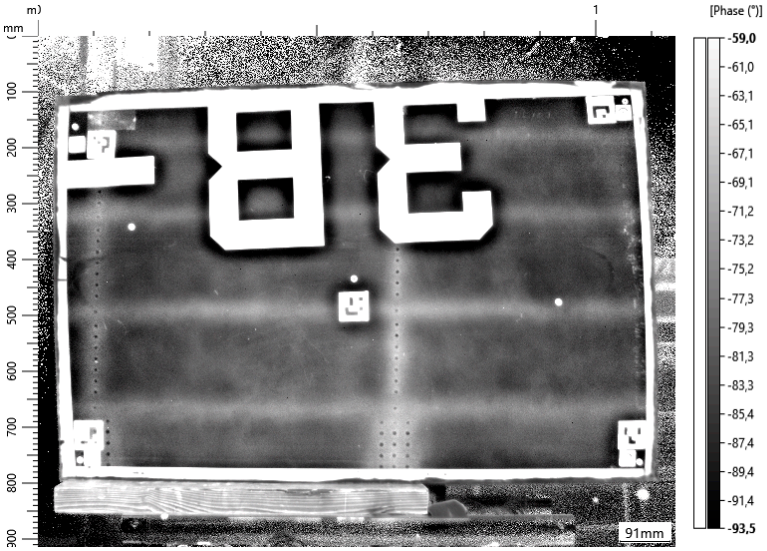

Figure 48: Panel 10587 @ 0.1Hz

0.1Hz

- Overall image is clear
- Rivet line is under the white painted surface is good visible including the separate rivets
- Rivet line under black sticker <u>not</u> visible
- Stringers are visible

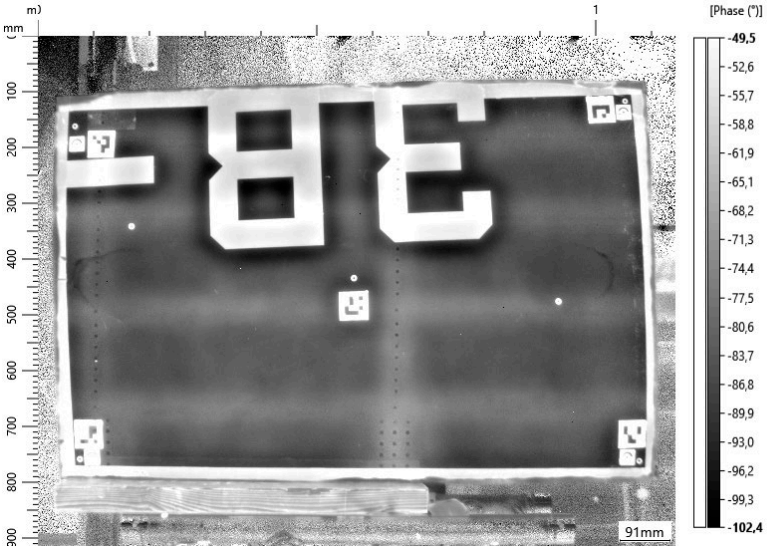

Figure 49: Panel 10587 @ 0.05Hz

0.05Hz

- Overall image is clear
- Rivet line is under the white painted surface is good visible including the separate rivets
- Rivet line under black sticker partly visible
- Stringers are visible but less than at 0.1Hz

Panel 10587:

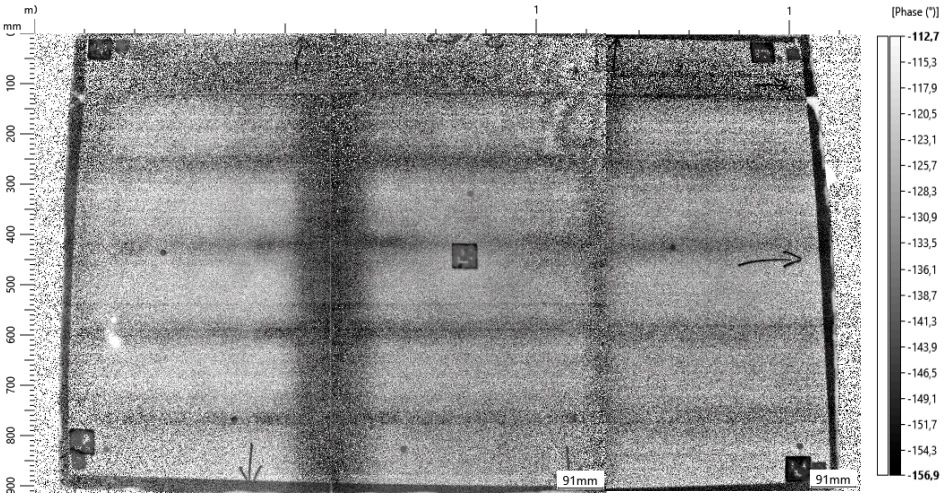

Figure 50: Panel 10597 @ 4Hz

4Hz

- The overall image is noisy due to the lack of heat (result of the high frequency)
- Contour of stringers and circumferential joint are visible
- Rivets not visible
- Longitudinal joint not visible due to the noise

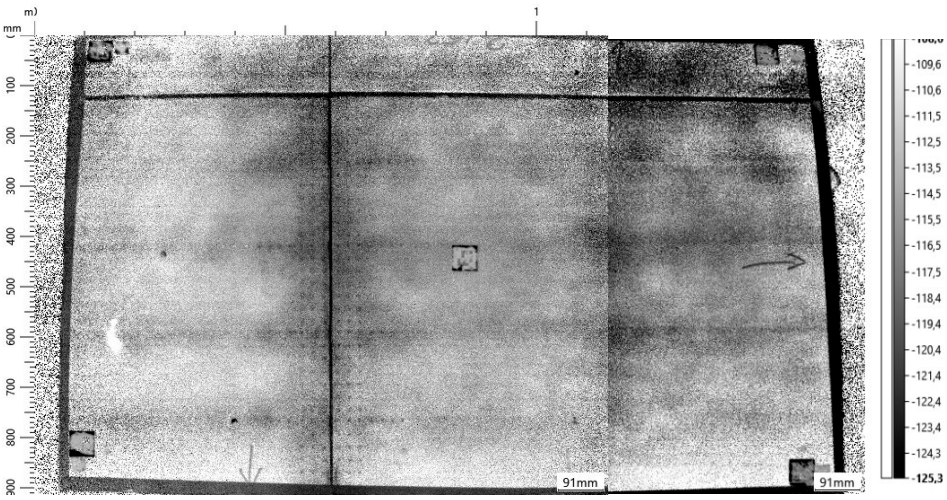

Figure 51: Panel 10597 @ 2Hz

2Hz

- The overall image is noisy due to the lack of heat (result of the high frequency)
- Stringers not reliable visible
- Circumferential joint is visible
- Rivets partly visible in circumferential joint
- Rivets in longitudinal joint not visible

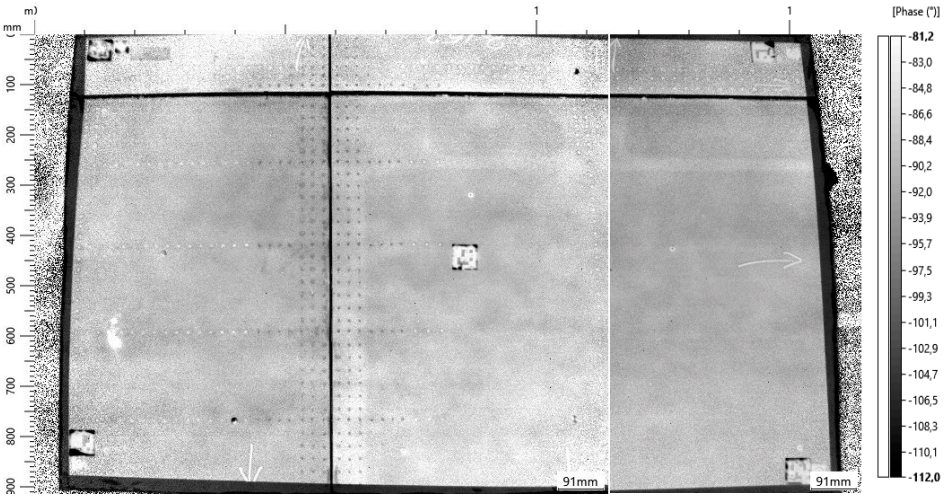

Figure 52:Panel 10597 @ 1Hz

1Hz

- Overall image is clean
- Rivet line not reliable visible
- Rivets in circumferential joint are visible
- Stringers are not visible
- Rivets in longitudinal joint are partly visible

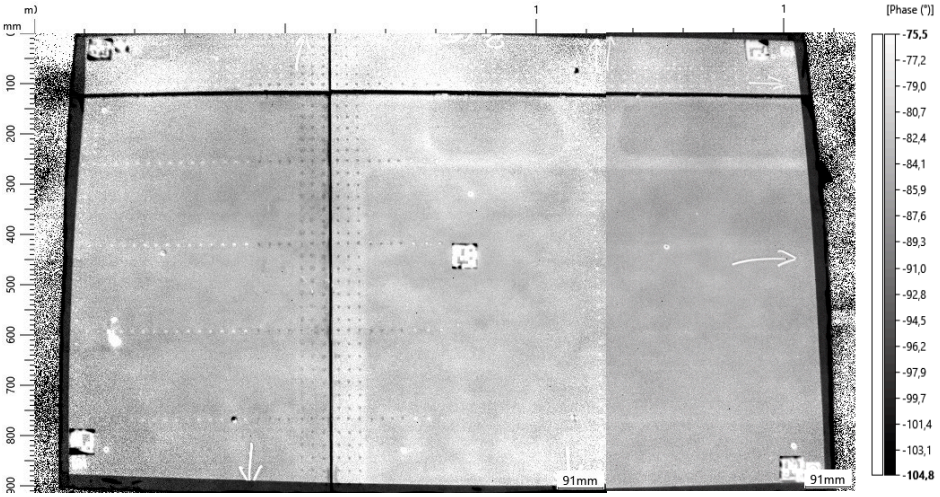

Figure 53: Panel 10597 @ 0.8Hz

0.8Hz

- Overall image is clean
- Rivet line is partly visible
- Rivets in circumferential joint are visible
- Stringers are not visible
- Rivets in stringers are visible
- Longitudinal joint is partly visible

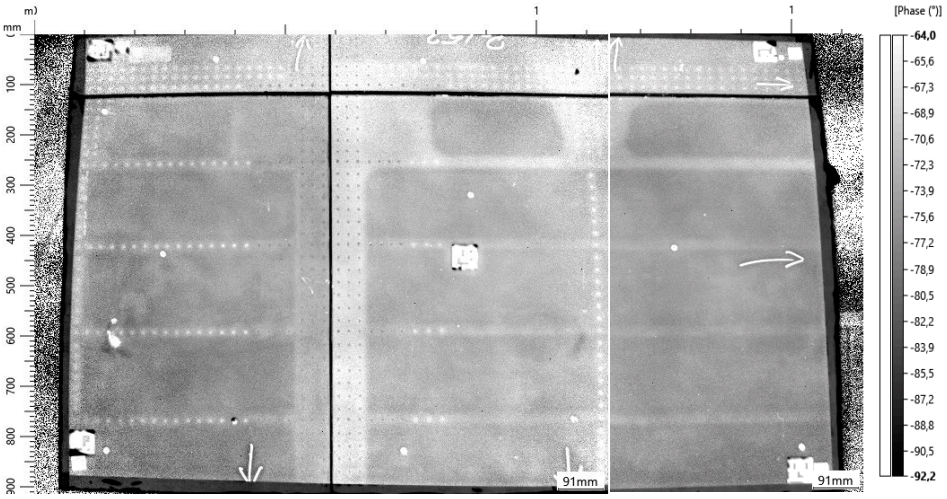

Figure 54: Panel 10597@ 0.5Hz

0.5Hz

- Overall image is clean
- Rivet line is visible
- Rivets in circumferential joint are visible
- Stringers are visible
- Rivets in stringers are visible
- Longitudinal joint is visible

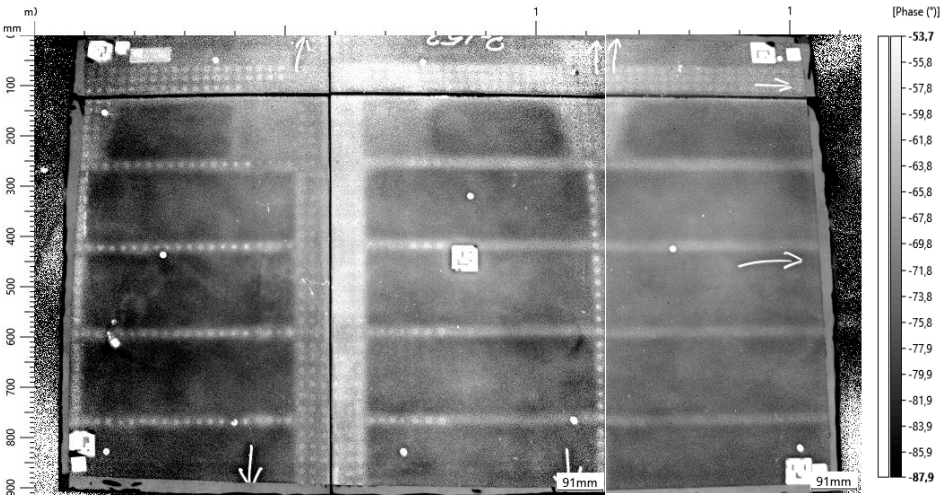

Figure 55: Panel 10597 @ 0.3Hz

0.3Hz

- Overall image is clean but the circumferential joint is starting to get saturated
- Rivet line is good visible
- Rivets in circumferential joint are partly visible
- Stringers are visible
- Rivets in stringers are visible
- Longitudinal joint is visible but also starting to get saturated

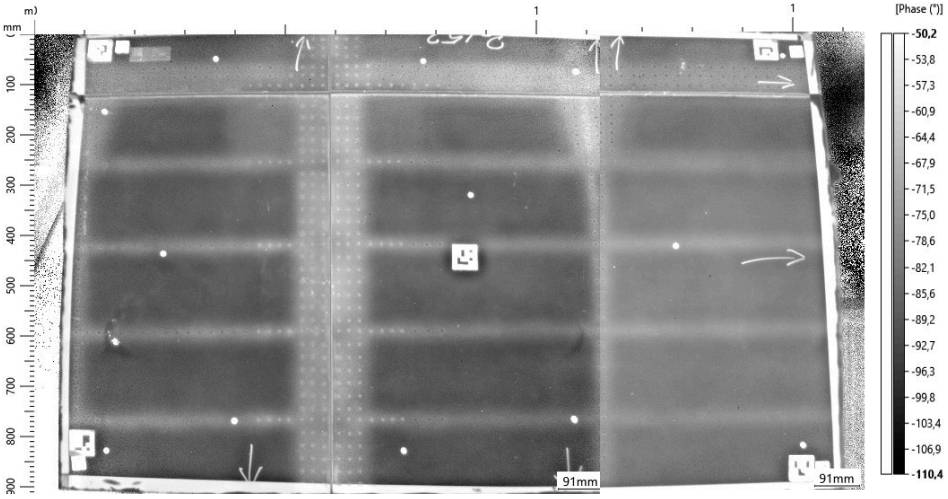

Figure 56: Panel 10597 @ 0.1Hz

0.1Hz

- Overall image is clean
- Rivet line is visible
- Rivets in circumferential joint are visible
- Stringers are visible
- Rivets in stringers are visible
- Rivets in longitudinal joint are partly visible

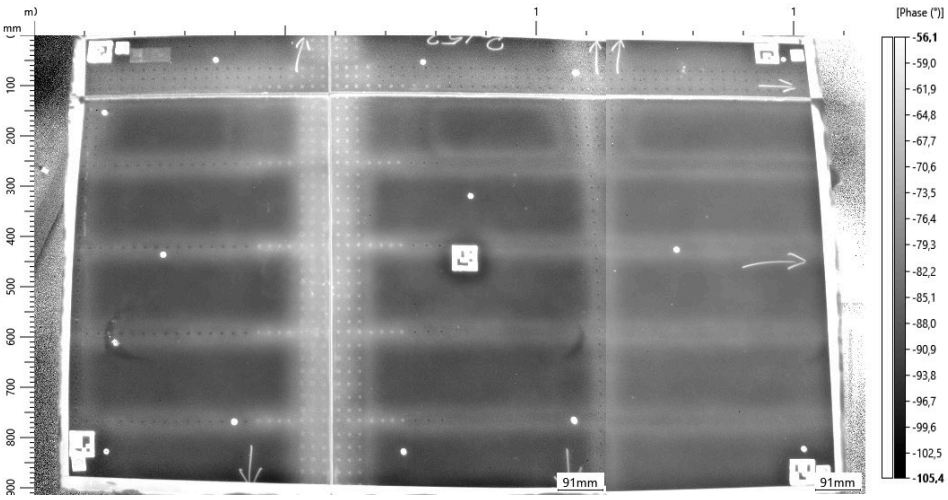

Figure 57: Panel 10597 @ 0.05Hz

0.05Hz

- Overall image is clean
- Rivet line is partly visible
- Rivets in circumferential joint are good visible
- Stringers are visible but starting to become fuzzier and wider.
- Rivets in stringers are visible
- Rivets in longitudinal joint are visible

Appendix B Overview of panels

NLR 10585
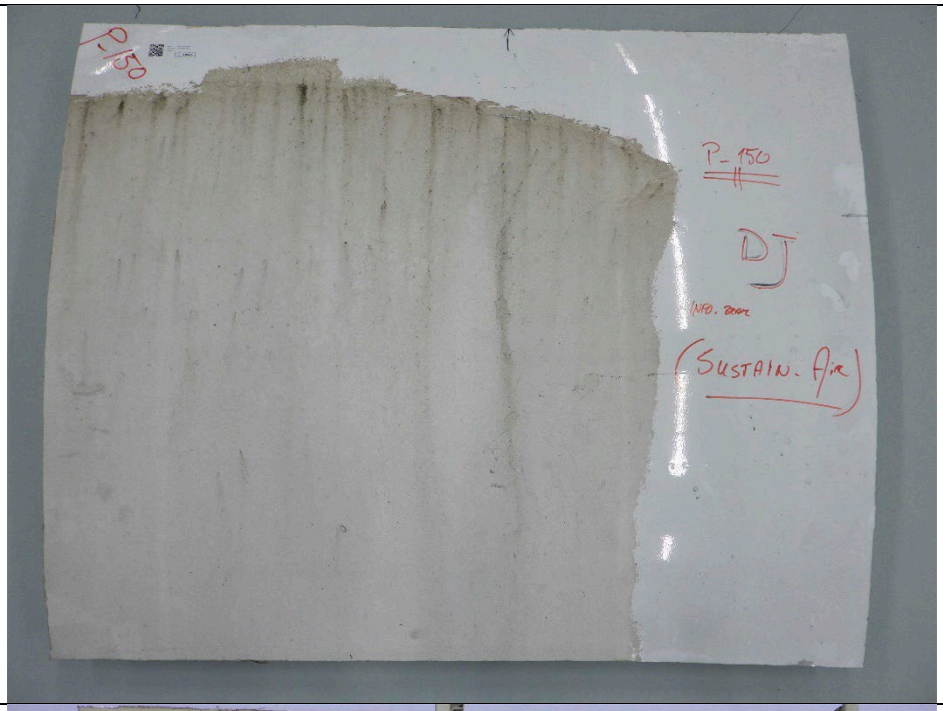


NLR 10586
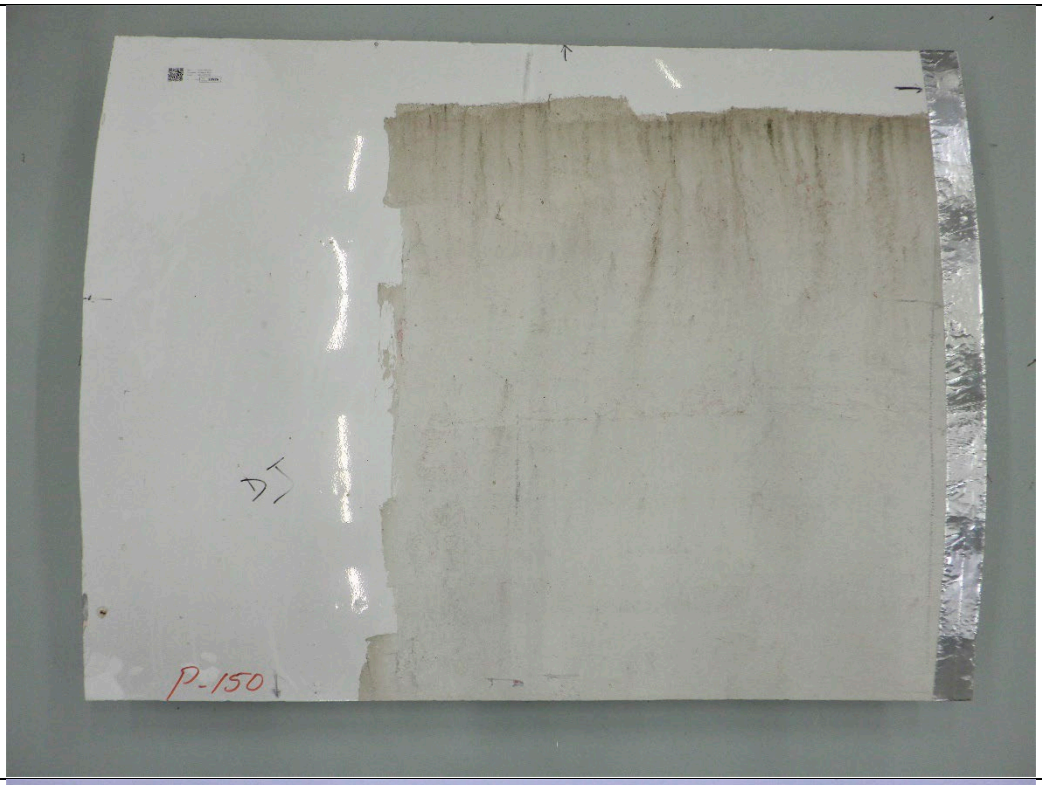


NLR 10587
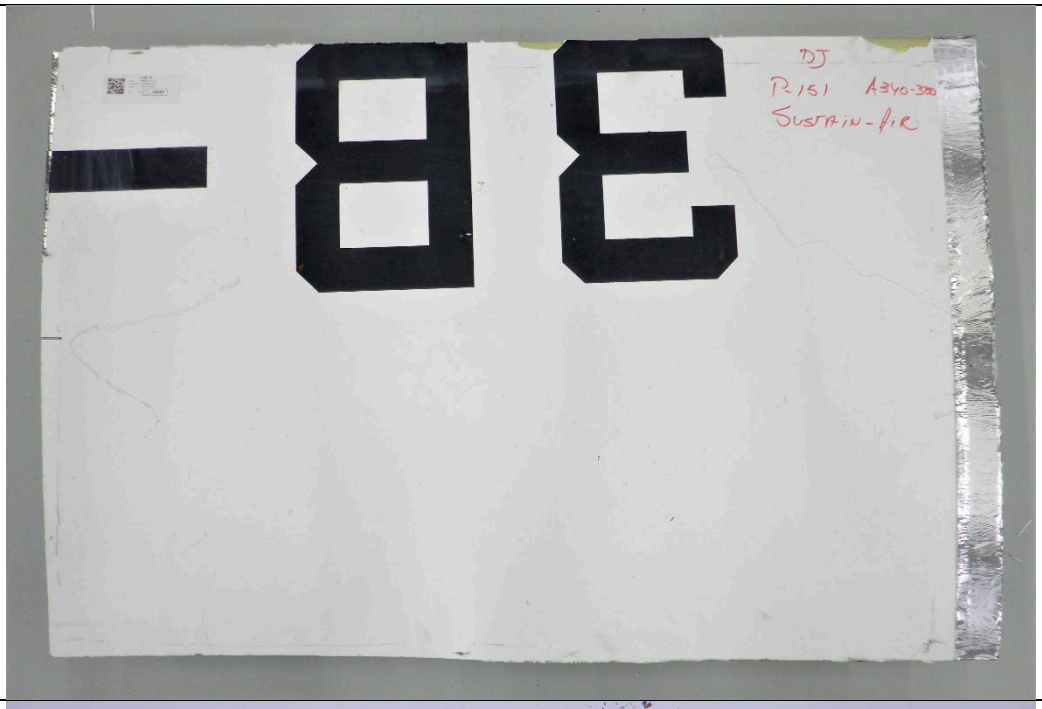


NLR 10588
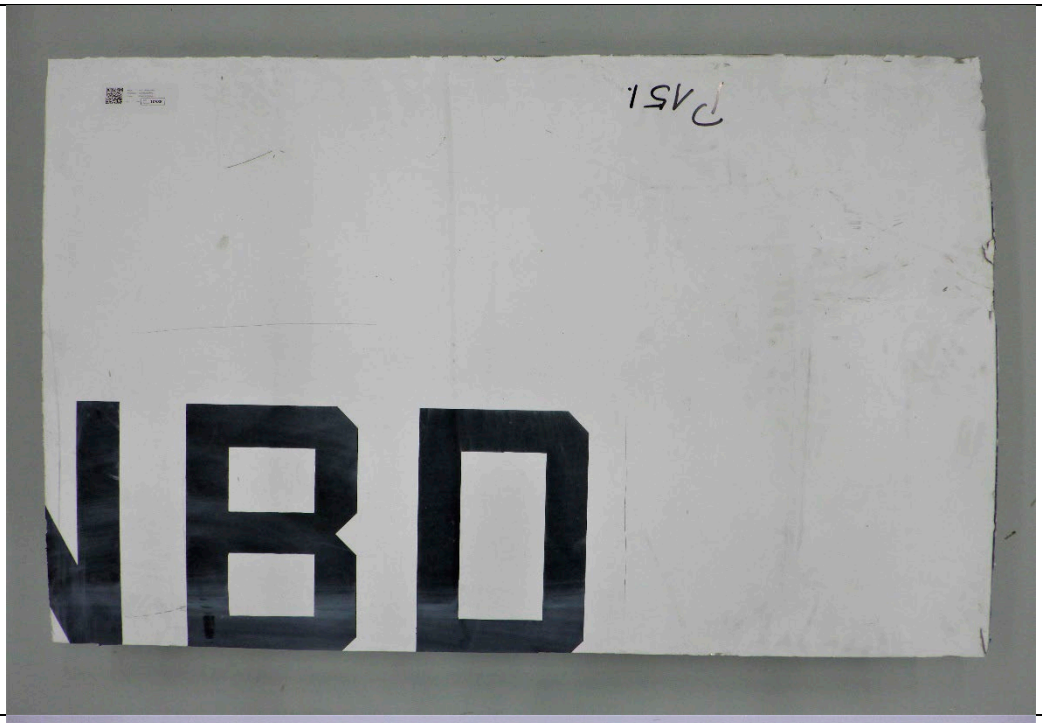


NLR 10589
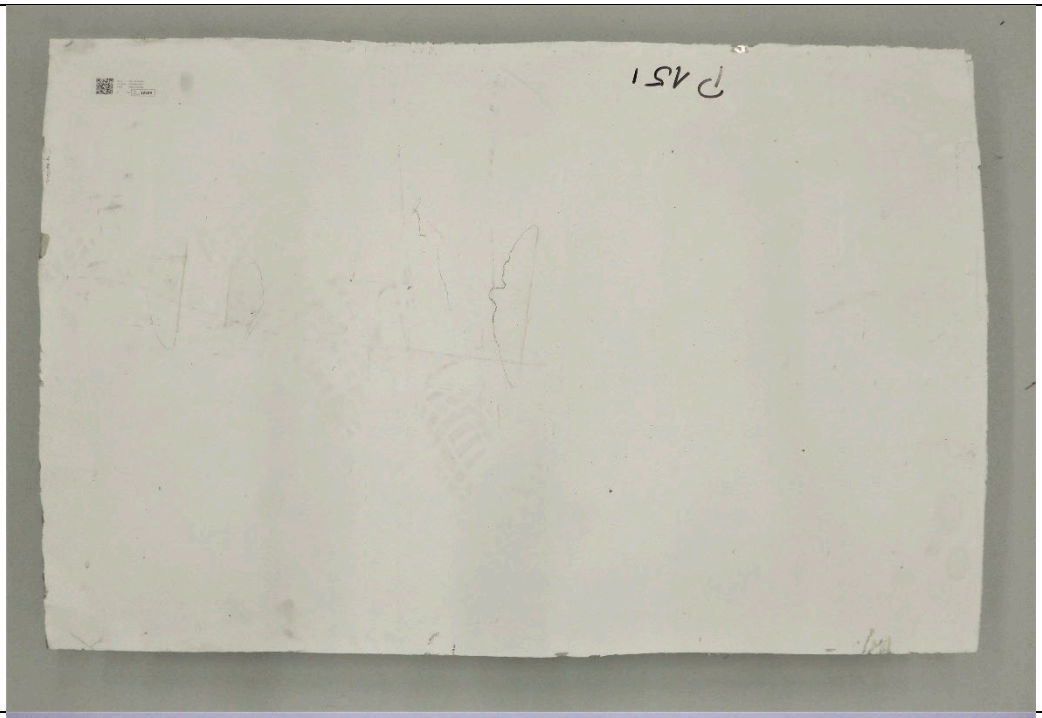


NLR 10590
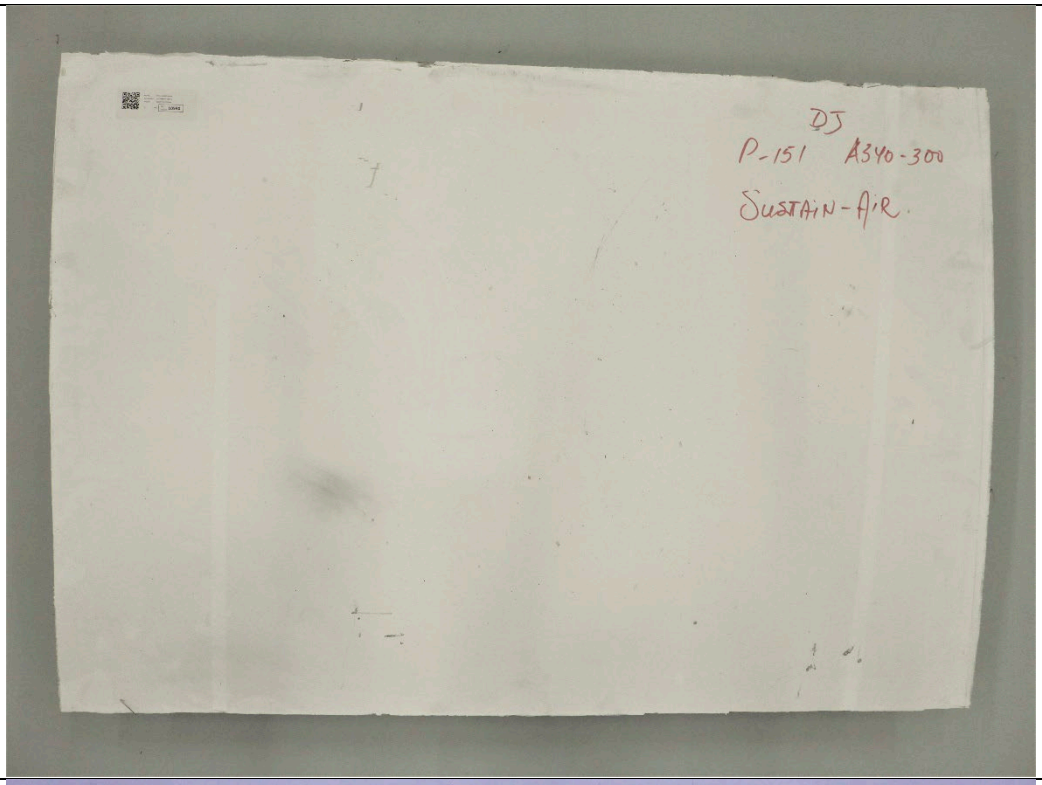


NLR 10591
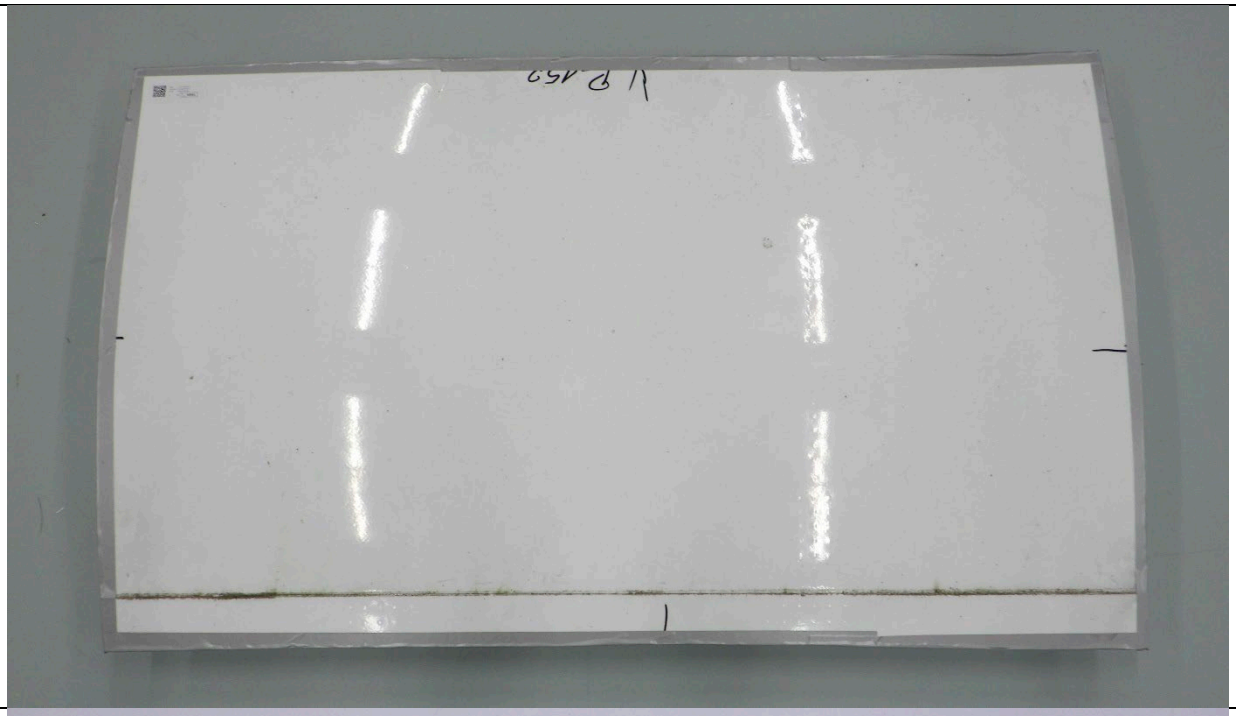


NLR 10592

NLR 10593

NLR 10594

NLR 10595

NLR 10596

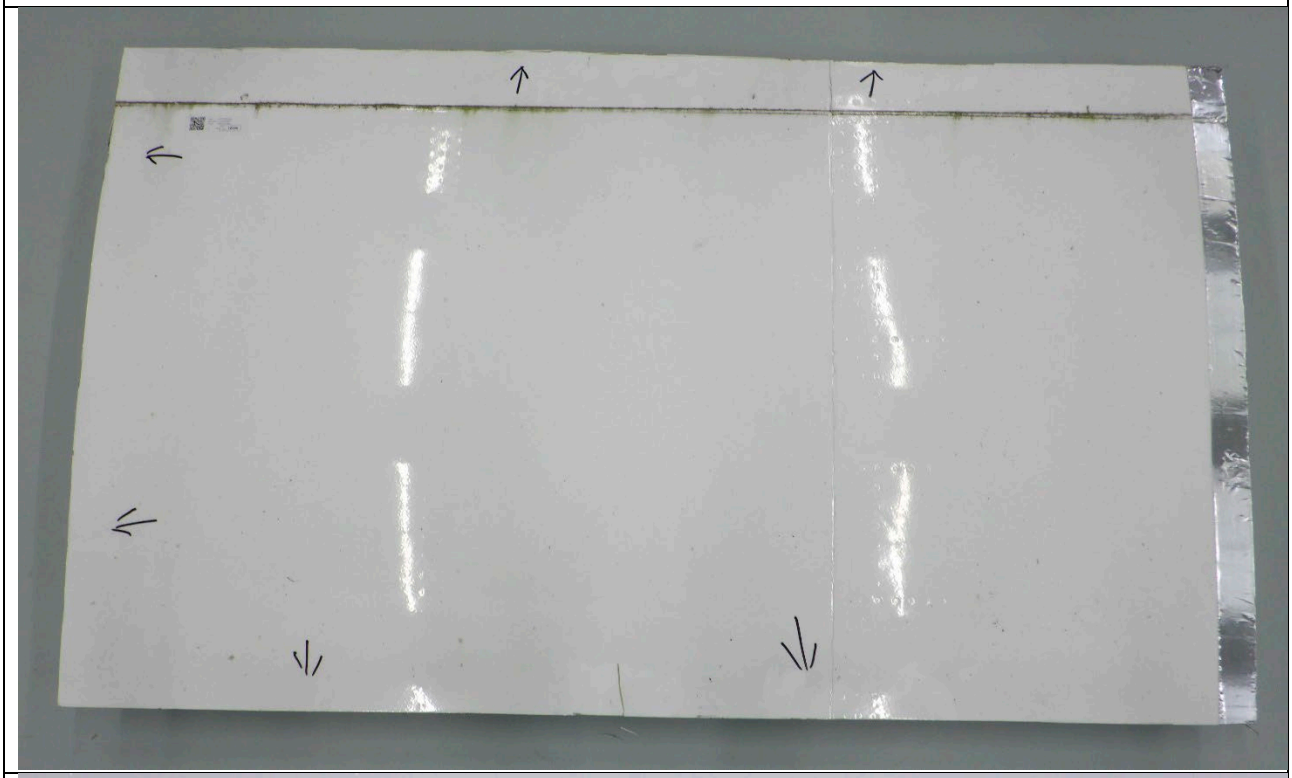

NLR 10597

NLR 10598

Appendix C Thermography results of all panels

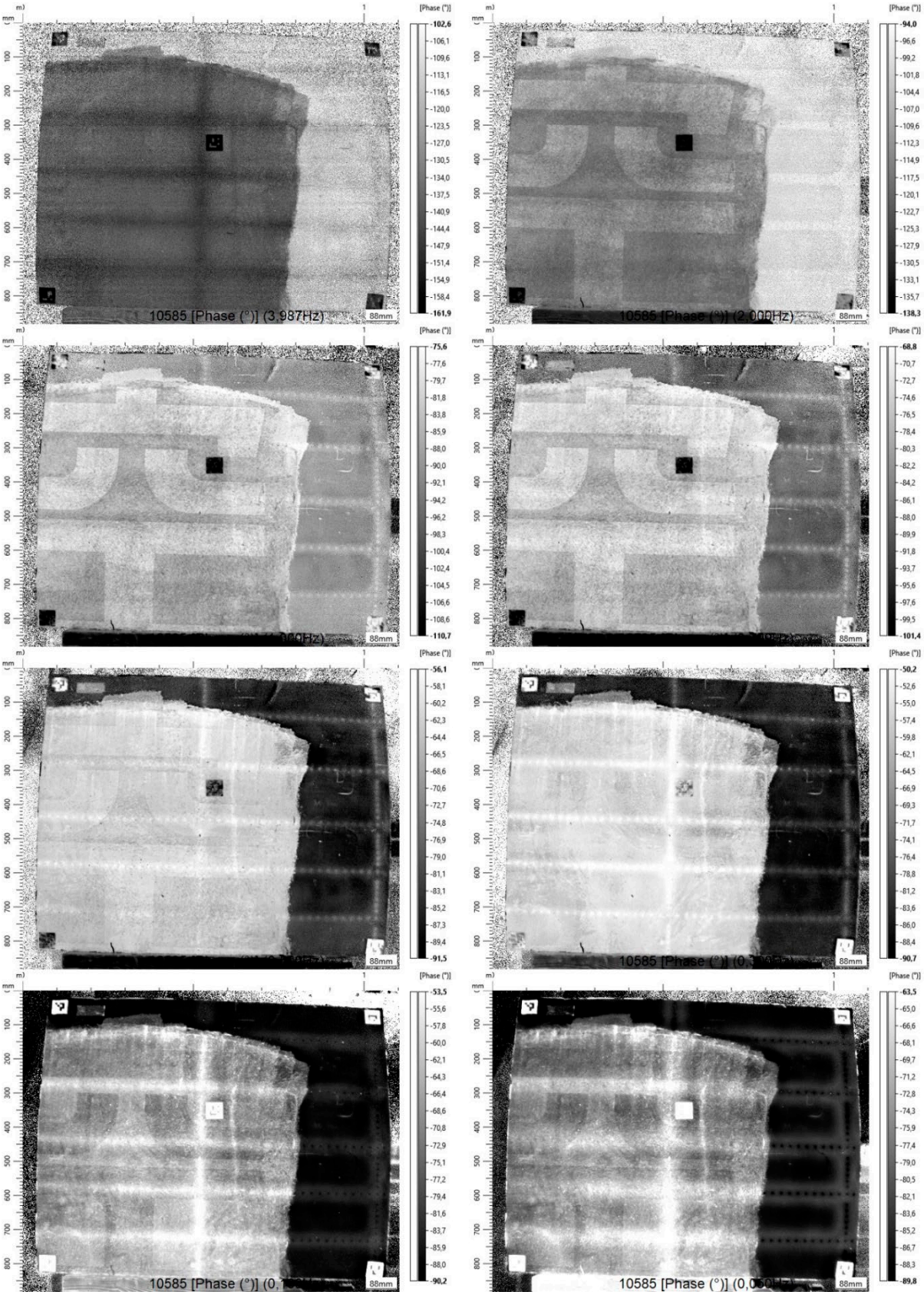

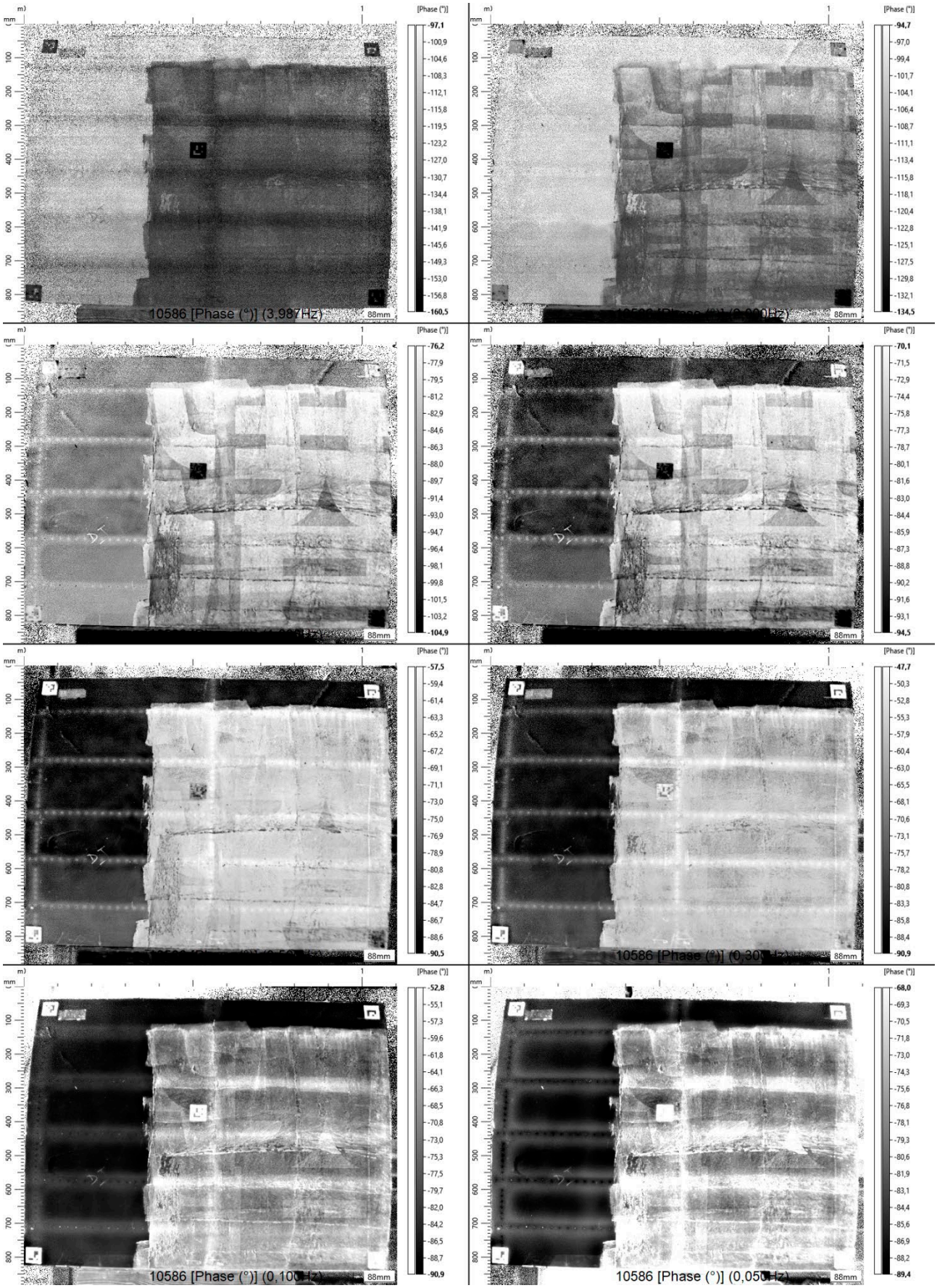
10586 [Phase (°)] (3,987Hz)
10586 [Phase (°)] (0,305 Hz)
10586 [Phase (°)] (0,100 Hz)
10586 [Phase (°)] (0,050 Hz)
88mm
[Phase (°)]

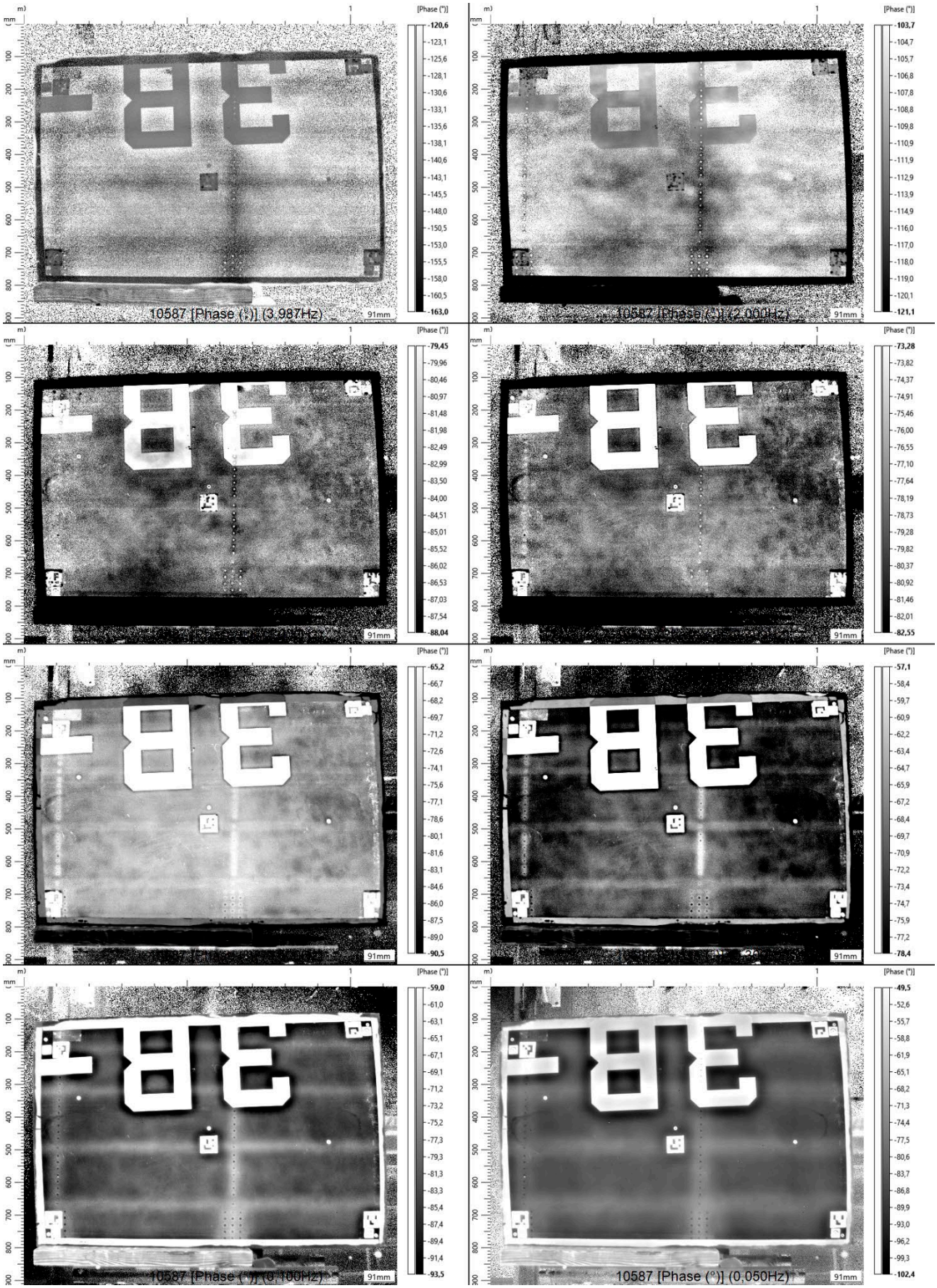
10587 [Phase (°)] (3,987Hz)
10587 [Phase (°)] (2,000Hz)
10587 [Phase (°)] (0,100Hz)
10587 [Phase (°)] (0,050Hz)
91mm
[Phase (°)]

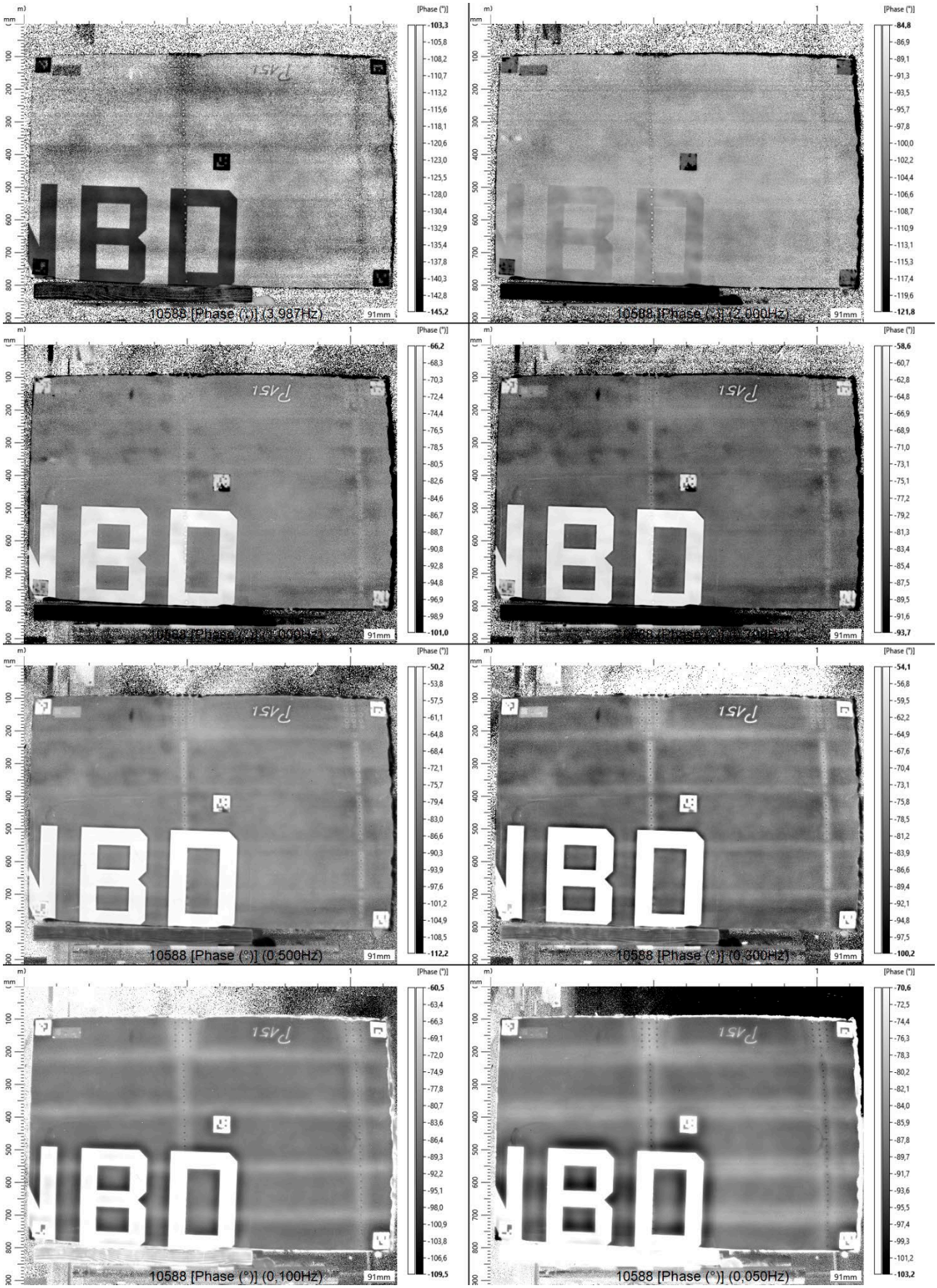
10588 [Phase (°)] (3,987Hz)
10588 [Phase (°)] (2,000Hz)
10588 [Phase (°)] (1,000Hz)
10588 [Phase (°)] (0,500Hz)
10588 [Phase (°)] (0,300Hz)
10588 [Phase (°)] (0,100Hz)
10588 [Phase (°)] (0,050Hz)
91mm
[Phase (°)]

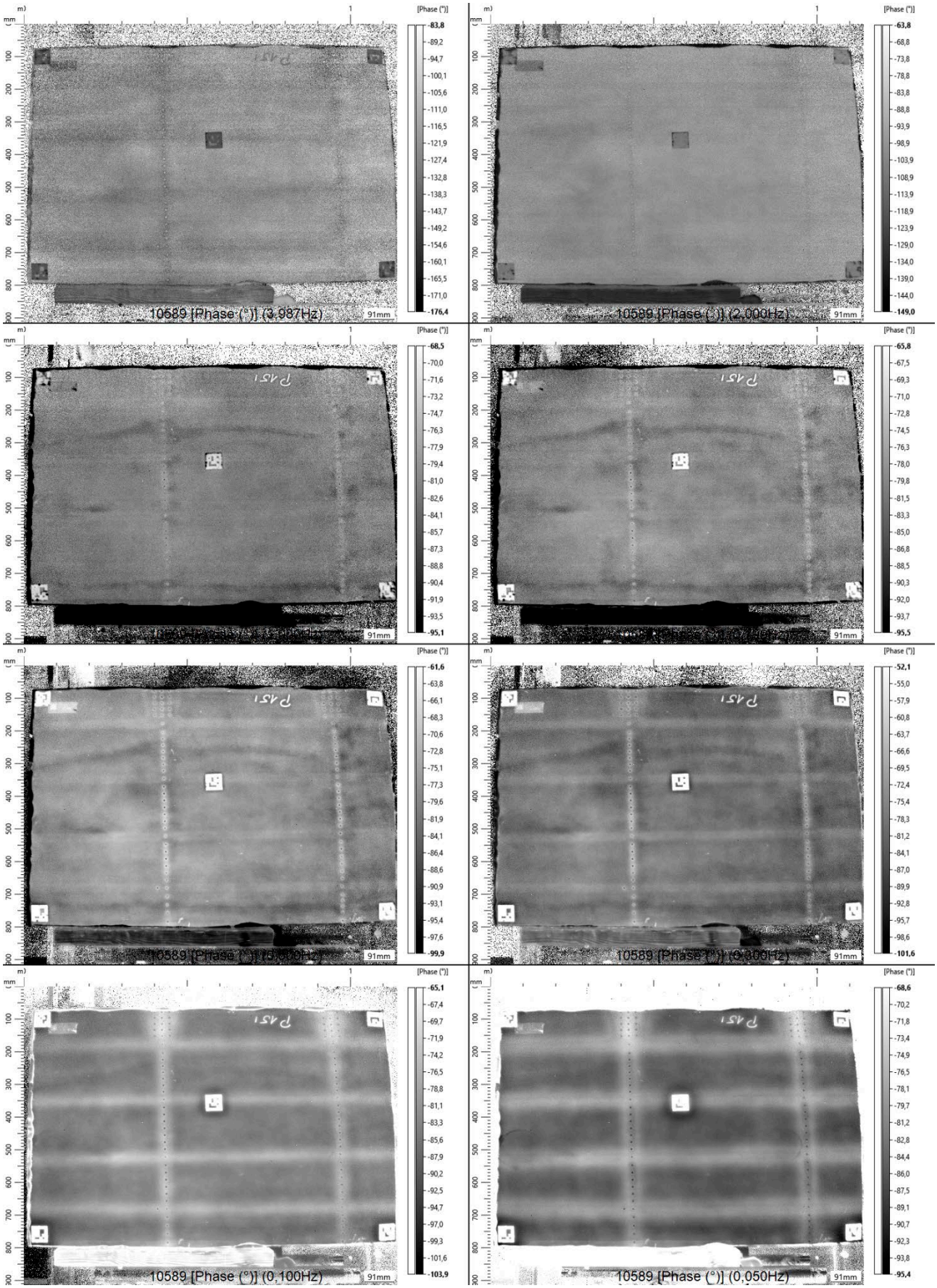
10589 [Phase (°)] (3,987Hz)
10589 [Phase (°)] (2,000Hz)
10589 [Phase (°)] (0,100Hz)
10589 [Phase (°)] (0,050Hz)
91mm
[Phase (°)]

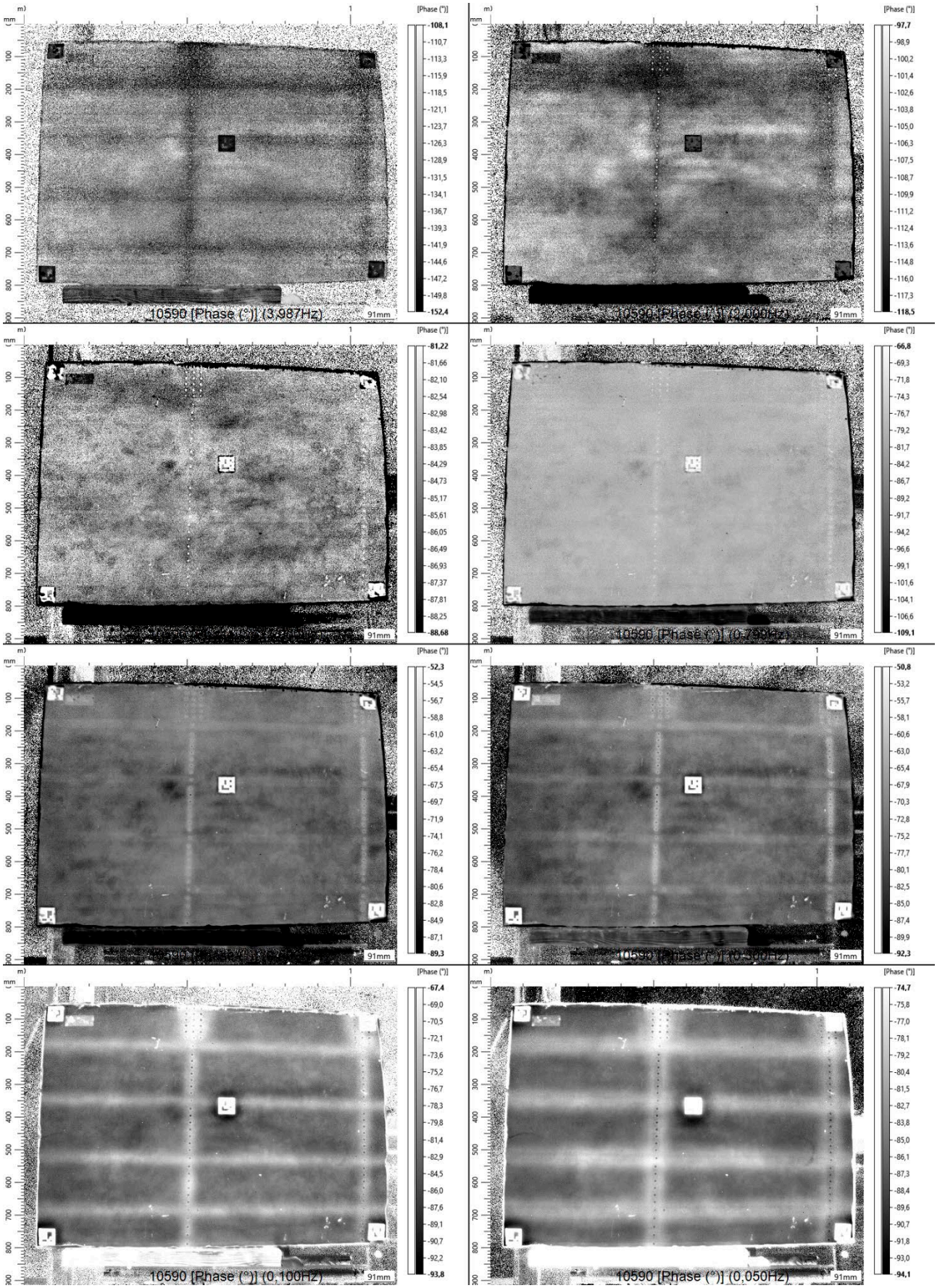
10590 [Phase (°)] (3.987Hz)
10590 [Phase (°)] (1.000Hz)
10590 [Phase (°)] (0.780Hz)
10590 [Phase (°)] (0.100Hz)
10590 [Phase (°)] (0.050Hz)
91mm
[Phase (°)]

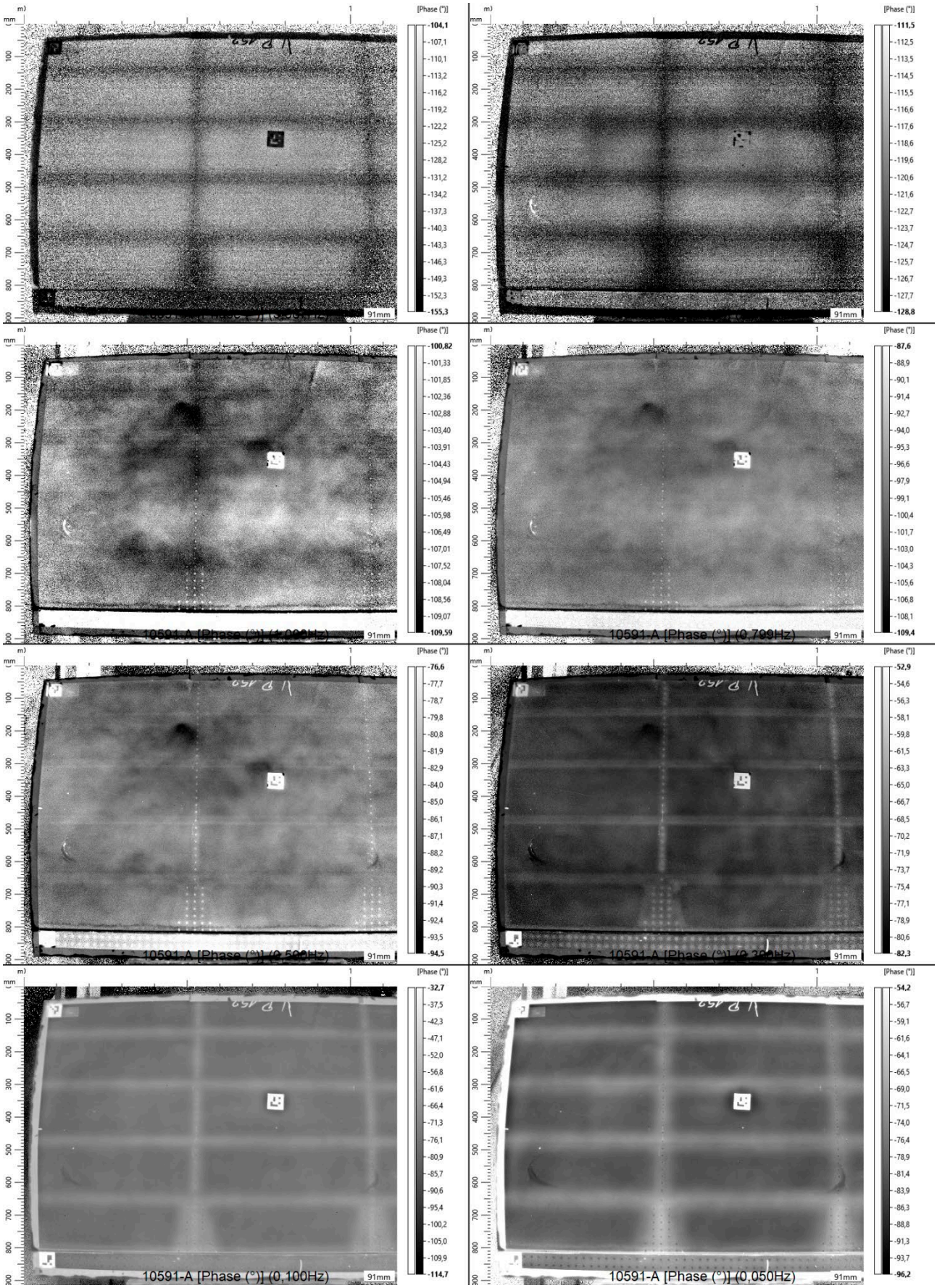
10591-A [Phase (°)] (0,100Hz)
10591-A [Phase (°)] (0,050Hz)

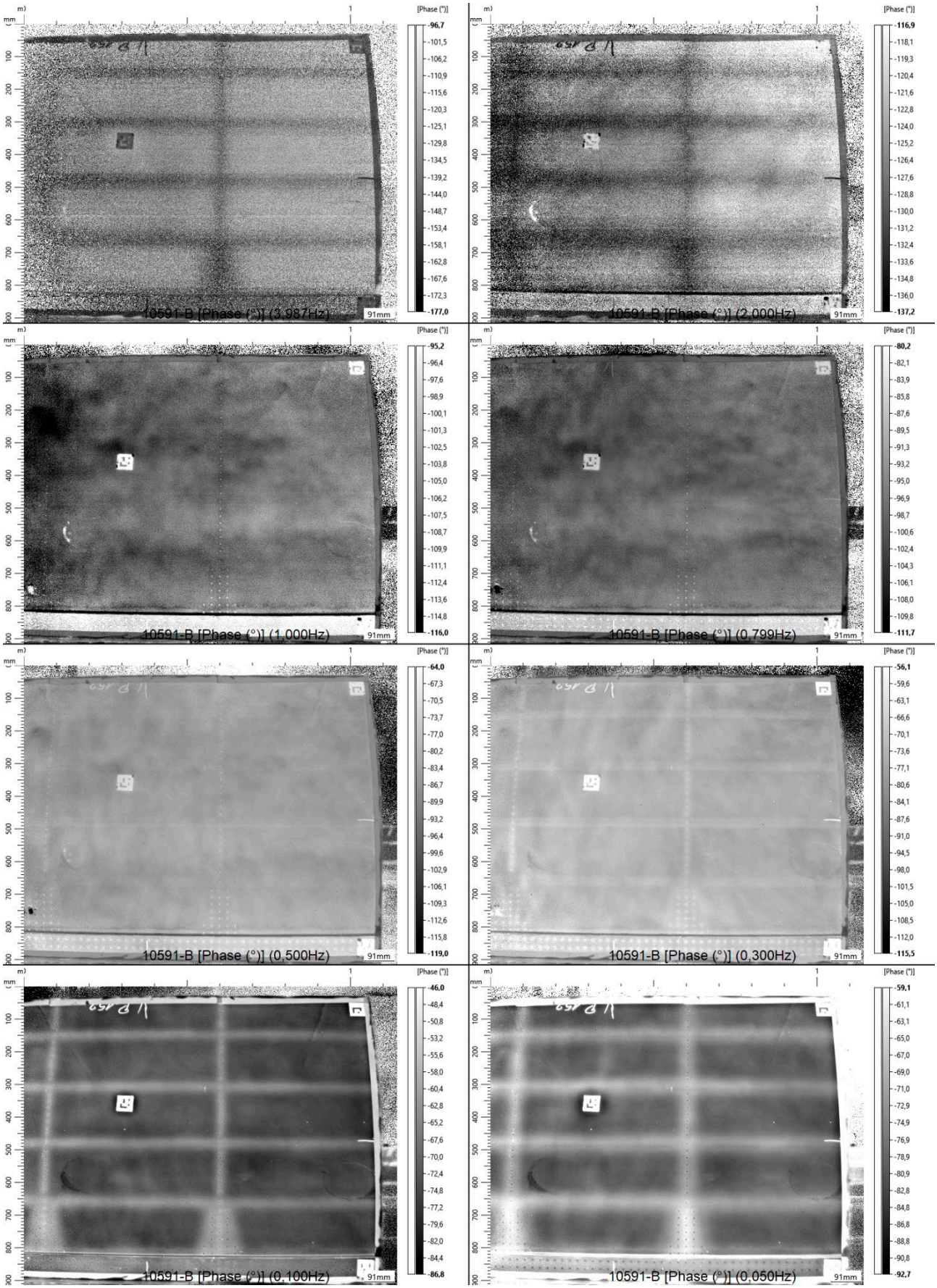
10591-B [Phase (°)] (3,987Hz)
10591-B [Phase (°)] (2,000Hz)
10591-B [Phase (°)] (1,000Hz)
10591-B [Phase (°)] (0,799Hz)
10591-B [Phase (°)] (0,500Hz)
10591-B [Phase (°)] (0,300Hz)
10591-B [Phase (°)] (0,100Hz)
10591-B [Phase (°)] (0,050Hz)

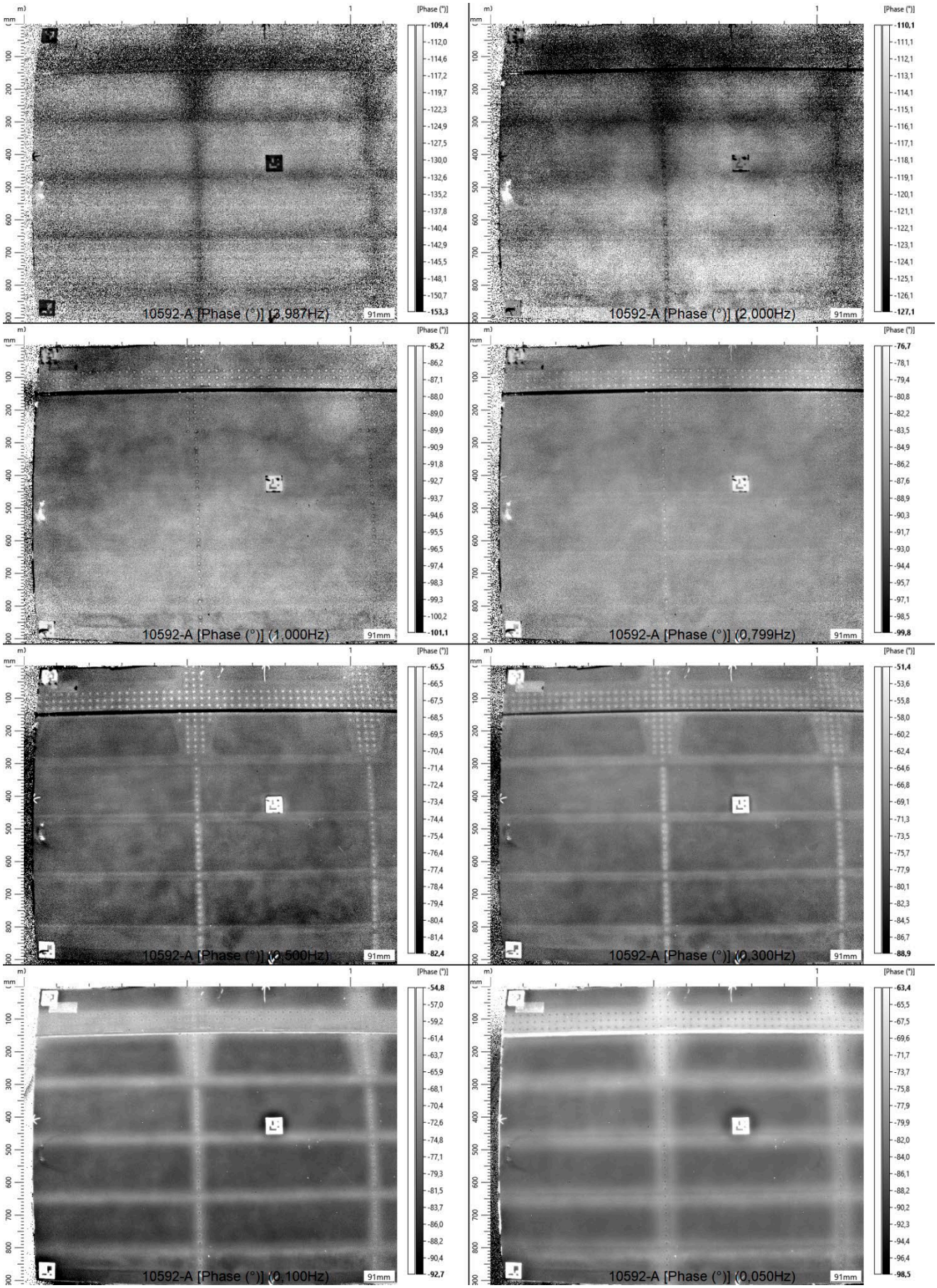
10592-A [Phase (°)] (2,987Hz)
10592-A [Phase (°)] (2,000Hz)
10592-A [Phase (°)] (1,000Hz)
10592-A [Phase (°)] (0,799Hz)
10592-A [Phase (°)] (0,500Hz)
10592-A [Phase (°)] (0,300Hz)
10592-A [Phase (°)] (0,100Hz)
10592-A [Phase (°)] (0,050Hz)
91mm
[Phase (°)]

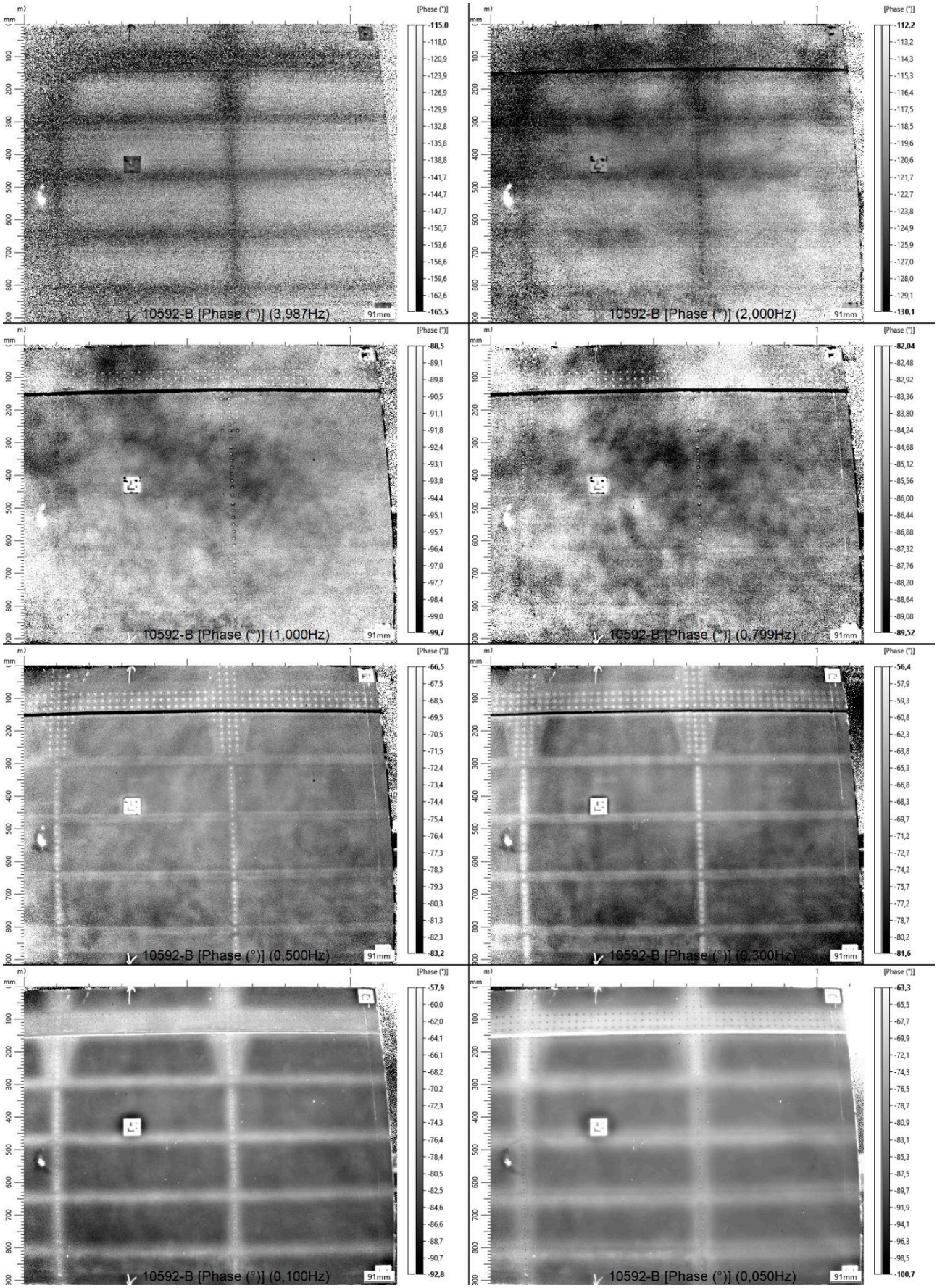
10592-B [Phase (°)] (3,987Hz)
10592-B [Phase (°)] (2,000Hz)
10592-B [Phase (°)] (1,000Hz)
10592-B [Phase (°)] (0,799Hz)
10592-B [Phase (°)] (0,500Hz)
10592-B [Phase (°)] (0,300Hz)
10592-B [Phase (°)] (0,100Hz)
10592-B [Phase (°)] (0,050Hz)

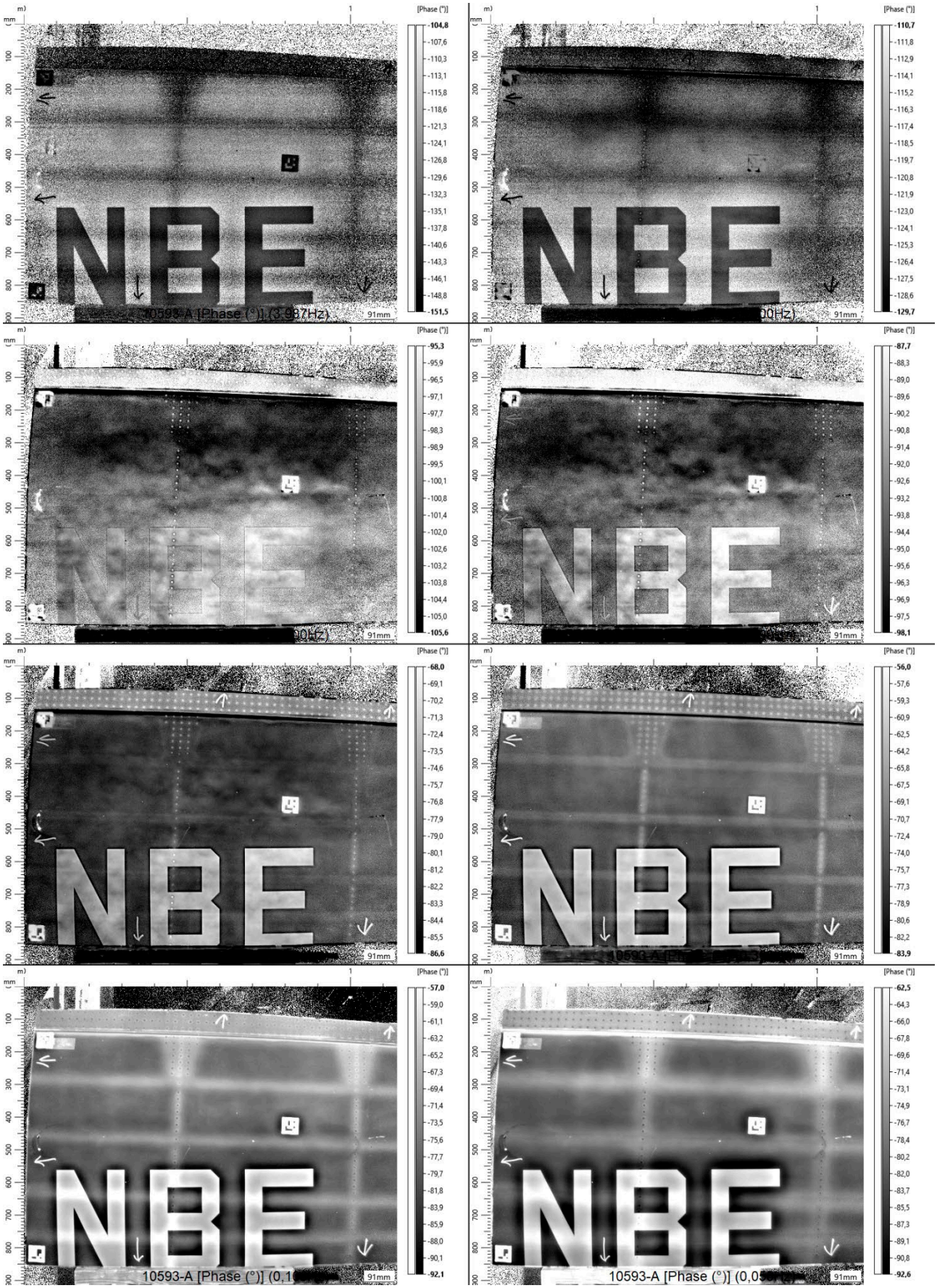
[Phase (°)]
NBE
91mm
10593-A [Phase (°)]

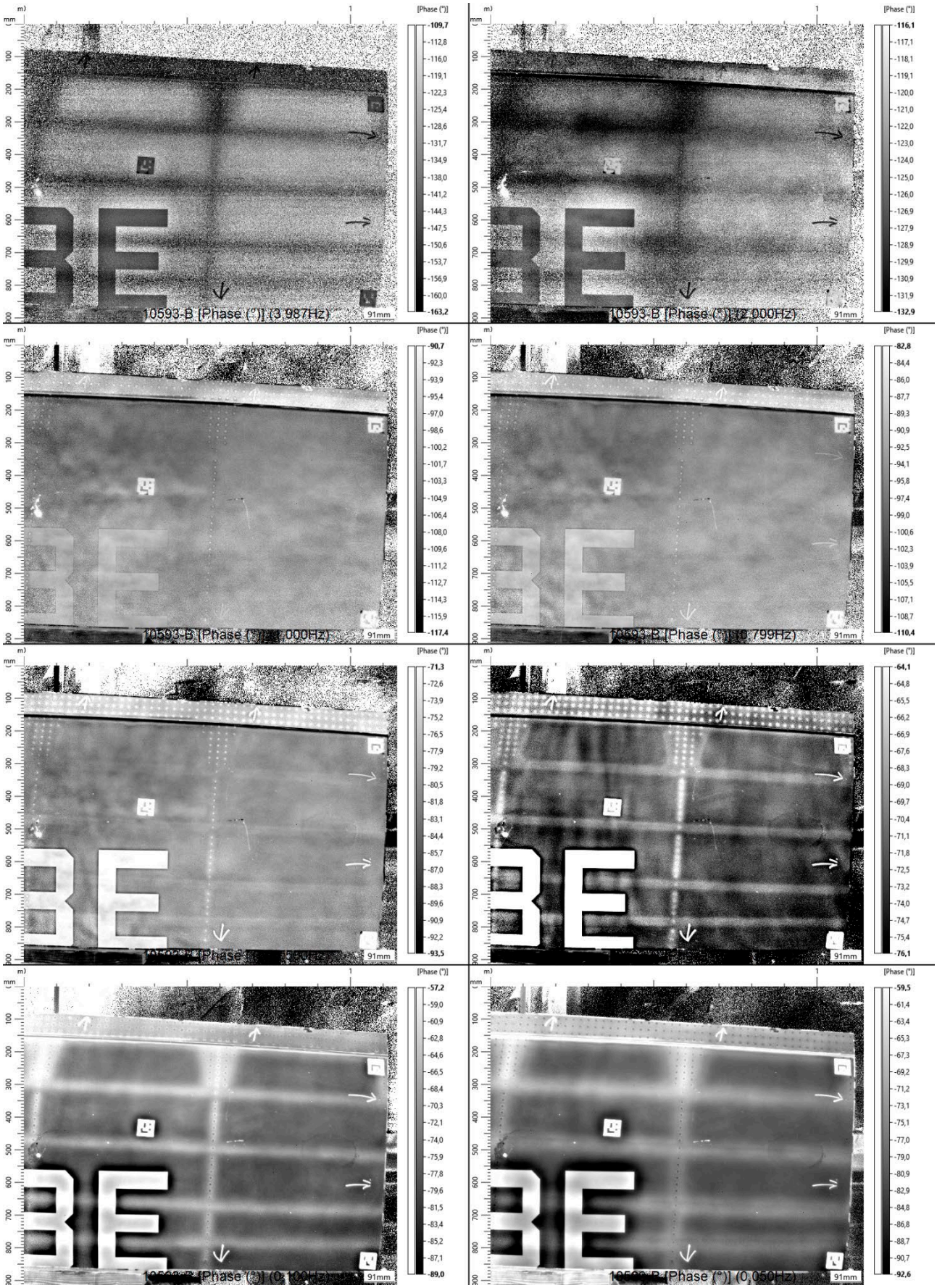
10593-B [Phase (°)] (3,987Hz)
10593-B [Phase (°)] (2,000Hz)
10593-B [Phase (°)] (0,799Hz)
10593-B [Phase (°)] (0,100Hz)
10593-B [Phase (°)] (0,050Hz)
91mm

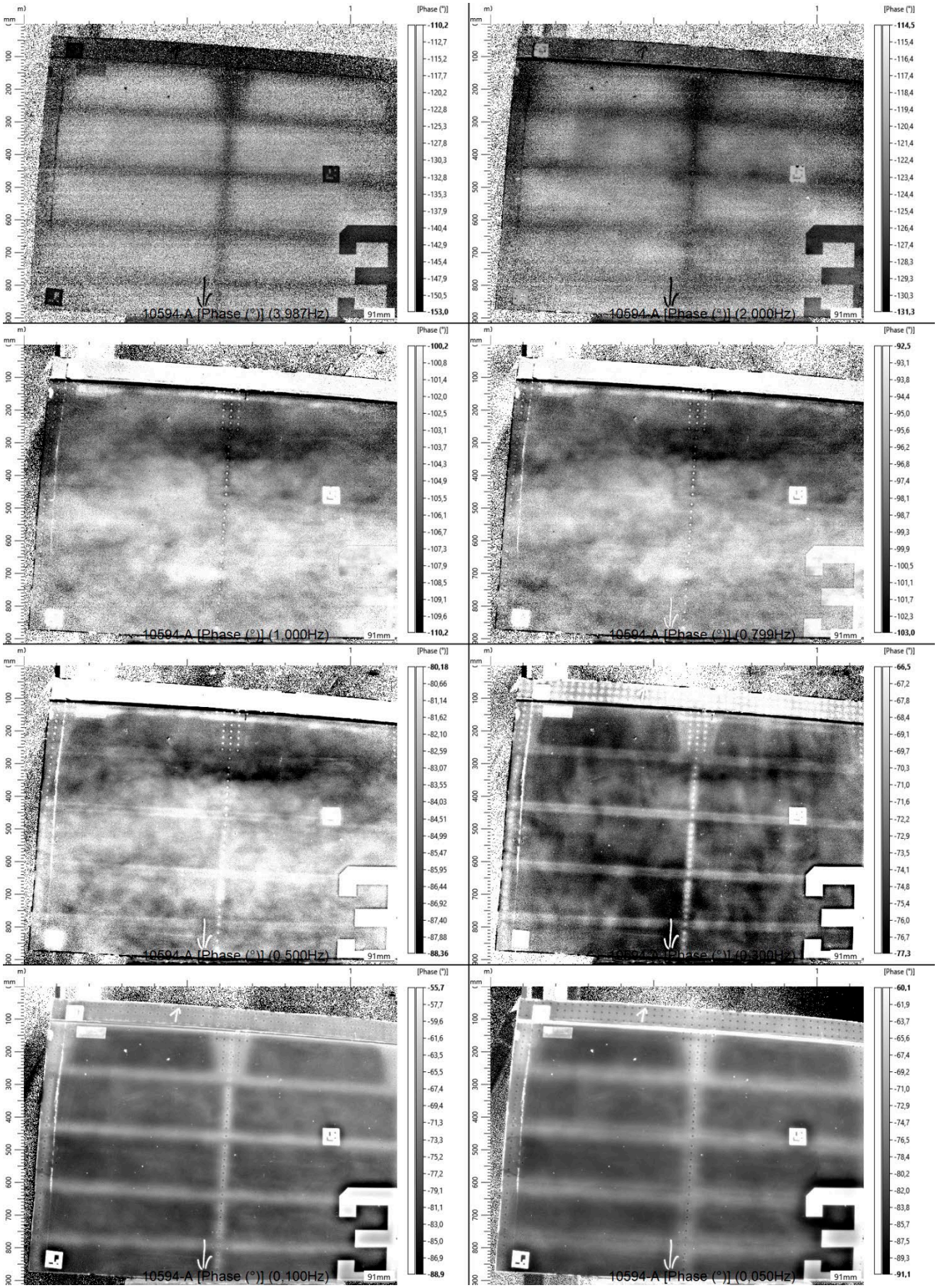
10594-A [Phase (°)] (3,987Hz)
10594-A [Phase (°)] (2,000Hz)
10594-A [Phase (°)] (1,000Hz)
10594-A [Phase (°)] (0,799Hz)
10594-A [Phase (°)] (0,500Hz)
10594-A [Phase (°)] (0,100Hz)
10594-A [Phase (°)] (0,050Hz)

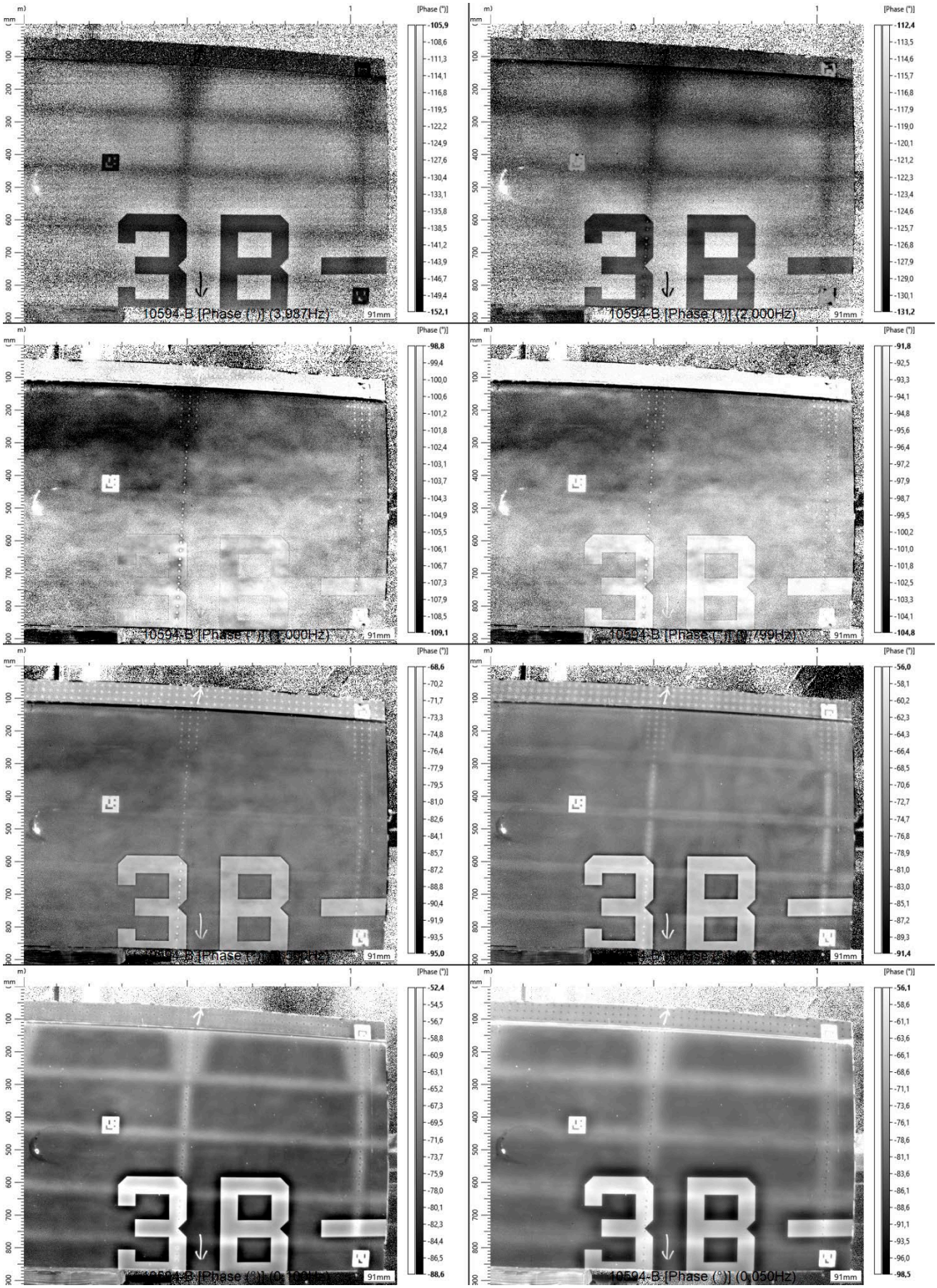
10594-B [Phase (°)] (3,987Hz)
10594-B [Phase (°)] (2,000Hz)
10594-B [Phase (°)] (1,000Hz)
10594-B [Phase (°)] (0,799Hz)
10594-B [Phase (°)] (0,100Hz)
10594-B [Phase (°)] (0,050Hz)
91mm
[Phase (°)]

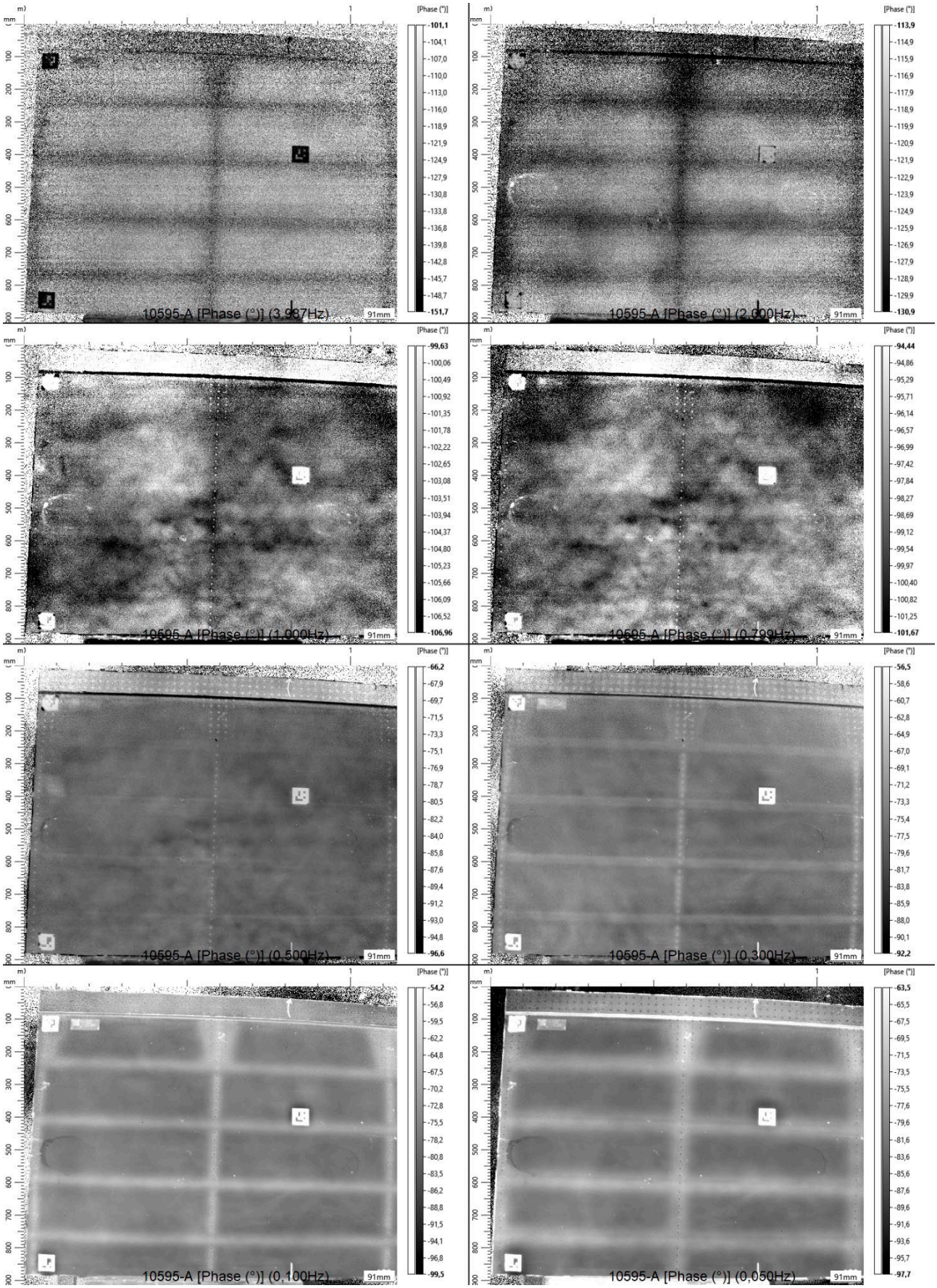
10595-A [Phase (°)] (3,987Hz)
10595-A [Phase (°)] (2,000Hz)
10595-A [Phase (°)] (1,000Hz)
10595-A [Phase (°)] (0,799Hz)
10595-A [Phase (°)] (0,500Hz)
10595-A [Phase (°)] (0,300Hz)
10595-A [Phase (°)] (0,100Hz)
10595-A [Phase (°)] (0,050Hz)

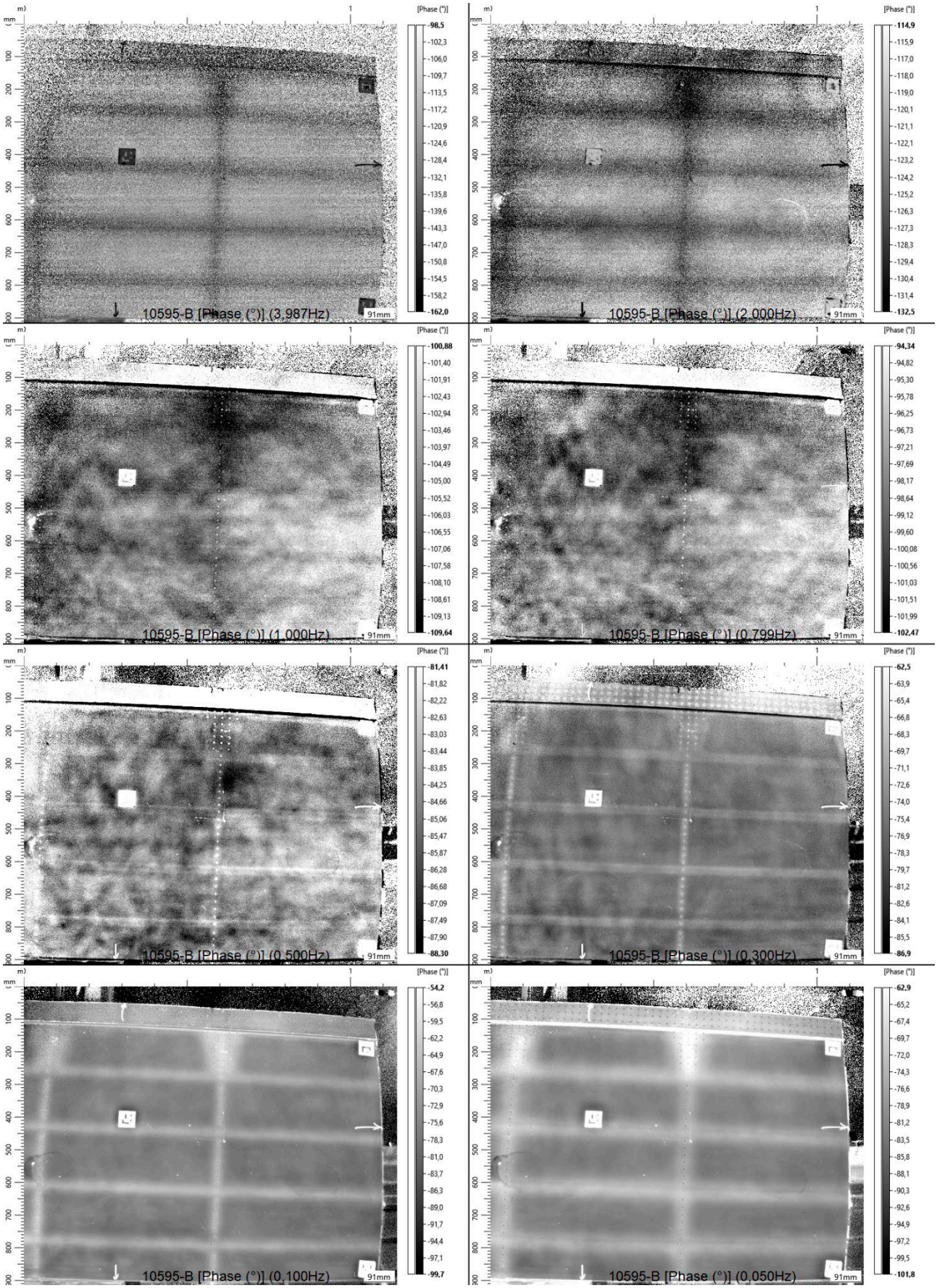
10595-B [Phase (°)] (3,987Hz)
10595-B [Phase (°)] (2,000Hz)
10595-B [Phase (°)] (1,000Hz)
10595-B [Phase (°)] (0,799Hz)
10595-B [Phase (°)] (0,500Hz)
10595-B [Phase (°)] (0,300Hz)
10595-B [Phase (°)] (0,100Hz)
10595-B [Phase (°)] (0,050Hz)

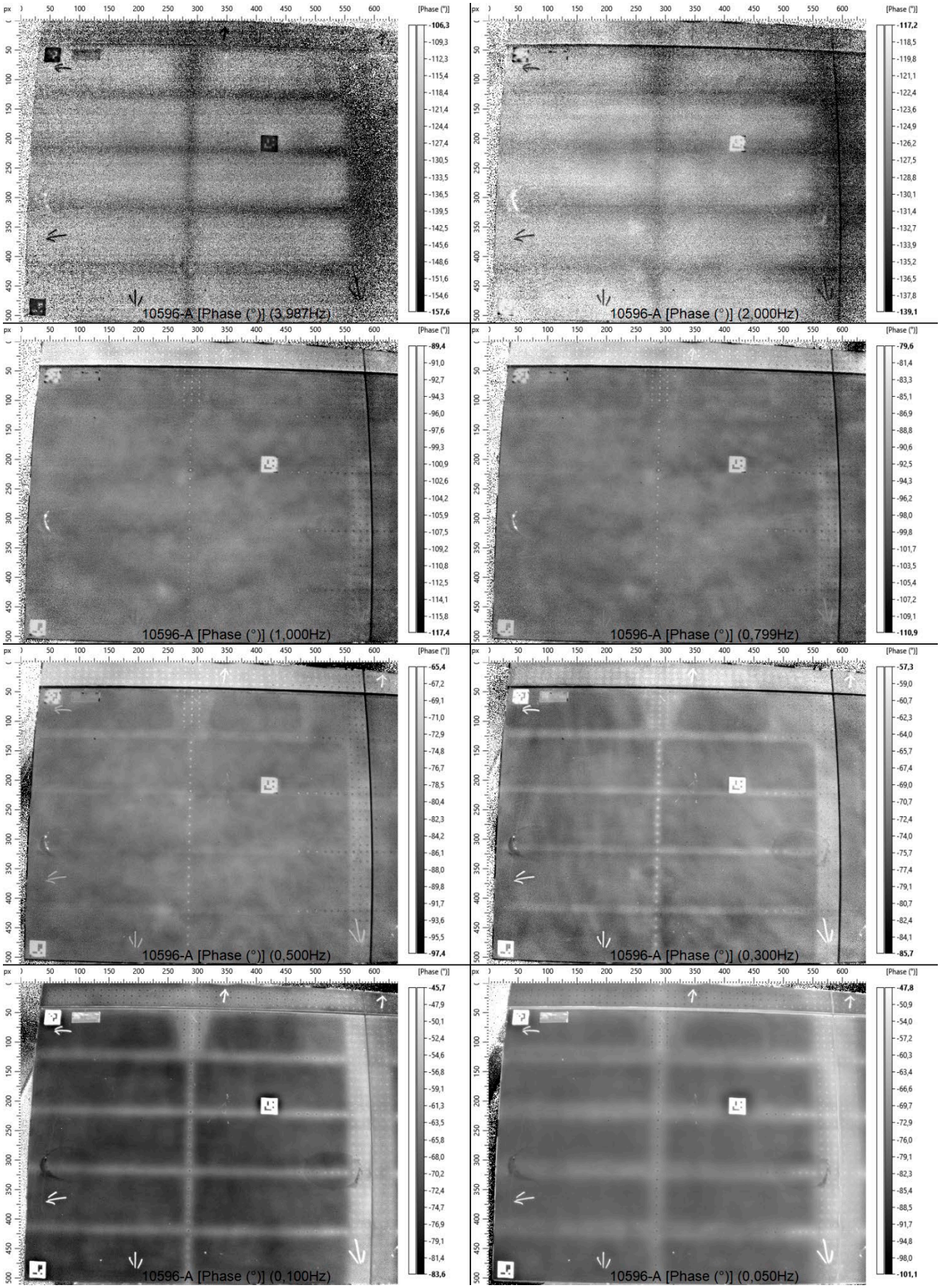
10596-A [Phase (°)] (3,987Hz)
10596-A [Phase (°)] (2,000Hz)
10596-A [Phase (°)] (1,000Hz)
10596-A [Phase (°)] (0,799Hz)
10596-A [Phase (°)] (0,500Hz)
10596-A [Phase (°)] (0,300Hz)
10596-A [Phase (°)] (0,100Hz)
10596-A [Phase (°)] (0,050Hz)

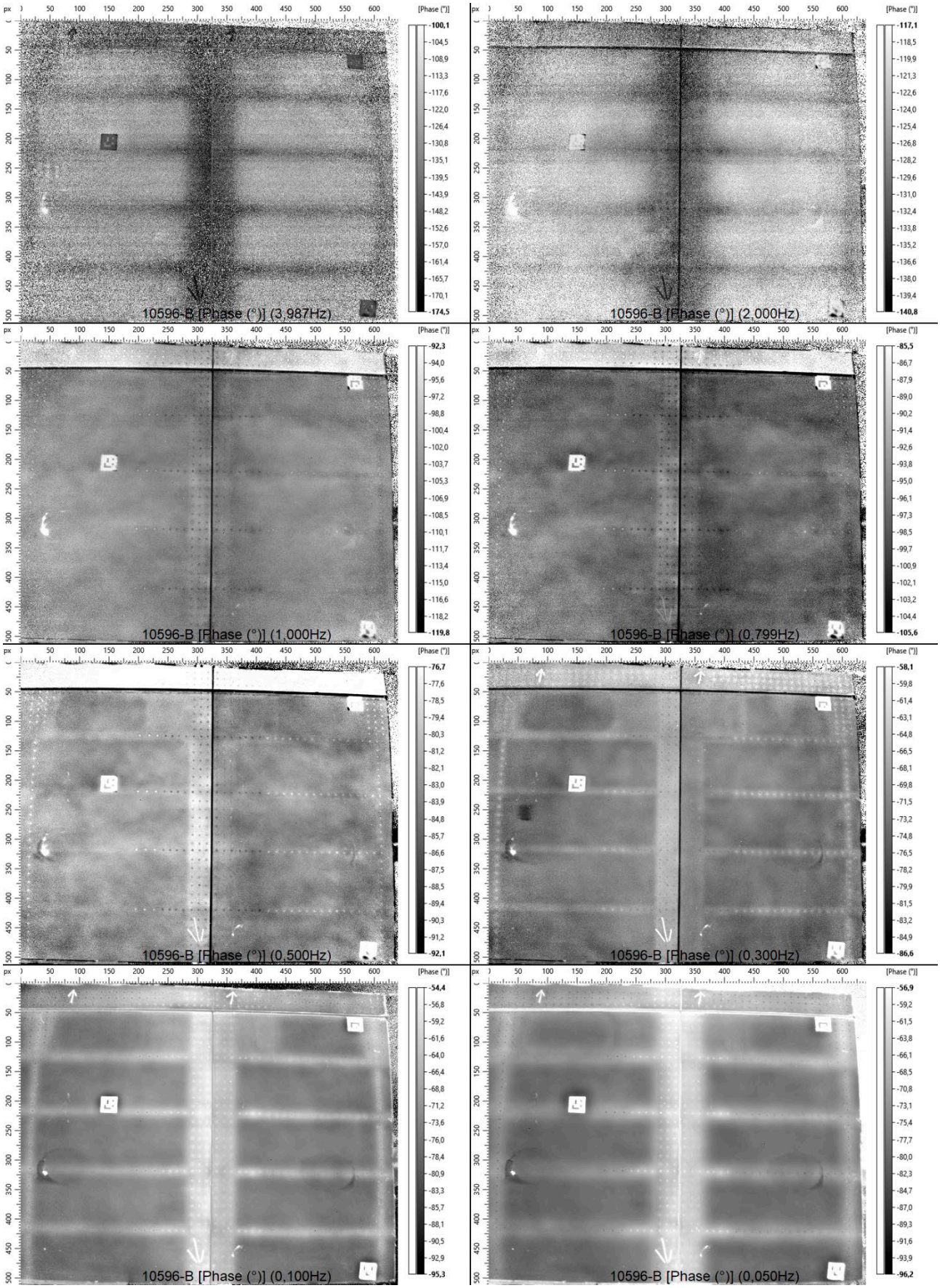
10596-B [Phase (°)] (3,987Hz)
10596-B [Phase (°)] (2,000Hz)
10596-B [Phase (°)] (1,000Hz)
10596-B [Phase (°)] (0,799Hz)
10596-B [Phase (°)] (0,500Hz)
10596-B [Phase (°)] (0,300Hz)
10596-B [Phase (°)] (0,100Hz)
10596-B [Phase (°)] (0,050Hz)

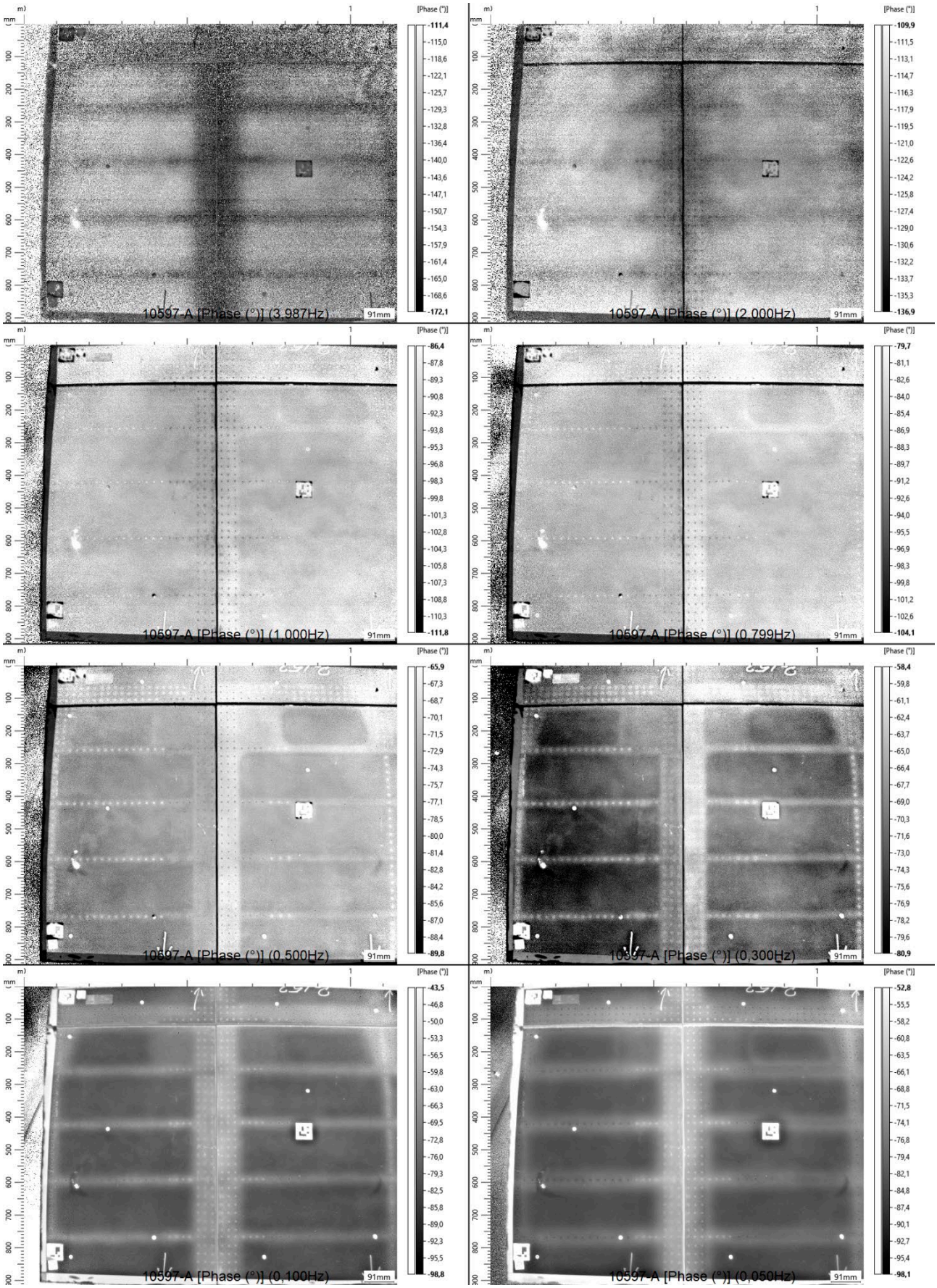
10597-A [Phase (°)] (3,987Hz)
10597-A [Phase (°)] (2,000Hz)
10597-A [Phase (°)] (1,000Hz)
10597-A [Phase (°)] (0,799Hz)
10597-A [Phase (°)] (0,500Hz)
10597-A [Phase (°)] (0,300Hz)
10597-A [Phase (°)] (0,100Hz)
10597-A [Phase (°)] (0,050Hz)
91mm
[Phase (°)]

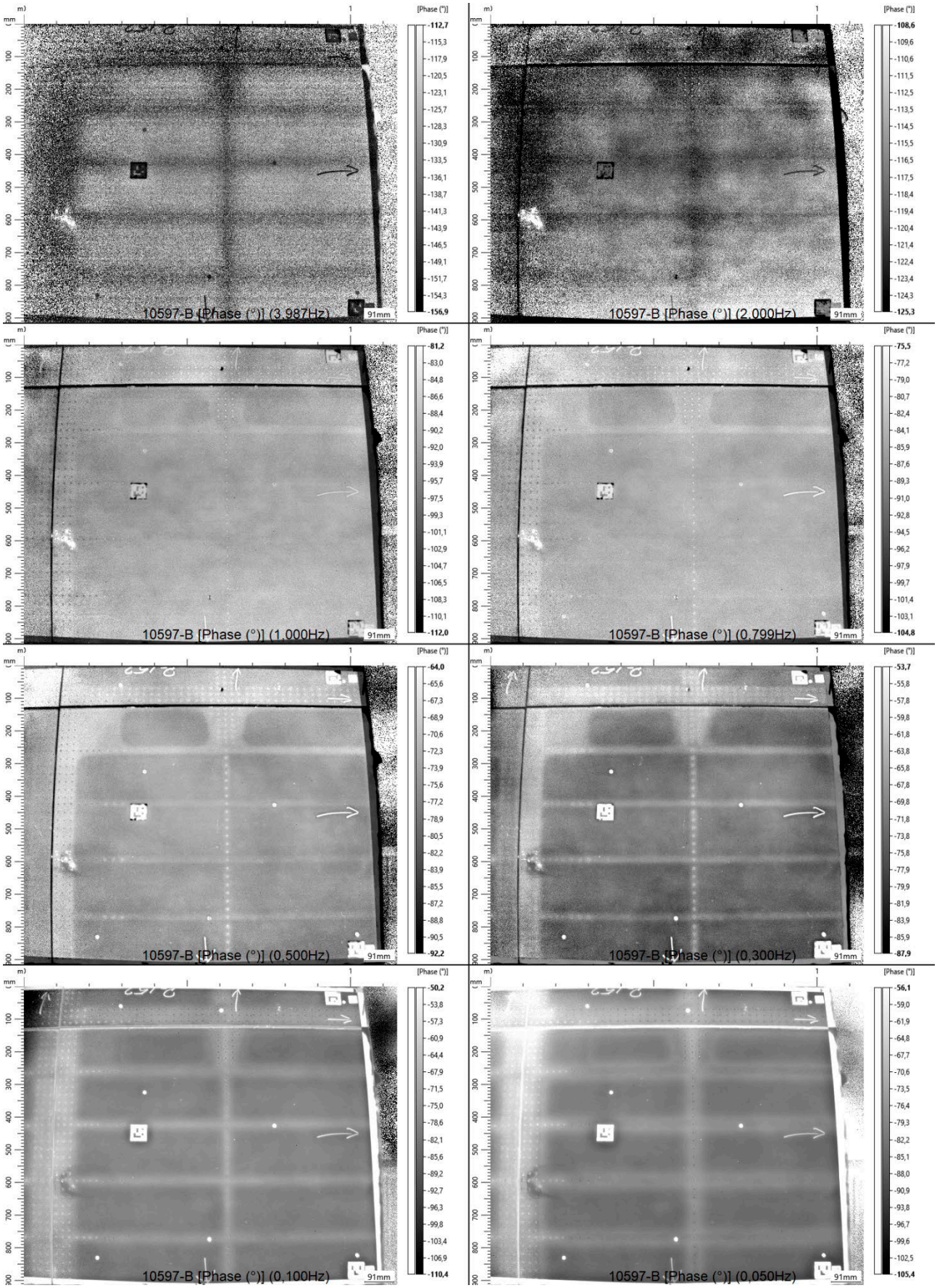
10597-B [Phase (°)] (3,987Hz)
10597-B [Phase (°)] (2,000Hz)
10597-B [Phase (°)] (1,000Hz)
10597-B [Phase (°)] (0,799Hz)
10597-B [Phase (°)] (0,500Hz)
10597-B [Phase (°)] (0,300Hz)
10597-B [Phase (°)] (0,100Hz)
10597-B [Phase (°)] (0,050Hz)

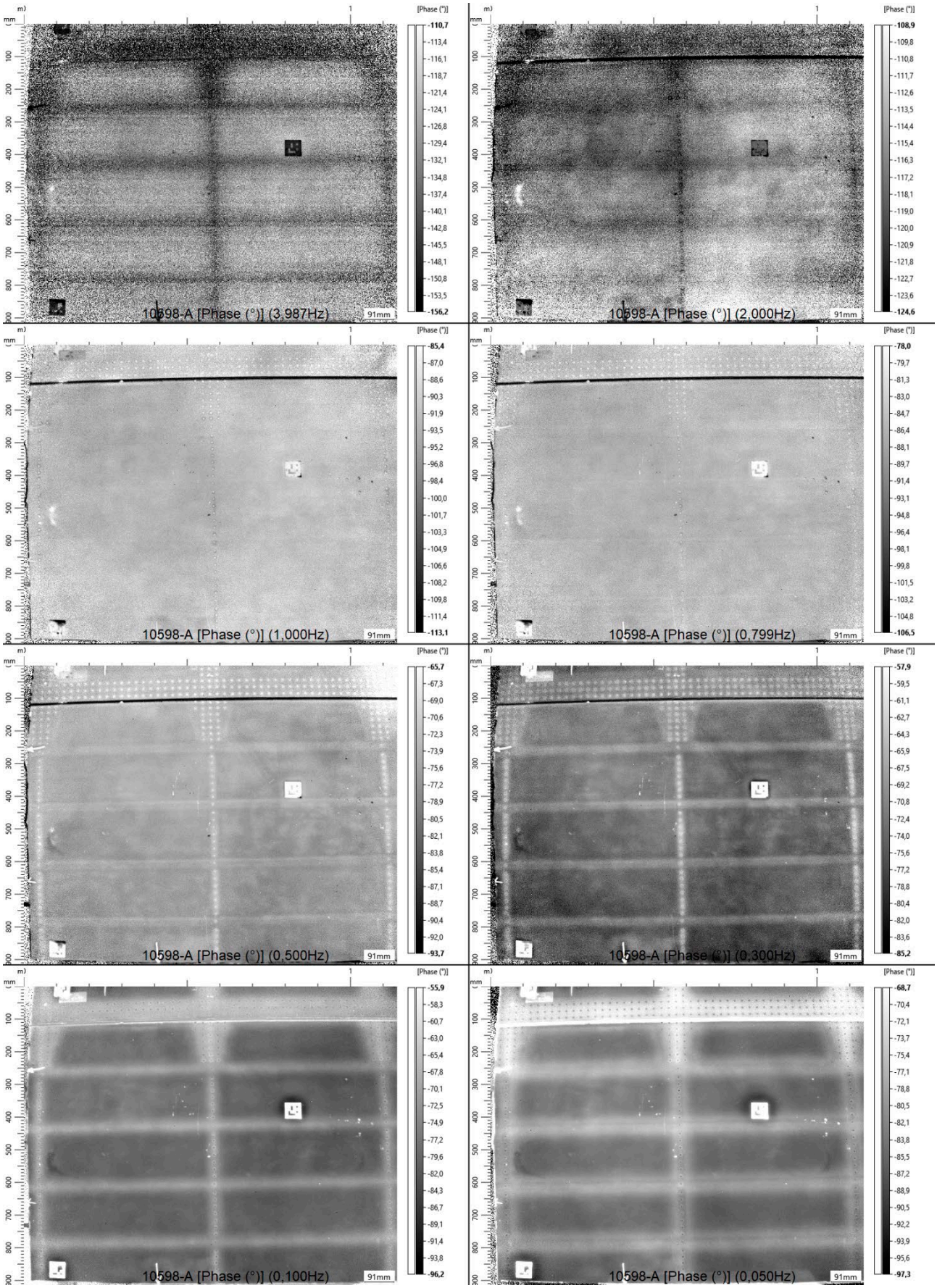
10598-A [Phase (°)] (3,987Hz)
10598-A [Phase (°)] (2,000Hz)
10598-A [Phase (°)] (1,000Hz)
10598-A [Phase (°)] (0,799Hz)
10598-A [Phase (°)] (0,500Hz)
10598-A [Phase (°)] (0,300Hz)
10598-A [Phase (°)] (0,100Hz)
10598-A [Phase (°)] (0,050Hz)
91mm
[Phase (°)]

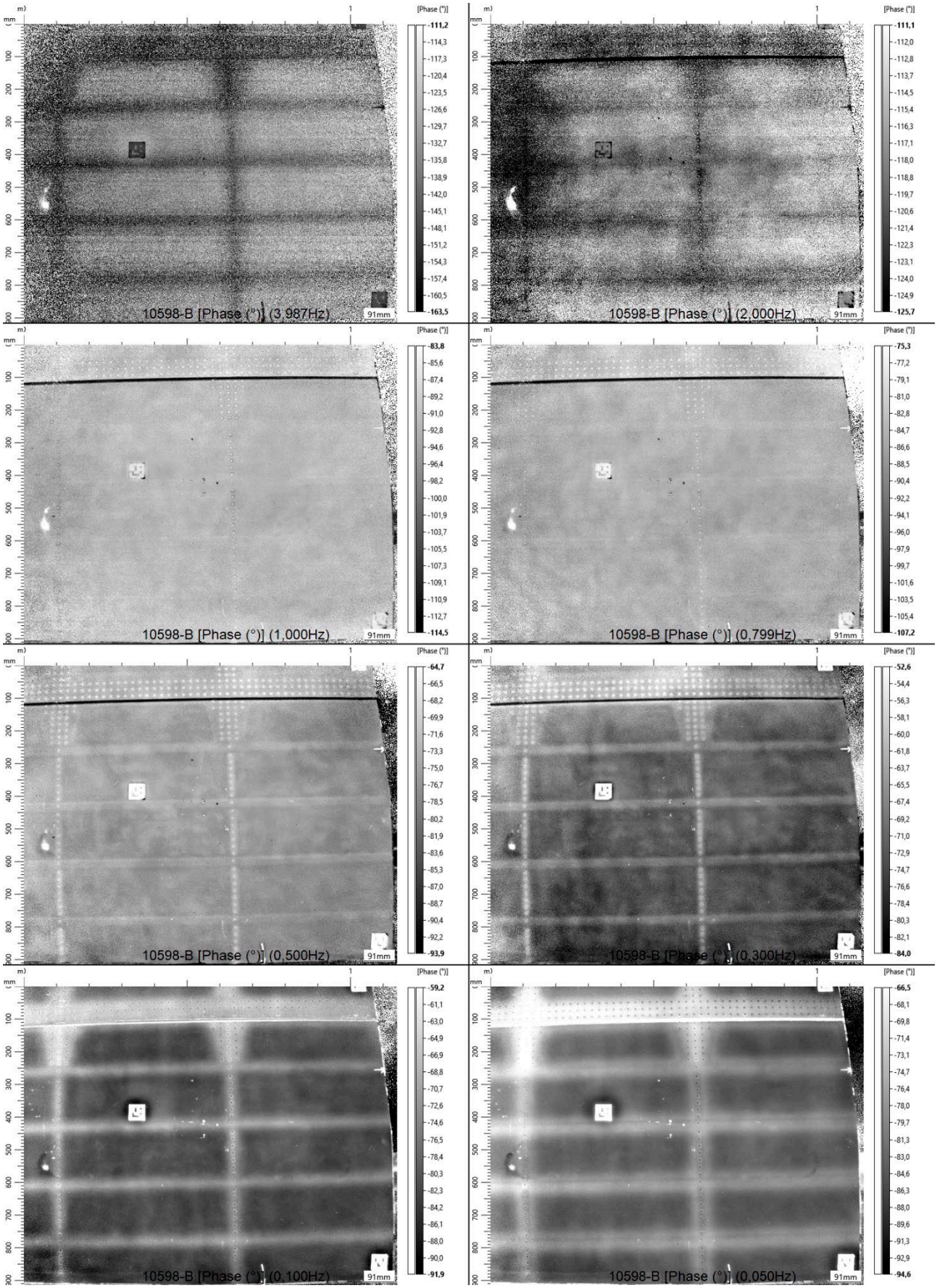
10598-B [Phase (°)] (3,987Hz)
10598-B [Phase (°)] (2,000Hz)
10598-B [Phase (°)] (1,000Hz)
10598-B [Phase (°)] (0,799Hz)
10598-B [Phase (°)] (0,500Hz)
10598-B [Phase (°)] (0,300Hz)
10598-B [Phase (°)] (0,100Hz)
10598-B [Phase (°)] (0,050Hz)

Dedicated to innovation in aerospace

Royal NLR - Netherlands Aerospace Centre

NLR operates as an objective and independent research centre, working with its partners towards a better world tomorrow. As part of that, NLR offers innovative solutions and technical expertise, creating a strong competitive position for the commercial sector.

NLR has been a centre of expertise for over a century now, with a deep-seated desire to keep innovating. It is an organisation that works to achieve sustainable, safe, efficient and effective aerospace operations.
The combination of in-depth insights into customers' needs, multidisciplinary expertise and state-of-the-art research facilities makes rapid innovation possible. Both domestically and abroad, NLR plays a pivotal role between science, the commercial sector and governmental authorities, bridging the gap between fundamental research and practical applications. Additionally, NLR is one of the large technological institutes (GTIs) that have been collaborating over a decade in the Netherlands on applied research united in the TO2 federation.

From its main offices in Amsterdam and Marknesse plus two satellite offices, NLR helps to create a safe and sustainable society. It works with partners on numerous programmes in both civil aviation and defence, including work on complex composite structures for commercial aircraft and on goal-oriented use of the F-35 fighter. Additionally, NLR helps to achieve both Dutch and European goals and climate objectives in line with the Luchtvaartnota (Aviation Policy Document), the European Green Deal and Flightpath 2050, and by participating in programs such as Clean Sky and SESAR.

For more information visit: **www.nlr.org**

Postal address
PO Box 90502
1006 BM Amsterdam, The Netherlands
e) info@nlr.nl **i)** www.nlr.org

Royal NLR
Anthony Fokkerweg 2
1059 CM Amsterdam, The Netherlands
p) +31 88 511 3113

Voorsterweg 31
8316 PR Marknesse, The Netherlands
p) +31 88 511 4444

Chamber of Commerce No. 41150373. VAT No. NL002760551B01